

12-2017

Characterizing the Adsorption-Bioavailability Relationship of PAHs Adsorbed to Carbon Nanomaterials in the Aquatic Environment

Erica N. Linard
Clemson University

Follow this and additional works at: https://tigerprints.clemson.edu/all_dissertations

Recommended Citation

Linard, Erica N., "Characterizing the Adsorption-Bioavailability Relationship of PAHs Adsorbed to Carbon Nanomaterials in the Aquatic Environment" (2017). *All Dissertations*. 2056.
https://tigerprints.clemson.edu/all_dissertations/2056

This Dissertation is brought to you for free and open access by the Dissertations at TigerPrints. It has been accepted for inclusion in All Dissertations by an authorized administrator of TigerPrints. For more information, please contact kokeefe@clemson.edu.

CHARACTERIZING THE ADSORPTION-BIOAVAILABILITY RELATIONSHIP OF
PAHS ADSORBED TO CARBON NANOMATERIALS IN THE AQUATIC
ENVIRONMENT

A Dissertation
Presented to
the Graduate School of
Clemson University

In Partial Fulfillment
of the Requirements for the Degree
Doctor of Philosophy
Environmental Toxicology

by
Erica N. Linard
December 2017

Accepted by:
Dr. Peter van den Hurk, Committee Chair
Dr. Stephen J. Klaine
Dr. Cindy Lee
Dr. Tanju Karanfil
Dr. William C. Bridges Jr.

ABSTRACT

Concurrent with the high applicability of carbon nanomaterials (CNM) in a variety of fields and the potential use for pollution remediation, there is the inevitable release of CNMs into the environment. As a consequence of their unique physicochemical properties, CNMs entering the environment will interact with both abiotic and biotic factors. With CNM concentrations estimated to range from parts per billion to low parts per million and their high adsorption affinity for organic contaminants, there is significant concern that CNMs will act as “contaminant transporters”. Even though adsorption and desorption of contaminants from CNMs play a significant role in the ultimate fate of adsorbed compounds, currently there is little conclusive information characterizing the relationship between adsorption behavior and bioavailability of CNM-adsorbed contaminants. The goal of the present research was to establish a comprehensive understanding of the key mechanisms influencing bioavailability of CNM-adsorbed organic contaminants. To accomplish this, I utilized a systematic approach to characterize the influence of CNM morphology, contaminant physicochemical properties, and contaminant mixtures on the resulting bioavailability of the adsorbed compounds, where polycyclic aromatic hydrocarbons (PAHs) were selected as a model class of organic contaminants.

Adsorption behavior of a suite of PAHs by suspended multi-walled carbon nanotubes (MWCNTs) and exfoliated graphene (GN) was characterized using batch adsorption isotherm techniques and fitting experimental data with established adsorption models. Bioavailability of CNM-adsorbed PAHs to *Pimephales promelas* (fathead

minnow) was quantified using bile analysis via fluorescence spectroscopy. Multiple linear regression techniques were used to assess the influence of CNM type, PAH physicochemical characteristics, and concentration effects on adsorption of PAHs by MWCNTs as well as to model the relationship between adsorption behavior and the resulting bioavailability of MWCNT-adsorbed PAHs.

While CNM structure and surface area differed, adsorption affinity was more influenced by PAH physicochemical characteristics. In particular, differences in adsorption of PAHs between MWCNT and GN became insignificant as hydrophobic and π - π interactions with the particular PAHs increased. Similarly, bioavailability of CNM-adsorbed PAHs was less influenced by the type of CNM and more influenced by the PAHs physicochemical properties, particularly the size and morphology of the PAH molecules.

A further investigation with a greater range of PAHs, showed that molecular morphology of small less hydrophobic PAHs was particularly influential on bioavailability when adsorbed to MWCNTs. Though adsorption of chemically similar PAHs was nearly identical in single-solute solutions, the resulting bioavailability was not the same and was attributed to differences in the PAH's π electron system as a function of structure and aromatic makeup. Additionally, modeling the relationship between adsorption affinity (i.e. $\text{Log } K_d$) and resulting bioavailability of MWCNT-adsorbed PAHs, showed a direct correlation when $\text{Log } K_d$ was greater than 2.5, where only the aqueous concentration of PAH remained bioavailable. However, lower adsorption affinity resulted in a variable amount of the MWCNT-adsorbed PAH remaining

bioavailable in an unpredictable manner. The results of this work also indicated that there was a concentration effect influencing adsorption affinity and bioavailability. This was determined to largely be a function of molecular surface area coverage of MWCNT resulting in a change of the adsorption process from more heterogenous to more homogenous.

Finally, adsorption of two pairs of chemically similar PAHs, (1) phenanthrene and anthracene and (2) fluoranthene and pyrene, in bi-solute mixtures confirmed that structural makeup of the molecule is significantly influential on the adsorption-bioavailability relationship. PAHs that have increased contact with the surface of MWCNT, such as anthracene being linear to align with the curved surface of the tube or fluoranthene being more flexible to bend with the curved surface of the tube, outcompeted their chemically similar isoforms. Competitive interactions between PAHs at the surface of MWCNT decreased adsorption affinity of both PAHs within the bi-solute system thus increased bioavailability of the adsorbed PAHs. However, the effect of competition on PAH bioavailability appeared to be greater for less hydrophobic PAHs (i.e. phenanthrene and anthracene) compared with the more hydrophobic PAH pair (i.e. fluoranthene and pyrene). This was attributed to adsorption affinity of phenanthrene and anthracene dipping below $\text{Log } K_d = 2.5$ due to competitive interactions in a bi-solute system. Similar to the single solute studies, only when $\text{Log } K_d > 2.5$ was bioavailability of adsorbed PAHs largely associated with just the aqueous concentration of PAH left in the system.

Overall, the results of this work indicate that there is a correlation between bioavailability of CNM-adsorbed PAHs and observed adsorption behavior in aqueous systems, which is largely driven by the adsorbate's physicochemical characteristics. Factors influencing CNM adsorption affinity of PAHs prior to organismal ingestion, such as concentration and competition, also influence bioavailability of the CNM-adsorbed PAHs in a similar manner. However, adsorption behavior of PAHs by CNMs in aqueous solution is not a perfect prediction of the resulting uptake of PAH into *P. promelas* bile, though my data does indicate an adsorption affinity threshold at which MWCNTs can significantly reduce bioavailability of the adsorbed PAHs. This work furthered our understanding in the factors that may predominantly influence the bioavailability of CNM-adsorbed organic contaminants and provided initial insight into the complex interactions that may occur after consumption on CNM-contaminant complexes that should be focused on in the future.

DEDICATION

I dedicate this work to the late Steve Klaine and his legacy in the ecotox field. Although he is not here today to see this work completed, I couldn't have gotten here without his training, science optimism, and continual support. He was an unforgettable mentor and friend, that helped shape me into the scientist I am today and made an impression that I will carry with me for life.

ACKNOWLEDGMENTS

First, I want to thank Dr. Peter van den Hurk; I am so incredibly appreciative of you becoming not only my advisor for the last year and half, but a lifetime mentor and friend. Without missing a beat, you helped me to seamlessly transition into your lab, tackle the major hurdles of a PhD program, and to remember the toxicological components of my work. You've always had an open door and ear that kept me grounded during the most stressful periods of this project. The unwavering support and help (often expedited help) you've provided me with throughout this process helped make this project happen; for that I cannot thank you enough. I am also thankful to you and Jeanne for opening your home to me during the holidays.

Thank you to my committee: Dr. Cindy Lee, Dr. William Bridges and Dr. Tanju Karanfil. I cannot express enough gratitude for the support that you each have given me throughout my dissertation and especially in the last year; you've kept me motivated, on track and always been ready to provide your expertise as I ran into road blocks during this project. Dr. Lee, beyond helping me to improve my technical understanding of organic chemistry and to improve as a scientific writer, reader and public speaker, you have been an excellent role model; helping me to develop my own balance and identity as a woman in the sciences, thank you. Thank you, Dr. Bridges, for the countless hours spent working with me to analyze my data and taking the time to teach me the "how and why" of each test or technique we used; I may not be an expert in statistics, but you have well equipped me with a set of skills in the field that I will continue to use in future research. Thank you, Dr. Karanfil, for your insight into nanomaterial-environmental

interactions and the opportunities to be involved in grant writing and publication reviews; this not only improved my working knowledge of nanomaterials in the environment, but also improved my critical thinking capabilities. A special thanks to Dr. Onur Apul, for acting as a mentor, always being available to help me work through “adsorption confusion”, and teaching me a number of the skills necessary to complete this dissertation.

I wouldn’t have been able to complete this work without the folks that dedicate so much time to making ENTOX and Cherry Farm run smoothly. Thank you, Ron Gossett, for building me experimental apparatuses, keeping Cherry Farm working regardless of the time of night, and always lending a hand to help. I’m extremely grateful for all your help and your friendship. Thank you to John Smink for your advisement on ICAUC protocols and guidance in the wet lab, as well as your support and friendship during the PhD process. Thank you, Norm Ellis, for always watching out for us at ENTOX and always being willing to help. Also, thank you to Rodney Merck and Rodney Morgan, the lab specialists at CETL, for always fixing the equipment I used although I wasn’t a regular there.

Thank you to many lab mates and fellow ENTOX students that provided help, insight or support during my time at Clemson. Special thanks to Lauren Sweet and Katherine Johnson for helping with sample preparation, water analysis, and exposure dissections; without your help, I would not have been able to complete the amount of work I did for this dissertation. Thank you, Sarah Au and Lauren Stoczynski, for helping prepare and clean Cherry Farm for inspection. Dr. Joe Bisesi, thank you for organizing

the logistics around attending nano specific meetings and including me in your plans; your insight in the field and support as a friend was especially helpful after the passing of Dr. Klaine. Thank you to Dr. Tafadzwa Kaisa, for lending or gifting me lab equipment to allow me to complete my dissertation. Thank you to Dr. Apparao Rao and Dr. Ramakrishna Podila for their insight into graphene interactions with PAHs and thank you to their students, Achyut Raghavendra and Mehmet Karakaya, for making and characterizing exfoliated graphene for me at the Clemson Nanomaterials Center. Thank you also to Mahmut Ersan, for characterizing carbon nanomaterial solutions. Thank you to Dr. Renea Hardwick for helping me to improve my skills as a teacher and teaching me different ways to be an engaging educator. Dr. Karen High and Dr. Julie Martin, I am so appreciative of your mentorship and helping me to prepare for an academic career. I learned an incredible amount during my meetings with each of you, and developed a new appreciation for education in the engineering and science field.

I would like to acknowledge the What's in Our Waters program and the numerous folks that were involved that made an impact on my personal growth during my time at Clemson. Janine Sutter, Cathleen Rees, and Charly McConnell, thank you for helping this program to expand and supporting me to attend conferences and workshops to speak on behalf of the program. Thank you, Namrata Sengupta, for recruiting and training me as project coordinator of this program, it was an extremely fulfilling experience. Thank you to Lauren Garcia-Chance and Christie Sampson for your hard work as co-coordinators and helping to grow the program into its full potential.

Finally, no amount of words can express the feeling of gratefulness and thanks to my loving and supportive parents, Karen and Terry Robinson. You were supportive and positive even when I wasn't, being the best cheerleaders I could've possibly had. Thank you for the care packages, words of encouragement, and willingness to make any potential visit work. I know that I wouldn't have gotten to this point without the two of you backing me. Michael Jensen, thank you for your patience and never wavering support; even when you were tasked with lab work on your visits you have always worked hard to reduce my stress and show your encouragement. Thank you to all the Kuehns, Robinsons, Linards, Blemkers, Joyce Long, and countless other family members and friends for your support, encouragement, and interest in my work over these years.

TABLE OF CONTENTS

	Page
TITLE PAGE	i
ABSTRACT.....	ii
DEDICATION	vi
ACKNOWLEDGMENTS	vii
LIST OF TABLES	xiv
LIST OF FIGURES	xv
 CHAPTER	
I. LITERATURE REVIEW	1
1.0 General Background of Carbon Nanomaterials	1
1.1 Adsorptions of HOCs By CNMs	2
1.1.1 Influence of Adsorbent Properties	2
1.1.2 Influence of Adsorbate Properties	5
1.1.3 Adsorption Models.....	8
1.2 CNMs in the Environment.....	10
1.2.1 Influence of CNMs on Contaminant Fate and Transport	11
1.2.2 Influence of CNMs on Contaminant Bioavailability and Toxicity	14
1.3 Polycyclic Aromatic Hydrocarbons: A Model Class of Contaminants	19
1.3.1 Exposure and Exposure.....	20
1.4 Motivation and Project Goals	21
1.5 References	24
 II. BIOAVAILABILITY OF CARBON NANOMATERIAL- ADSORBED POLYCYCLIC AROMATIC HYDROCARBONS TO PIMPHALES PROMELAS: INFLUENCE OF ADSORBATE MOLECULAR SIZE AND CONFIGURATION.....	 33
2.1 Introduction.....	33
2.2 Materials and Methods.....	35

Table of Contents (Continued)	Page
-------------------------------	------

2.2.1 Chemicals and Particles	35
2.2.2 CNM Characterization	35
2.2.3 Suspension of CNM.....	36
2.2.4 Adsorption Isotherms	36
2.2.5 Organismal Care	38
2.2.6 Bioavailability Assays	39
2.2.7 Bile Analysis	40
2.2.8 Statistical Analysis	41
2.3 Results and Discussion	41
2.3.1 Influence of CNM Type on Adsorption.....	42
2.3.2 Influence of PAH Properties on Adsorption.....	48
2.3.3 Bioavailability of PAHs Adsorbed to MWCNT and GN	50
2.3.4 Relationship Between Adsorption Behavior and Bioavailability of MWCNT and GN Adsorbed PAHs	53
2.3.5 Effect of Biological Conditions on Bioavailability	60
2.4 Conclusions	62
2.5 References	63

III. CHARACTERIZATION AND MODELING THE ADSORPTION-BIOAVAILABILITY RELATIONSHIP OF PAHS BY MWCNTS	68
--	----

3.1 Introduction	69
3.2 Materials and Methods.....	71
3.2.1 Materials	71
3.2.2 Adsorption Isotherms	72
3.2.3 Isotherm Modeling.....	73
3.2.4 LFER Modeling	74
3.2.5 Bioavailability Assays	75
3.2.6 Statistical Analysis and Model Development	78
3.3 Results and Discussion	80
3.3.1 Adsorption Isotherm Modeling.....	80
3.3.2 Adsorption Mechanisms	87
3.3.3 Influence of Adsorbate Properties on Adsorption	91
3.3.4 Linear Free Energy Relationship (LFER).....	96
3.3.5 Bioavailability of PAHs Adsorbed to MWCNT	100
3.3.6 Characterizing the Relationship Between Bioavailability and Adsorption	104
3.3.7 Development of Predictive Bioavailability Model	109
3.4 Conclusions	114

Table of Contents (Continued)	Page
3.5 References	116
IV. INVESTIGATING THE INFLUENCE OF COMPETITIVE ADSORPTION BY MWCNTS AND THE IMPACT ON ADSORBED-PAH BIOAVAILABILITY TO <i>P. PROMELAS</i>	121
4.1 Introduction.....	121
4.2 Materials and Methods.....	122
4.2.1 Materials	122
4.2.2 Adsorption Isotherms.....	123
4.2.3 Adsorption Models.....	124
4.2.4 Solid-phase Extraction	125
4.2.5 Bioavailability Assays	126
4.2.6 Bile Analysis.....	127
4.2.7 Statistical Analysis.....	128
4.3 Results and Discussion	129
4.3.1 Single-Point Competitive Adsorption.....	129
4.3.2 Adsorption in Bi-solute Systems	131
4.3.3 Bioavailability of MWCNT-adsorbed PAHs in Single and Bi-solute Systems	138
4.4 Conclusions.....	143
4.5 References.....	145
V. CONCLUSIONS.....	148
APPENDICES	153
A: Chemical Characteristics	154
B: CNM Characterization	156
C: Supporting Information for Organismal PAH and CNM Exposures.....	160
D: Adsorption Model Fitting	163
E: JMP Outputs for LFER Models	164
F: JMP Outputs for Bioavailability Model.....	168

LIST OF TABLES

Table	Page
2.1 Freundlich isotherm model parameters for adsorption of PAHs by GN and MWCNTs in the presence of NOM.....	43
3.1 Nonlinear sorption models used to fit adsorption isotherms of all PAHs to MWCNTs.....	74
3.2 Fitting parameters of nonlinear models to adsorption isotherms of PAHs on MWCNT	83
3.3 Actual and predicted responses in RFUs \pm 95% confidence interval for <i>P. promelas</i> in PAH-spiked treatments containing MWCNT	104
4.1 Nonlinear sorption models used to fit adsorption isotherms of PAHs to MWCNTs.....	125
4.2 Fitting parameters of Freundlich and Polyani-Manes nonlinear models to adsorption isotherms of PAHs on MWCNT	135
A.1 Adsorbate physico-chemical properties	154
B.1 Morphological characteristics of adsorbents measured before and after adsorption of 2 mg C/L NOM.....	156
B.2 Micro Raman of exfoliated graphene (GN) and multi-walled nanotubes (MWCNT) with PAHs adsorbed.....	157
C.1 Standard curves of PAHs used to calculate PAH equivalent concentration in bile samples and the calculated bile bioconcentration factor (BCF _{bile})	161
D.1 Freundlich model fitting parameters of adsorption isotherms above and below the “isotherm transition point”	163

LIST OF FIGURES

Figure	Page
1.1 Schematic outlining sources of CNM release and expected pathways in which CNMs reach various environmental compartments	11
2.1 Adsorption isotherms of PAHs by MWCNT and GN on a mass and surface area basis	44
2.2 Distribution of PAH adsorption between GN and MWCNT on a mass and surface area basis	45
2.3 Relationship between surface area normalized GN/MWCNT partition coefficient and selected PAH physicochemical properties.....	47
2.4 Adsorption normalized by hydrophobic character plotted as a function of equilibrium concentration	50
2.5 Response of <i>P. promelas</i> to PAHs in the absence and presence of CNMs.....	52
2.6 Relationship between the measured and the predicted response of <i>P. promelas</i> from each treatment.....	53
2.7 Comparison of bioavailability index across all treatments containing MWCNT and GN.....	57
2.8 Relationship between bioavailability index from CNM exposures with PAH physicochemical characteristics.....	59
2.9 Bioavailability index as a function of (A) surface heterogeneity and (B) % CNM surface area coverage.	61
3.1 Adsorption isotherms of PAHs fit with the A) Freundlich model, B) Langmuir model C) Polanyi-Manes model, and D) Dual-Langmuir model	82
3.2 Correlation Curve of PAHs adsorbed to MWCNTs	85

List of Figures (Continued)

Figure	Page
3.3 The relationship between single point adsorption descriptors (K_d) with the equilibrium concentration (C_e) of the PAHs by MWCNTs in log-log plot	88
3.4 Residuals of predicted q_e vs actual q_e	88
3.5 The relationship between PAH molecular surface area and (A) the equilibrium concentration and (B) calculated adsorption descriptor ($\text{Log } K_d$) at the isotherm curvature point.	91
3.6 The relationship between single point adsorption descriptors (K_d) and PAH physicochemical characteristics.....	93
3.7 Log-log plot of PAH adsorption by MWCNT as a function of equilibrium concentration normalized for hydrophobicity.....	94
3.8 Plot of experimental training and external validation single point adsorption descriptors ($\text{Log } K_d$) against predicted values from developed LFER models.....	100
3.9 Response of <i>P. promelas</i> in PAH bioavailability assays with and without MWCNT present.....	101
3.10 Comparison of bioavailability index across all PAHs at the “low” and “high” concentrations.	106
3.11 Descriptive boxplot of % response reduction to each of the PAHs due to the presence of MWCNT at all concentrations	107
3.12 Relationship between the ratio of concentration in the <i>MWCNT</i> treatments to the <i>PAH only</i> treatments in water and bile, as a function of the adsorption descriptor ($\text{Log } K_d$)	112
3.13 Plot of predicted distribution coefficient of PAH between bile and MWCNT ($K_{\text{bileMWCNT}}$) against experimentally obtained values for the training and validation data set.....	119

List of Figures (Continued)

Figure	Page
4.1 Schematic of experimental set up of bioavailability assays.....	127
4.2 Single point adsorption descriptors (K_d) of the primary adsorbate plotted against the competitor adsorbate.	131
4.3 Adsorption isotherms of PAHs by MWCNTs without and with competitor	136
4.4 Polyani-model based correlation curves of PAHs adsorbed by MWCNT alone and in the presence of the competitor PAH.	138
4.5 Comparison of the concentration of PAH measured in bile of fish exposed to treatments with and without MWCNT in single and bi-solute exposures.	139
4.6 The reduction in bile concentration (%) of PAHs as a function of adsorption	141
4.7 Comparison of the uptake of each PAH from MWCNT into bile in single solute and bi-solute exposures.....	143
B.1 TEM images of GN and MWCNT in moderately hard water and in the presence of NOM	158
B.2 Raman spectra for MWCNTs and GN.....	158
B.3 Concentration of suspended MWCNTs and GN measured via UV-vis absorbance	159
C.1 Concentration of suspended MWCNTs and GN measured via UV-vis absorbance	160
C.2 Images of <i>P. promelas</i> intestinal tract from PAH and CNM exposures	161
C.3 Relationship between single Log BCF _{bile} values for each PAH and the measured partitioning of PAHs into bile from the bioavailability assays (Log K _{ibile}).....	162

CHAPTER ONE

LITERATURE REVIEW

1.0 General Background of Carbon Nanomaterials

Although carbon nanomaterials (CNMs) have been produced naturally and unintentionally for decades, the discovery of fullerene in 1985 and multi-walled carbon nanotubes in 1991 led to extensive interest in the use of these materials in various commercial products (Andrews et al., 2002; Klaine et al., 2008; Gogotosi and Presser, 2014). Carbon nanomaterials are composed of graphitic carbon that can occur in sp , sp^2 , and sp^3 hybridization, allowing for a wide range of structures and properties (Gogotosi and Presser, 2014). Of the carbeneous nanomaterials, CNTs and graphene have been considered the most promising in terms of commercial applications due to their remarkable thermal, mechanical, electronic and biological properties (Scida et al. 2011). Two-dimensional graphene is composed of six-membered sp^2 hybridized carbon atom rings in a one-atom thick sheet (Apul and Karanfil, 2015; Zhao et al., 2014a). Carbon nanotubes are essentially graphene sheets rolled into cylinders that are produced as either individual graphene cylinders that can be capped or uncapped, known as single walled nanotubes (SWCNTs), or as concentric open-ended graphene cylinders, known as multi-walled carbon nanotube (MWCNTs) (Dai, 2002). Carbon nanotubes are currently the most popular and efficiently produced carbon nanomaterial. In 2015 the global CNT market was estimated at 2.26 billion USD, but is expected to grow to 5.64 billion USD by 2020 with electronics and semiconductors being the largest application (Ren et al., 2011). In recent years graphene, as well as multilayered graphene and oxidized graphene, has gained significant attention for its promising applications in electronic films, aerospace, composites, biosensors, filtration, etc., though the limitation on the growth of the graphene market is attributed to expensive equipment and inability to mass produce quality graphene (Mauter and Elimelech, 2008).

1.1 Adsorption of HOCs By CNMs

The high specific surface area of CNTs and graphene as well as their hydrophobicity make them particularly good adsorbents of organic materials, including natural organic matter and a wide range of non-polar hydrophobic organic contaminants (HOCs). While this property suggests potential use in pollution remediation of organic contaminants it also brings concern as to the potential risk they may pose by altering the fate of adsorbed organics (Baun et al. 2008; Ren et al 2011; Klaine et al., 2008). As such, much research has been devoted to understanding the mechanisms driving adsorption of organic contaminants to CNMs. Studies have largely concluded that adsorption to CNMs is driven by π - π bonding, hydrophobic interactions, hydrogen-bonding and electrostatic interactions. Although, morphological differences in CNMs, such as structure, length, thickness, diameter, pore size distribution, surface functionalization, number of layers or walls, can all influence adsorption behavior (Apul and Karanfil, 2015; Zhao et al., 2014a). Likewise adsorbate physicochemical characteristics, such as hydrophobicity, size, polarizability, or even morphology, can also greatly influence adsorption (Apul and Karanfil, 2015; Yang et al., 2006). Overall, though adsorption of HOCs by graphene and CNTs is largely driven by π - π bonding (Chen et al., 2007; Zhao et al., 2014a), differences in adsorption behavior by the two materials have been observed due to interactions with the adsorbate (Apul et al., 2013; Wang et al., 2014).

1.1.1 Influence of Adsorbent Properties

Because most CNMs consisting of sp^2 hybridized carbons with the graphene hexagonal lattice as the building block, structural and morphological differences largely account for differences in adsorption interaction with HOCs. For most carbon nanomaterials, adsorption capacity is positively correlated with surface area and pore volume, as increases in these parameters mean an increase in potential adsorption sites (Apul and Karanfil, 2015; Apul et al, 2013; Zhao et al., 2014a). Theoretical surface area of a single sheet of graphene is estimated to

be 2630 m²/g, although due to aggregation and/ or wrinkling in aqueous solution the actual surface area of graphene is found to be closer to 400-600 m²/g (Wang et al., 2014; Apul et al., 2013). The surface area of multilayered graphene, reported to range from 100 – 150 m²/g, is related to the degree of exfoliation and the number of layers; with limited exfoliation and a high number of layers the material will more closely resemble graphite with a surface area reported to range from 4 to 8 m²/g (Wang et al., 2009; Zhao et al, 2014b; Zhu and Pignatello, 2005). The surface area of CNTs depends on the length, diameter and number of walls of the tube. Most studies have largely found the average surface area of purchased and/or made SWCNTs and MWCNTs to fall within the size range of 373±176 m²/g and 216±159m²/g, respectively (Apul and Karanfil, 2015). The interlayer spacing (i.e. < 0.34nm) in multi-layered graphene, carbon nanotubes, and graphite is inaccessible to molecules even as small as N₂, therefore adsorption largely occurs on the outer surface of dispersed CNMs (Pan and Xing, 2008; Laurent et al., 2010; Wang et al., 2009). While aggregation of CNMs in aqueous solution can reduce the surface area, CNT aggregates can create interstitial channels and grooves as additional adsorption sites (Pan and Xing, 2008; Zhang et al., 2009), while graphene aggregates can cause folding or formation of micropores as additional adsorption sites (Zhao et al., 2014b; Wang et al., 2014). Though some studies have denoted differences in micropore volume between CNTs and graphene, a majority of studies have concluded that these structural differences between 2D or quasi 2D graphene and 1D CNTs do not alter the mechanism of adsorption (Zhao et al., 2014b). Normalization of adsorption by CNMs specific surface area and micropore volume are largely effective in reducing the difference in observed adsorption capacity for the same compound, suggesting that the mechanisms driving adsorption of HOCs for graphene, graphite and CNTs are similar (Zhao et al., 2014b; Apul et al., 2013; Yang et al., 2006).

Beyond surface area and pore size influences on adsorption, surface chemistry can dramatically alter the adsorption capacity of CNMs. Presence of amorphous carbon or impurities

due to material synthesis can hinder access of HOCs to adsorption sites (Apul and Karanfil, 2015; Gotovac et al., 2007). Additionally, oxidation of CNMs during material preparation can decrease the hydrophobicity of adsorption sites, deform or alter micropores, and disrupt the graphitized structure of carbon, generally decreasing CNM adsorption capacity (Zhao et al., 2014b; Apul and Karanfil, 2015; Stankovich et al., 2006). Because defect sites, such as amorphous carbon, edges or metal impurities, are more reactive to oxygen, CNMs of different structures may have different levels or sites of oxygenation which may alter adsorption behavior (Apul and Karanfil, 2015; Yang et al., 2006; Zhao et al., 2014a). Surface functionalization of CNMs alter the electron donating and accepting properties of CNMs, thus can impact the types of adsorbates adsorbed (i.e. polar vs nonpolar) and in part determines the strength of the π - π interactions (Dinadayalan and Leszczynski, 2010; Radovic and Bockrath, 2005). Regardless, the influence that surface functionalization has on CNM adsorption capacity has been found to be more dependent on the type of adsorbate than the type of the adsorbent (Pan and Xing, 2010).

Curvature of a graphitic material has also been shown to impact adsorption of HOCs; the curved surface of CNTs creates a diversity of C-C bond lengths unlike the flat surface of graphene which has only single length of C-C bond. Different C-C bonds are suggested to alter adsorption strength, especially for planar molecules, like aromatic hydrocarbons, that have different favorable “stacking” positions based on the bond type (Tournus and Charlier, 2005; Li et al., 2013a). For single layered graphene, wrinkling of the surface can create additional high energy groove sites for adsorption (Wang et al., 2014). Further, differences in morphology along with the degree of edge sites and number of layers cause graphene and CNTs to have distinct electrical properties (Wang et al., 2009). The difference in electronic reactivity is partially due to the delocalization of π -conjugated orbitals across the graphene surface making the basal plane of graphene/graphite electrochemically inert while the localized orbitals at the defect and edge sites of graphene and CNTs create a higher degree of electronic activity (Tachikawa and Kawabata,

2009; Zhu and Pignataello, 2005). As the diameter of CNTs becomes greater than 1 nm, the C-C bond lengths become uniform and the strain of π -orbital misalignment is reduced, thus allowing for greater adsorbate binding energy that is more reminiscent of binding with graphene (Dinadayalan & Leszczynski, 2010). This decrease in CNT surface curvature is related to increased π - π interactions due to increased contact and better alignment of planar molecules with the surface of CNTs (Gotovac et al. 2007; Apul et al. 2012a). In general, π - π interactions and hydrophobic forces are attributed to driving the physical adsorption of HOCs to CNTs although they are not considered strong enough to allow for charge transfer between the compounds and the CNT surface (Tournus et al., 2005; Rajesh et al., 2009). In contrast, several studies suggest that while these interactions also significantly contribute to the adsorption of HOCs by graphene, other mechanisms such as electrostatic interactions are responsible for stabilizing adsorption (Wang et al., 2014; Bjork et al., 2010; Zhu and Pignataello, 2005).

1.1.2 Influence of Adsorbate Properties

Nonspecific attractions and hydrophobic forces are considered the main interactions promoting adsorption of HOCs by CNMs. The strength of these interactions is dependent on HOCs physicochemical characteristics, particularly the molecules size, polarity, and polarizability which likewise contribute to the compounds' hydrophobicity (Apul and Karanfil, 2015). In linear solvation energy relationship (LSER) models developed to predict adsorption of various HOCs to CNTs, the most dominant parameter was one representing the adsorbate hydrophobicity followed by the adsorbate's ability to accept and donate hydrogen bonds (Apul et al., 2012b). In addition to these parameters, Xia et al. (2010) also found the compound's polarizability to be a significant contributing factor. Generally, adsorption of HOCs by CNMs tends to increase with increasing compound hydrophobicity and that normalization of adsorption capacity by the molecule's hydrophobicity (i.e. octanol-water partitioning coefficient or aqueous solubility) diminishes the observed adsorption differences between comparable compounds

(Brooks et al., 2012; Yang et al., 2006; Zhu and Pignatello, 2005; Wang et al. 2014). However, differences in size or functional groups can also alter a compound's adsorption affinity beyond the hydrophobic effects. Larger molecules have been observed to have a lower adsorption affinity for CNTs, graphene, and graphite than smaller, less hydrophobic compounds (Wang et al., 2014; Yang et al., 2006; Pan and Xing, 2008). This is largely attributed to the inability of larger molecules to access the available micropores and the increase of steric hindrance between molecules adsorbed on the CNM surface (Apul and Karanfil, 2015; Wang et al. 2014; Pan and Xing, 2008). Numerous studies have noted that adsorption of especially small HOCs, such as naphthalene, may be driven by a combination of mechanisms such as pore filling in addition to the surface adsorption observed for most adsorbates (Wang et al., 2014; Yang et al., 2006).

Because most adsorption occurs on the surface of CNM through nonspecific interactions, adsorption energy increases with a decreased distance between the adsorbate and CNM surface as well as with increased contact (Pan and Xing, 2008). Along with molecular size, the adsorbate's morphology can significantly impact the ability of a molecule to get close enough to the CNM's surface for strong adsorption. Studies have suggested an adsorption advantage of planar molecules by both curved CNTs and graphene, due to increased surface contact and increased van der Waals interactions. Moreover, linear planar molecules have been observed to have a greater adsorption capacity due to better ability to align with the curved surface of CNTs; this advantage is less pronounced on wide diameter CNTs where the surface resembles the flat surface of graphene (Gotovac et al., 2007; Apul et al., 2012a). Although studies have also observed that non-planar compounds, such as biphenyl, are less impacted by adsorption competition than rigid planar compounds (Apul et al 2012a). Likewise, the adsorption of nonplanar 2-phenylphenol is less site selective than planar compounds, suggesting that the flexibility of nonplanar compounds allow them to better twist to access sites that may not be accessible to a rigid planar compound (Zhang et al., 2009).

Compounds of similar structure or in a similar compound class typically have a similar mechanism of adsorption. Zhu and Pignatello (2005) found that when a wide range of HOCs adsorption isotherms were normalized by the compound's hydrophobicity, the compounds from the same class collapsed onto a single isotherm line, though remaining distinctly different from other compounds classes. Similarly, Wang et al. (2008) found that the similarly structured aromatics, phenanthrene and naphthalene, had comparable adsorption when adsorbed by a range of adsorbents, though 1-naphthol, a compound of similar size but with a functional group, adsorbed quite differently. The presence of functional groups and the compound's polarity greatly determine the strength of the electron-donor-acceptor (EDA) interaction with the CNM surface and the strength of π - π interactions (Keiluweit and Kleber, 2009). The graphitic surface of graphene and CNTs can either donate or accept electrons, thus interactions with substituted and unsubstituted compounds can be vastly different (Pan and Xing, 2008; Zhu and Pignatello, 2005). Typically for aromatic compounds, such as polycyclic aromatic hydrocarbons (PAHs), π - π bonds form between the graphitic surface carbons and the C=C double bonds of the carbon rings (Pan and Xing, 2008; Yang et al 2006; Apul and Karanfil, 2015; Zhao et al., 2014b). PAHs are considered to behave as electron donors towards graphitic surfaces, where donor strength increases with polarizability and likewise improves the chances of charge transfer/ electrostatic intermolecular interactions (Zhu and Pignatello, 2005; Martinex and Iverson, 2012). Additionally, it has been suggested that aromatics with a smaller HOMO-LUMO (highest occupied molecular orbital energy and lowest unoccupied molecular orbital) gap may have a greater affinity for CNMs (Pan and Xing, 2008). As previously mentioned, the electronic properties of CNMs, including π orbitals (i.e. HOMO and LUMO energy levels) is partially dependent on CNM structure; the regions of delocalized π electrons will influence adsorption and may do so differentially for different CNMs (Oleszczuk et al., 2009; Bjork et al, 2010; Apul and Karanfil, 2015). Ultimately the occurrence of electrostatic interactions depends on the nature

of the charge on both the CNM and the adsorbates; CNMs with low functionalization and unsubstituted aromatic hydrocarbons are more likely to engage in nonspecific interactions and π - π bonding (Zhao et al., 2014b; Pan and Xing, 2008).

1.1.3 Adsorption Models

Several linear and nonlinear models exist that are commonly used to describe the adsorption of HOCs by CNMs. Generally, the process is considered heterogenous due to the presence of a range of adsorption sites possessing different energy levels as a function of surface defects, edges, groove regions etc. (Kah et al., 2011). In high solute concentrations, it has also been proposed that heterogenous adsorption will occur with condensation and multilayer formation (Pan and Xing, 2008). Although existing adsorption models were originally used to describe gas adsorption onto adsorbents, they are also applicable to describe adsorption of HOCs by CNMs in aqueous systems. These models help to empirically explain the observed adsorption process and provide insight into the adsorption mechanisms of HOCs by CNMs. Six of the most commonly used models to describe adsorption of HOCs by CNMs, charcoal and geo-sorbents are Freundlich (FM), Langmuir (LM), Brunauer-Emmett-Teller (BET), dual-mode (DMM), dual-Langmuir (DLM) and Polyani-Manes (PMM) (Kah et al., 2011). Although FM and LM can be linearly transformed, the other four models cannot. The Freundlich model, a special form of the PMM, assumes a distribution of adsorption sites with various surface energies, where molecules will first occupy the high-energy sites before the lower energy sites and there is the potential of multilayer formation. Data that fit this model would be linear when log transformed and adsorption would continually increase to some degree (Kah et al., 2011; Yang et al., 2006). On the other hand, the Langmuir model assumes a homogenous distribution of adsorption sites and shows a characteristic plateau representative of a maximum adsorption capacity reached after a monolayer has been formed (Kah et al., 2011). The BET model also assumes that after the formation of the first monolayer, multiple layers will then form due to condensation as

concentrations approach the solubility limit. The dual-mode model assumes that both partitioning and adsorption are occurring, where the process of partitioning is linear and the adsorption process follows the same assumptions as the Langmuir model. Due to the lack of a flexible domain and the small spaces between layers of CNMs such as CNT and graphene, partitioning of compounds into the nanoparticle is not considered a likely process (Kah et al., 2011). Dual-Langmuir model assumes the existence of only two different types of sites, high and low energy, where a maximum adsorption capacity exists for each (Kah et al., 2011; Yang et al., 2006). The Polanyi-Manes theory assumes that adsorption is related to the distance the molecule is from the adsorbent's surface (i.e. adsorption space) and the attractive forces between the adsorbate and adsorbent (i.e. adsorption potential) (Yang and Xing, 2010). Adsorption capacity is independent of temperature, but dependent on the potential space available and the molecule's size, where the higher the adsorption potential the greater the adsorption affinity (Yang and Xing, 2010). For describing heterogeneous adsorption of compounds to activated carbon and CNMs, the Freundlich model and Polanyi-Manes have often been recognized as the models with the best fit (Yang and Xing, 2010; Pan and Xing, 2008; Oleszczuk et al., 2009). Additionally, Yang et al (2006) suggested that the PMM was applicable to describe adsorption to flat surfaces and pore filling. In contrast, Kah et al (2011), found that the DLM model had the best fit when assessing a wide concentration range of PAHs adsorbed to CNTs. The authors suggested that this fit may not necessarily be due to the existence of only two types of adsorption sites, but rather that the model represented different accessibilities to the available adsorption sites that were created during aggregation. Fitting adsorption models over wide equilibrium concentrations often results in the inability of the models to describe the whole adsorption process (Wang et al., 2014; Kah et al, 2011). Overall, it is important to note that while such empirical models can provide insight into the potential mechanisms of adsorption, they are limited in the range of concentration they can

describe and are apt to misinterpretation when additional processes are occurring such as aggregation or competition.

1.2 CNMs in the Environment

Concurrent with the increase of production and use of products containing engineered nanomaterials is their increased entrance into the environment (Klaine et al., 2008; Mueller and Nowack, 2008). Because CNMs are made up of carbon and can resemble already naturally present carbon materials in the environment, it has been difficult to measure actual concentrations (von der Kammer et al., 2012; Peterson et al., 2011; Gottschalk, et al., 2013). However predictive models using information on the worldwide production volume and flow coefficient of CNMs, have provided estimates of CNMs expected in various environmental compartments (Figure 1.1) (Mueller and Nowack, 2008; Peterson and Henry, 2012). Depending on the environmental compartment and proximity to release points, environmentally relevant concentrations of CNMs are estimated to range from parts per billion to low parts per million range (Velzebor et al., 2013; Peterson et al., 2011; Gottschalk et al., 2013).

As a consequence of their “nano” dimensions, nanomaterials possess physicochemical properties unique from their bulk counterparts. As such nanomaterials are reactive thus interact with abiotic and biotic factors in the environment, in many cases causing potential concern for human and environmental health (Apul and Karanfil, 2015; Nowack et al., 2012). The fate and transport of CNMs in the natural environment are largely driven by aggregation and suspension behaviors, that are greatly influenced by environmental conditions such as ionic strength, pH, the presence of natural organic matter, and media porosity (Lin et al., 2010a; Chen et al., 2008; Hofmann and von der Kammer, 2009). Due to their hydrophobicity, pristine CNMs are prone to aggregation upon entering into an aqueous system, thus likely to settle out into sediment (Saleh et al., 2008; Schwyzer et al., 2011). However, upon entering any natural water source, CNMs will interact with natural organic matter (NOM) which will help disperse and stabilize CNMs in

the water column (Schwyzer et al., 2011; Hyung et al, 2007; Lu and Su, 2007). This can increase the mobility of CNMs, thus altering their fate and organismal exposure. Additionally, a majority of CNMs entering into the environment have likely already undergone some level of transformation either because of their specific application, aging or during the release process and are no longer considered pristine (Zhao et al., 2014a). Because of CNMs high adsorption affinity, they are also prone to readily adsorb a wide array of contaminants either during processing or upon entering the environment where contaminants are already present. As such, though some nanomaterials are inert themselves, they can become indirectly toxic through interactions with co-occurring contaminants (Velzebor et al., 2013; Baun et al, 2008; Zhao et al., 2014a).

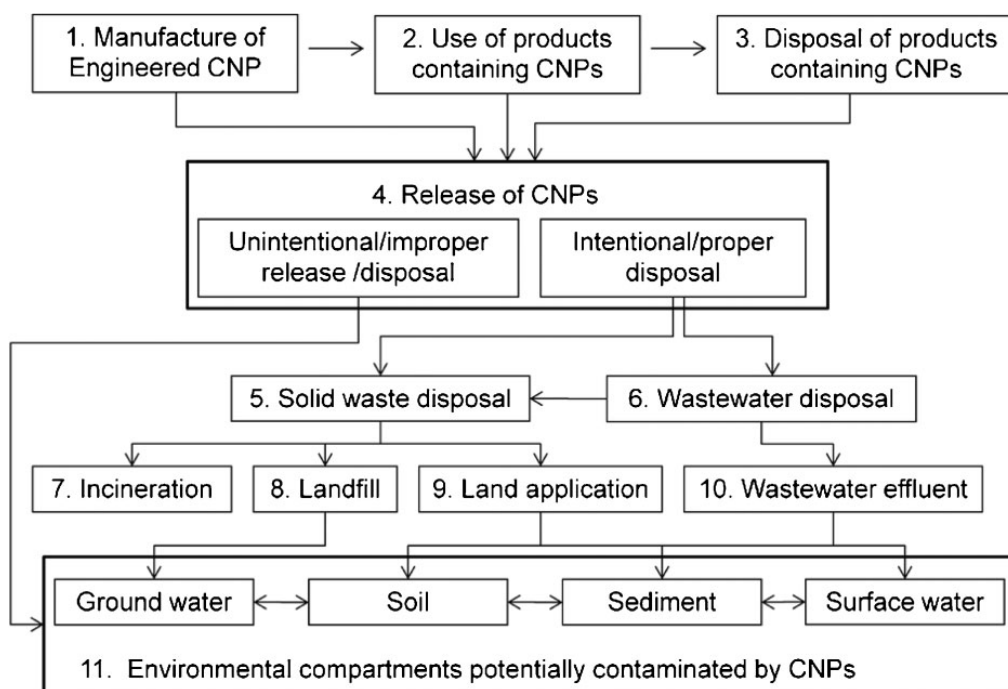


Figure 1.1. Schematic outlining the sources of CNM release and expected pathways in which CNMs reach various environmental compartments (Peterson and Henry, 2012).

1.2.1 Influence of CNMs on Contaminant Fate and Transport

In the environment, the presence of natural organic matter (NOM) and/or other colloids has been generally found to reduce the bioavailability of hydrophobic contaminants due to sequestration; however, the potential of CNMs to facilitate the transport or alter the fate of adsorbed contaminants is distinctly different than that of NOM or natural colloids due to the adsorptive interactions with HOCs (Riding, et al., 2015; Zhang et al., 2011a). For example, CNTs can significantly reduce mobility of organic contaminants compared to reference material octadecyl (C_{18}) in soil even at high flow rates due to the significantly higher adsorption capacity of CNTs (Li et al., 2013a). The preference of a wide range of contaminants, including organic, inorganic and metals, to bind to CNMs over sediment, soil or organic matter is attributed to the physicochemical characteristics the adsorbent (Zhang et al., 2011a; Josko et al., 2013). Co-transport of contaminants via CNMs in soil and sediment matrices is significantly influenced by the morphology of CNMs and aggregation behavior. Though CNTs and graphene have higher surface area on which to adsorb contaminants, CNMs that aggregate in looser bundles, such as spherical fullerenes, are more effectively transported through porous media (Fang et al., 2013; Jaisi and Elimelech, 2009; Zhang et al., 2009). Beyond CNM aggregation behavior, CNM mobility is largely dependent on the soil particle size and content makeup, where transport decreases with decreasing particle size due to effective filtration of the soil matrix (Fang et al., 2013). Surface chemistry of the CNMs can also influence potential translocation of adsorbed contaminants (Wang et al. 2012; Hu et al. 2014). Oxidized or functionalized CNMs tend to be more hydrophilic causing them to be more easily transported and to release hydrophobic adsorbed compounds more easily due to a lower adsorption affinity (Zhao et al., 2014a; Zhang et al., 2011a; Sun et al., 2013a).

In aqueous systems, dispersal, strength of adsorption and rate of desorption are considered the most influential properties driving contaminant transport (Hoffman and von der Kammer, 2009). Irreversible adsorption or particularly strong adsorption can hinder the release

of contaminants even if the CNMs are transported throughout the environment (Hofmann and von der Kammer, 2009; Li et al., 2013a). However, the adsorption and desorption of contaminants can be influenced by the aqueous solution chemistry such as ionic strength, pH, and presence of NOM (Chen et al., 2008; Hyung et al., 2007; Zhang et al., 2011b). It is important to note that the role that NOM plays in mediating or enhancing transport of CNM adsorbed contaminants is largely dependent on the type and concentration of NOM present. The enhanced suspension of CNMs by NOM or oxidation has been shown to increase the mobility, transport distance and release of adsorbed contaminants (Lin et al., 2010b; Zhao et al., 2014a). Further, Hu et al. (2014), found that the presence of NOM increased the release of more hydrophobic polycyclic aromatic hydrocarbons (PAHs), although it retarded the uptake of less hydrophobic PAHs. On the other hand, the presence of NOM can also 1) increase the competition of adsorption sites on the surface of CNMs, causing contaminants to remain in the environment thus accessible for biodegradation and bioaccumulation, or 2) inhibit desorption of adsorbed contaminants (Zhang et al., 2011b; Apul et al., 2013; Wang et al. 2009; Sun et al., 2013a).

Beyond the potential effects that CNMs can have on the transport of co-occurring contaminants, CNMs can drastically alter the ultimate fate and environmental residency of adsorbed contaminants. Organic contaminants released into the environment, in the absence of CNMs, often undergo some degree of aging or biodegradation mediated by microbial communities (Eijsackers et al., 2001; Towell et al., 2011). The presence of CNMs can cause a longer retention time of contaminants in the environment by reducing the biodegradation and mineralization efficiency of adsorbed contaminants (Towell et al., 2011; Riding et al., 2015). Although microbes and bacteria can still access some fraction of the adsorbed contaminant, the portion that is actually bioaccessible is reduced (Towell et al., 2011). Towell et al. (2011) observed the extent of mineralization differed depending on CNM type, where mineralization decreased as MWCNT>SWCNT>fullerene. This was attributed to CNM adsorption capacity and

aggregation behavior of the different types of CNMs. CNMs have also been shown to increase the ageing time of contaminants due to the inability of abiotic factors, such as light exposure, to access the adsorbed molecules (Cui et al., 2011; Zhou et al., 2013; Xia et al. 2013). This differs from the influence of natural colloids or NOM on adsorbed contaminants, which are more susceptible to abiotic factors than CNMs and are prone to release the adsorbed contaminant (Schwarzenbach et al., 2003; Turco et al., 2011).

1.2.2 Influence of CNMs on Contaminant Bioavailability and Toxicity

Ingestion of CNMs is considered the main route of exposure to aquatic organisms although interactions at the gills can also occur (Jackson et al., 2013; Hou et al., 2013). Investigations of CNT bioaccumulation in a wide range of organisms including *Daphnia magna*, various fish species, invertebrates and earthworms have largely concluded CNTs to have low bioaccumulative potential as they do not cross intestinal cells or absorb into tissues (Edgington et al., 2010; Peterson et al., 2009; Bisesi et al., 2015). For larger organisms such as fish, CNTs are compartmentalized in the gut and readily excreted, though the level of dispersion and aggregation of the materials can influence the rate of egestion (Peterson et al., 2009; Su et al., 2013). Indirect CNT toxicity has been observed in *D. magna* at high concentration as a result of gut impaction or blockage at the gills (Peterson and Henry, 2012; Edgington et al., 2010). Further, the ingestion of CNTs has been shown to alter the mucous cell morphology causing edema in the submucosa of the gastrointestinal tissue of *P. promelas* (Bisesi, et al., 2015). Graphene and graphene oxide have been observed to have higher antibacterial properties than other CNMs, which has been attributed to the thinness of the material (Zhao et al., 2014a). If graphene remains in single sheets, it has the potential to puncture cell membranes, due to its sharp edges, thus causing cell death (Zhang et al 2012). However, this is considered a larger concern for graphene oxide (GO) as the oxidation on the surface of the material will hinder the aggregation of GO; due to van der Waals forces, graphene will quickly aggregate in aqueous

systems, becoming much thicker and less likely to cause membrane damage (Zhao et al., 2014a). Graphene toxicity was found to be insignificant in *Caenorhabditis elegans* and crustaceans, though current literature investigating graphene toxicity is still in its infancy (Zhao et al., 2014a). In general, toxicity of CNMs themselves largely depends on the concentration, degree of dispersion and the functionalization or coating that exist in the material (Hou et al., 2013).

Due to CNM's high adsorption affinity for organic contaminants and influence on adsorbate fate, there is considerable concern for the materials to behave as "contaminant transporters" once released into the environment (Baun et al., 2008). Greater retention of contaminants in environmental compartments (e.g. soil) and/or reduced degradation of contaminants due to CNM adsorption has the potential to increase exposure to local organismal residents beyond the anticipated exposure in CNM-free environments (Li et al., 2013a; Towell et al., 2011). The enhanced influence on bioavailability, either negatively or positively, by CNMs over other black carbon sources is attributed to the unique adsorption behavior (Ferguson et al., 2008; Xia et al. 2012). Contaminants within the same class (i.e., PCBs, PAHs, estrogenic compounds, etc.) have been observed to have similar bioaccumulative trends that are a function of the compound's chemical and structural makeup (Xia et al., 2012). MWCNTs have been shown to enhance the bioaccumulation of compounds that are ionizable, such as pentachlorophenol and ibuprofen, due to the change in chemistry both at the gill and in the digestive tract (Sun et al., 2013b; Chen et al., 2014). Although sediment and water concentrations of these ionizable compounds can be reduced by adsorption to CNMs, the change in pH and solution chemistry once at the gills or ingested can significantly alter the binding behavior thus leading to potential release and accumulation (Sun et al. 2014; Chen et al., 2014; Myers et al., 2016). However, for less hydrophobic ionizable compounds that have a lower adsorption affinity for CNTs, such as diphenhydramine (DPH), MWCNTs were found to not significantly alter DPH uptake due to exposure levels remaining the same (Myers et al., 2016). The bioavailability of neutral organic

contaminants adsorbed to CNMs, like PAHs, is not much affected by change in solution pH (Wang et al., 2011; Linard et al., 2015). Additionally, Zindler et al. (2016) recently observed that regardless of surface functionalization or diameter, the bioavailability and toxicity of CNT-adsorbed phenanthrene to *D. magna* did not differ. This suggests that for neutral compounds CNT physicochemical properties have little influence on the adsorbed compound's bioavailability (Zindler et al., 2016). From the literature, the largest driver in dictating the influence CNMs will have on neutral aromatic compounds bioavailability is adsorption affinity, which would explain the contrasting results related to bioavailability of CNM-adsorbed PAHs. Largely, the bioavailability of phenanthrene, a small three-ringed PAH, has been observed to be enhanced when adsorbed to fullerenes, SWCNTs and MWCNTs in fish and *D. magna* (Baun et al., 2008; Su et al., 2013; Zindler et al., 2016; Wang et al., 2011). Though for PAHs with higher adsorption affinity, such as pyrene and fluoranthene, bioavailability was significantly reduced when adsorbed to CNTs (Peterson et al., 2009; Linard et al., 2015). In accordance, it was found that bioaccumulation of organochlorine compounds in medaka was significantly reduced for the highly hydrophobic compounds (i.e. $\text{Log } K_{ow} > 6$), but was slightly enhanced for the less hydrophobic compounds ($\text{Log } K_{ow} < 6$) (Hu et al., 2010). It has also been observed that bioavailability of several polychlorinated biphenyls (PCBs) and polybrominated diphenyl ethers (PBDEs) to benthic invertebrates was reduced with the amendment of CNTs in the sediment (Ferguson et al., 2008; Parks et al. 2013). Adsorption studies have shown that the presence of the aromatic rings within these types of compounds enhances their interaction with CNMs; therefore, the influence on bioavailability of these compounds is likely driven by the strength of interaction with the CNM in question. Similarly, Xia et al. (2012) concluded that the degree of hydrophobic interactions between CNTs and the contaminant would largely drive the degree to which bioavailability would be reduced. Although perfluororchemicals (PFCs) are aliphatic with hydrophilic and hydrophobic groups, the high adsorption affinity of MWCNTs for these

compounds, due to hydrophobic interactions, significantly reduced the bioaccumulation of PFOS in *Chironomus plumosus* larvae (Xia et al., 2012). As chain length of PFCs partially drives their hydrophobic interactions with CNMs, future studies should investigate the bioavailability of CNM-adsorbed aliphatic contaminants and the relationship to chain length (Li et al., 2013b).

The level of dispersion or aggregation, which is partially driven by CNM morphology, is also suggested to have a significant impact on bioavailability of CNM-adsorbed contaminants. Peterson et al. (2009) observed that while there was not a significant difference in the degree that SWCNTs and MWCNTs reduced the bioaccumulation of pyrene in earthworms, MWCNTs did increase the rate of pyrene depuration to a greater extent than SWCNTs. Due to the smaller diameter of SWCNTs than MWCNT, SWCNT aggregate bundles are typically more compact (Zhang et al., 2009). Similarly, in an aquatic exposure of SWCNT-adsorbed PAH, phenanthrene, fish exposed to the more stable suspension had a lower level of phenanthrene measured in the intestinal tissue (Su et al., 2013). Although the stable suspension had a higher adsorption capacity for the compound, it was egested much more quickly, indicating that increased aggregation of CNTs in the gut tract led to a higher retention time allowing for greater desorption of the compound (Su et al., 2013). The desorption of phenanthrene CNTs in simulated human gastrointestinal fluids significantly increased with increasing CNT diameter. This was attributed to higher accessibility to the phenanthrene molecules by bile salts and other solubilizing digestive components due to a lack of micropores on the low curvature surface (Wang et al., 2011). This indicates that bioavailability of CNM adsorbed contaminants is partially driven by CNM morphology and suggests enhanced bioavailability of compounds adsorbed to flatter/low curvature surfaces, like graphene.

The presence of NOM has been found to have various influences on the bioavailability and toxicity of CNM-adsorbed contaminants depending on the environmental compartment and the type of contaminant adsorbed. In general, the ability of NOM to disperse CNMs has been

considered to increase the rate and ability of organisms to effectively egest ingested CNMs (Edgington et al., 2008; Peterson et al., 2009). However, due to MWCNT's adsorption of NOM, the speciation of copper was altered, leaving a greater concentration of free copper in the water thus increasing *D. magna* copper toxicity (Kim et al., 2010). Similarly, NOM has been found to inhibit the effectiveness of CNMs to reduce the bioavailability of adsorbed organic contaminants. Due to competition for adsorption sites by NOM, Shen et al. (2013) observed an increase in the bioaccumulation factor of PAHs in benthic invertebrates compared with MWCNT-amended sediment without NOM. In contrast, the presence of fulvic acid ameliorated the enhanced toxicity of PFOS adsorbed to graphene oxide in fish. Fulvic acid promoted the aggregation of graphene oxide (GO) in the intestine and accelerated the excretion of GO-PFOS complexes thus neutralizing the enhanced bioaccumulation effect of PFOS from GO (Qiang et al. 2016). There have also been observed cases where the presence of NOM has little effect on the bioavailability of CNM-adsorbed contaminants (Myers et al., 2016; Linard et al., 2015; Yan et al., 2017). This can be due to a number of factors such as different binding affinities of different types of NOM for CNMs or low preference of the adsorbed compound to interact with present NOM (Linard et al., 2015; Wang et al., 2008).

Further, the habitat, feeding habits and gut physiology of an organism drive the level of exposure and bioavailability potential of adsorbed contaminants (Shen et al., 2013; Peterson et al., 2009; Ferguson et al., 2008). Ferguson et al. (2008) found that PAH bioaccumulation in polychaetes was significantly reduced compared to the PAH tissue concentration in copepods exposed to the same SWCNT amended sediment. This was partially attributed to the feeding habits of the organisms; because the polychaetes were selective in the particle size that they would ingest compared to the copepods, the reduced PAH concentration was likely due to the polychaetes rejection of CNT-associated particles (Ferguson et al., 2008; Rust et al., 2004). Depending on the feeding state and digestive system of the organism, adsorbed contaminants can

desorb from CNMs and be subsequently absorbed in the gastrointestinal tract (Arnot and Gobas, 2006; Wang et al., 2011; Su et al., 2013). In the case of the antibiotic roxithromycin (ROX), the increased bioaccumulation observed in juvenile carp due to MWCNT presence was attributed to the binding competition of digestive biomolecules at MWCNT surface thus promoting ROX release (Yan et al. 2017). Most studies have concluded that for CNM-contaminant ingested complexes, solubilization and desorption of the contaminants is dependent on the presence and concentration of bile salts (Sun et al., 2013; Yan et al., 2017; Wang et al., 2011; Maldonado-Valderrama et al., 2011). Moreover, though the digestive tract is considered one of the most significant routes of exposure to CNM-adsorbed contaminants, this is highly dependent on the digestive time and residency of CNMs in the organism, which can vary from species to species.

1.3 Polycyclic Aromatic Hydrocarbons: A Model Class of Contaminants

Polycyclic aromatic hydrocarbons (PAHs) are one of the most ubiquitous organic pollutants present in the environment. They are a natural form of creosote and are also formed by the incomplete combustion of organic materials, their presence in the environment is due to natural and anthropogenic sources (Manoli and Samara, 1999). The largest source of PAH emissions are fossil fuels, wildfires, consumer products and oil production (Zhang and Tao, 2009). As semivolatile compounds, a majority are first released into the atmosphere; after atmospheric chemical and physical interactions take place they are deposited in soil and water (Maliszewska-Kordybach, 1999). Although PAHs can be degraded abiotically and biotically, concentrations remain consistent and high in the environment due to continual input (Simpson et al., 1995, Haritash and Kaushik, 2009). Concentrations in the aquatic environment can range from ng/L to as high as mg/L, depending on the compound's water solubility limit and/or the distance from point sources, such as concentrated run off locations (D'Adamo et al 1997; Baumard et al, 1998, Simpson et al., 1995).

Structurally PAHs are planar molecules comprised of two or more fused benzene rings, though can also contain non-aromatic structures like pentacyclic rings or alkyl side chains (Baird and Luch, 2010). Due to the delocalized π electrons on the aromatic rings, the compounds are particularly stable, hydrophobic, and will readily associate with other carbon containing materials in the environment including soil, sediment and colloids (Maliszewska-Kordybach, 1999; Ma et al., 2010). PAHs are also known to have a high adsorption affinity for CNMs, which is largely governed by hydrophobic effects and π - π interactions with the nanomaterial's carbon rings (Yang et al, 2006). Because environmentally released CNMs would likely interact with previously present PAHs, the adsorption relationship between PAHs and CNMs has been well studied. As such, this PAH-CNM adsorption relationship provides a good base from which to investigate how more complex, environmentally relevant conditions may be influential on contaminant-CNM relationships in general.

1.3.1 Exposure and Metabolism

Organismal exposure to PAHs in the aquatic environment can either be through absorbance across the gills or skin, if freely dissolved in the water column, or through ingestion of PAH-contaminated sediment or organic matter (Baumard et al., 1998; Beyer et al, 2010). Similarly, organismal exposure to CNM-adsorbed PAHs largely occurs through ingestion, where PAHs then have the potential to be absorbed across the intestinal tract (Beyer et al., 2010). While acute toxicity can lead to oxidative stress, chronic exposure normally leads to other effects such as lowered immune system, developmental and reproductive alteration, and in some cases mortality (Jen et al., 2011; Lotufom, 1997; de Maagd and Vethaak, 1998). Due to some PAHs or their metabolites being mutagenic and carcinogenic, it is not surprising that a number of them are listed on EPA's priority pollutant list. However, most vertebrates, including fish, efficiently metabolize PAHs in the liver via cytochrome P-450 enzymes (Kannan and Perrotta, 2008). The hydrophilic metabolites are then readily excreted from the body either through the bile or urine

(Beyer et al., 2010). For some small PAHs that are less hydrophobic, the parent compound can be directly excreted without undergoing any biotransformation (Tukikene, 1995). The bioaccumulative potential of PAHs with < 5 rings is considered relatively low in vertebrates due to efficient metabolism, thus biomagnification of PAHs in higher trophic level is not largely observed (Bleeker and Verbuggen, 2009). As such, analysis of tissue concentrations for PAHs are not considered to be well correlated with exposure (Beyer et al., 2010). Instead, the highly fluorescent nature of most PAHs allows PAH exposure to be quantified quickly and easily through fluorescence analysis of urine or bile (Beyer et al., 2010; Aas et al., 2000). Relative fluorescence intensity is directly proportional to PAH concentrations in the bile and water, and has become a standard procedure to assess uptake and bioavailability of PAHs (van der Oost et al., 2003; Aas et al., 2000; Güngördü, 2011). The ease of quantifying PAH exposure and concentration, makes PAHs an ideal class of contaminants to use in this study, to assess the influence of CNM adsorption on bioavailability.

1.4 Motivation and Project Goals

Current published data pertaining to the bioavailability of contaminants adsorbed to CNMs are sparse and sporadic. Studies have used different organisms, different types of CNMs, different organic contaminants, different background solutions and a variety of environmental conditions. Consequently, the comparison of results is difficult and general conclusions cannot be made at this point. Although adsorption behavior is very influential on the associated bioavailability of CNM-adsorbed PAHs (Wang et al., 2011), there is still a gap in understanding how contaminant-CNM interactions influence bioavailability of the adsorbed contaminant. Establishment of a fundamental understanding of the driving mechanisms behind bioavailability of CNM-adsorbed contaminants will significantly improve our ability to predict both environmental fate and biological impacts of CNMs.

The overall research goal of this work was to establish a comprehensive understanding of the key mechanisms influencing bioavailability of CNM-adsorbed organic contaminants. To accomplish this, I utilized a systematic approach to characterize the influence of CNM morphology, contaminant physicochemical properties, and contaminant mixtures on the resulting bioavailability of the adsorbed compounds, where PAHs were selected as a model class of organic contaminants. Focusing on the following specific objectives made this possible.

- 1) *Examine the influence of CNM type on the bioavailability of adsorbed PAHs.* This was achieved by developing adsorption isotherms for naphthalene (NAP), phenanthrene (PHEN), anthracene (ANT) and fluoranthene (FLU) by MWCNTs and exfoliated graphene, followed by quantifying the resulting bioavailability of each PAH to *Pimphales promelas* via bile analysis. Bioavailability was described in the form of a bioavailability index that allowed for direct comparison between the fraction of CNM-adsorbed PAH that was taken up into the bile as a function of adsorption.
- 2) *Determine the relationship between adsorption behavior and resulting bioavailability of CNT-adsorbed PAHs.* Adsorption behavior and the resulting bioavailable fraction of seven different adsorbed PAHs was quantified via adsorption isotherms and bile analysis. Multiple linear regression was used to assess the difference in adsorption affinity and the bioavailable fraction of seven different PAHs when adsorbed to MWCNTs as a function of the compound's physical, chemical and structural characteristics.
 - a. *Develop a predictive model to describe the bioavailability of CNT-adsorbed PAHs.* Generalized linear regression techniques were used to select and estimate the most influential factors controlling the bioavailability of CNT-adsorbed PAHs, where bioavailability was represented by the distribution coefficient of PAHs between MWCNT and bile.

Investigate how bioavailability of CNT-adsorbed PAHs is influenced when PAHs are present in mixtures. Single and bi-solute adsorption isotherms and bioavailability assays were conducted for two distinct PAH pairs, (1) PHEN and ANT and (2) FLU and PYR (pyrene), where the PAHs within each pair were chemically similar yet structurally different. Comparison of the change in adsorption and bioavailability of individual PAHs when present in the mixture provided insight into how competition at the MWCNT surface can alter both adsorption and resulting bioavailability.

1.5 References

- Aas, E.; Beyer, J.; Goksoyr, A. Fixed wavelength fluorescence (FF) of bile as a monitoring tool for polyaromatic hydrocarbon exposure in fish: An evaluation of compound specificity, inner filter effect and signal interpretation. *Biomark.* **2000**, 5 (1), 9-23.
- Andrews, R.; Jacques, D.; Qian, D.; Rantell, T. Multiwalled carbon nanotubes: Synthesis and application. *Acc. Chem. Res.* **2002**, 35, 1008-1017.
- Apul, O.G.; Karanfil, T. Adsorption of synthetic organic contaminants by carbon nanotubes: A critical review. *Water Res.* **2015**, 68, 34-55.
- Apul, O.G.; Shao, T.; Zhang, S.; Karanfil, T. Impact of carbon nanotube morphology on phenanthrene adsorption. *Environ. Tox. Chem.* **2012a**, 31(1), 783-788.
- Apul, O.G.; Wang, O.; Zhou, Y.; Karanfil, T. Adsorption of aromatic organic contaminants by graphene nanosheets: Comparison with carbon nanotubes and activated carbon. *Water. Res.* **2013**, 47, 1648-1654.
- Apul, O.G.; Wang, Q.; Shao, T.; Rieck, J.R.; Karanfil, T. Predictive model development for adsorption of aromatic contaminants by multi-walled carbon nanotubes. *Environ. Sci. Technol.* **2012b**, 47, 2295-2303.
- Arnot, J.A.; Gobas, F.A.P.C. A review of bioconcentration factor (BCF) and bioaccumulation factor (BAF) assessments for organic chemical in aquatic organisms. *Environ. Rev.* **2006**, 14, 257-297.
- Baird, W.M.; Luch, A. *Carcinogenic Polycyclic Aromatic Hydrocarbons.* **2010**; 14.06
- Baumard, P.; Budzinski, H.; Garrigues, P.; Sorbe, J.C.; Burgeot, T.; Bellocq, J. Concentrations of PAHs (polycyclic aromatic hydrocarbons) in various marine organisms in relation to those in sediments and to trophic level. *Mar. Pollut. Bull.* **1998**, 36 (12), 951-960
- Baun, A.; Sorensen, S.N.; Rasmussen, R.F.; Hartmann, N.B.; Koch, C.B. Toxicity and bioaccumulation of xenobiotic organic compounds in the presence of aqueous suspensions of aggregates of nano-C60. *Aquat. Toxicol.* **2008**, 86, 379-387.
- Beyer, J.; Jonsson, G.; Porte, C.; Krahn, M.M.; Ariese, F., Analytical methods for determining metabolites of polycyclic aromatic hydrocarbon (PAH) pollutants in fish bile: a review. *Environ. Toxicol. Pharmacol.* **2010**; 30: 224-244.
- Bisesi, J.H. Jr.; Ngo, T.; Ponnayolu, S.; Liu, K.; Lavelle, C.M.; Afrooz, A.R.M.N.; Saleh, N.B.; Ferguson, P.L.; Denslow, N.D.; Sabo-Attwood, T. Examination of single-walled carbon nanotubes uptake and toxicity from dietary exposure: Tracking movement and impacts in the gastrointestinal tract. *Nanomaterials.* **2015**, 5, 1066-1086.

Bjork, J.; Hanke, F.; Palma, C.; Samori, P.; Cecchini, M.; Persson, M. Adsorption of aromatic and anti-aromatic systems on graphene through π - π stacking. *J. Phys. Chem. Lett.* **2010**, 1, 3407-3412.

Bleeker, E.A.J.; Verbuggen, E.M.J. Bioaccumulation of polycyclic aromatic hydrocarbons in aquatic organisms. *RIVM report 601779002*; National Institute for Public Health and the Environment: Netherlands, **2009**.

Brooks, A.J.; Lim, H-N.; Kilduff, J.E. Adsorption uptake of synthetic organic chemicals by carbon nanotubes and activated carbons. *Nanotech.* **2012**, 23, 294008; doi:10.1088/0957-4484/23/29/294008.

Chen, J.; Chen, W.; Zhu, D. Adsorption of nonionic aromatic compounds to single-walled carbon nanotubes: Effects of aqueous solution chemistry. *Environ. Sci. Technol.* **2008**, 42, 7225-7230.

Chen, Q.; Yin, D.; Hu, X.; Wang, R.; Zhang, C. The effect of nC60 on tissue distribution of ibuprofen in *Cyprinus carpio*. *Sci. Total., Environ.* **2014**, 496, 453-460.

Chen, W.; Duan, L.; Zhu, D. Adsorption of polar and nonpolar chemical to carbon nanotubes. *Environ. Sci. Technol.* **2007**, 41, 8295-8300.

Cui, X.Y.; Jia, F.; Chen, Y.X.; Gan, J. Influence of single-walled carbon nanotubes on microbial availability of phenanthrene in sediment. *Ecotoxicology.* **2011**, 20, 1277-1285.

D'Adamo, R.; Pelosi, S.; Trotta, P.; Sansone, G. Bioaccumulation and biomagnification of polycyclic aromatic hydrocarbons in aquatic organisms. *Mar. Chem.* **1997**, 56, 45-49.

Dai H. Carbon nanotubes: opportunities and challenges. *Surf. Sci.* **2002**, 500, 218-241.

de Maagd, P.G-J.; Vethaak, A.D. Biotransformation of PAHs and their carcinogenic effect in fish. In *The Handbook of Environmental Chemistry*; Neilson, A.H., Ed.; Springer-Verlag: Berlin, Heidelberg, **1998**, 3 (Part J), 266-308.

Dinadayalane, T.C.; Leszczynski, J. Remarkable diversity of carbon-carbon bonds: Structures and properties of fullerene, carbon nanotubes and graphene. *Struct. Chem.* **2010**, 21, 1155-1169.

Edgington, A.J.; Roberts, A.P.; Taylor, L.M.; Alloy, M.M.; Reppert J.; Rao, A.M.; Mao, J.; Klaine, S.J.; The influence of natural organic matter on the toxicity of multiwalled carbon nanotubes. *Environ. Tox. Chem.* **2010**, 29 (11), 2511-2518.

Eijsackers, H.; Van Gestel, C.A.M.; De Jonge, S.; Muijs, B.; Slijkerman, D. Polycyclic aromatic hydrocarbon-polluted dredged peat sediments and earthworms: a mutual inference. *Ecotoxicology.* **2001**, 10, 35-50.

Fang, J.; Shan, X.-q.; Wen, B.; Haung, R. Mobility of TX100 suspended multiwalled carbon nanotubes (MWCNTs) and the facilitated transport of phenanthrene in real soil columns. *Geoderma* **2013**, 207, 1-7.

Ferguson, P.L.; Chandler, G.T.; Templeton, R.C.; Demarco, A.; Scrivens, W.A.; Englehart, B.A. Influence of sediment-amendment with single-walled carbon nanotubes and diesel soot on bioaccumulation of hydrophobic organic contaminants by benthic invertebrates. *Environ. Sci. Technol.* **2008**, 42: 3879-3885.

Gogotosi, Y.; Presser, V. *Carbon nanomaterials*. Taylor & Francis Group, LLC: Boca Raton, Florida, **2014**.

Gotovac, S.; Honda, H.; Hattori, Y.; Takahshi, K.; Kanoh, H.; Kaneko, K. Effect of nanoscale curvature of single-walled carbon nanotubes on adsorption of polycyclic aromatic hydrocarbons. *Nano Lett.* **2007**, 7(3), 583-587.

Gottschalk, F.; Sun, T.; Nowack, B. Environmental concentrations of engineered nanomaterials: Review of modeling and analytical studies. *Environ. Poll.* **2013**, 181, 287-300.

Güngördü, A. Evaluation of PAH metabolites in bile of common Carp, *Cyprinus carpio*, with fixed wavelengths fluorescence in a field and laboratory study. *Polycyclic Aromat. Compd.* **2011**, 31, 84-96.

Haritash, A.P.; Kaushik, C.P. Biodegradation aspects of polycyclic aromatic hydrocarbons (PAHs): a review. *J. Hazard. Mater.* **2009**, 169, 1-15.

Hofmann, T.; von der Kammer, F.. Estimating the relevance of engineered carbonaceous nanoparticle facilitated transport of hydrophobic organic contaminants in porous media. *Environ. Poll.* **2009**, 157, 1117-1126.

Hou, W.C.; Westerhoff, P.; Posner, J.D. Biological accumulation of engineered nanomaterials: A review of current knowledge. *Environ. Sci.: Processes Impacts.* **2013**, 15, 103-122.

Hu, X.; Li, J.; Chen, Q.; Lin, Z.; Yin, D. Combined effects of aqueous suspensions of fullerene and humic acid on the availability of polycyclic aromatic hydrocarbons: Evaluated with negligible depletion solid-phase microextraction. *Sci. Tot. Environ.* **2014**, 498, 12-21.

Hu, X.; Liu, J.; Zhou, Q.; Lu, S.; Liu, R.; Cui, L.; Yin, D.; Mayer, P.; Jiang, G. Bioavailability of organochlorine compounds in aqueous suspensions of fullerene: Evaluated with medaka (*Oryzias latipes*) and negligible depletion solid-phase microextraction. *Chemosphere.* **2010**, 80, 693-700.

Hyung, H.; Fortner, J.D.; Hughes, J.B.; Kim, J.H. Natural organic matter stabilizes carbon nanotubes in the aqueous phase. *Environ. Sci. Technol.* **2007**, 41, 179-184.

Jackson, P.; Jacobsen, N.R.; Baun, A.; Birkedal, R.; Kuhnel, D.; Jensen, K.A.; Vogel, U.; Wallin, H. Bioaccumulation and ecotoxicity of carbon nanotubes. *Chem. Cent. J.* **2013**, 7(154), 1-21.

Jaisi, D.P.; Elimelech, M. Single-walled carbon nanotubes exhibit limited transport in soil columns. *Environ. Sci. Technol.* **2009**, 43 (24), 9161-9166.

Jen, H.A.; Pan, C-H.; Diawara, N.; Chang-Chien, G-P.; Lin, W-Y.; Huang, C-T.; Ho, C-K.; Wu, M-T. Polycyclic aromatic hydrocarbon-induced oxidative stress and lipid peroxidation in relation to immunological alteration. *Occup. Environ. Med.* **2011**, 68, 653-658.

Josko I, Oleszczuk P, Pranagal J, Lehmann J, Xing B, and Cornelissen G. Effect of biochars, activated carbon and multiwalled carbon nanotubes on phytotoxicity of sediment contaminated by inorganic and organic pollutants. *Ecol. Eng.* **2013**, 60, 50-59.

Kah, M.; Zhang, X.; Jonker, M.T.O.; Hofmann, T. Measuring and modeling adsorption of PAHs to carbon nanotubes over a six order of magnitude wide concentration range. *Environ. Sci. Technol.* **2011**, 45 (14), 6011-6017.

Kannan, K.; Perrotta, E. Polycyclic aromatic hydrocarbons (PAHs) in livers of California sea otters. *Chemosphere.* **2008**, 71, 649-655

Keiluweit, M. and Kleber, M. molecular-level interactions in soils and sediments: The role of aromatic π -systems. *Environ. Sci. Technol.* **2009**, 43, 3421-3429.

Kim, K-T.; Edgington, A.J.; Klaine, S.J.; Cho, J-W.; Kim, S.D. Influence of multiwalled carbon nanotubes dispersed in natural organic matter on speciation and bioavailability of copper. *Environ. Sci. Technol.* **2010**, 43, 8979-8984.

Klaine, S.J.; Alvarez, P.J.J.; Batley, G.E.; Fernandes, T.F.; Handy, R.D.; Lyon, D.Y.; Mahendra, S.; McLaughlin, M.J.; Lead, J.R. Nanomaterials in the environment: Behavior, fate, bioavailability and effects. *Environ. Tox. Chem.* **2008**, 27 (9), 1825-1851.

Laurent, C.; Flahaut, E.; Peigney, A. The weight and density of carbon nanotubes verses the number of walls and diameter. *Carbon.* **2010**, 48 (10), 2994-2996.

Li, S.; Turaga, U.; Shrestha, B.; Anderson, T.A.; Tramkumar, S.S.; Green, M.J.; Das, S.; Canas-Carrell, J.E. Mobility of polyaromatic hydrocarbons (PAH) in soil in the presence of carbon nanotubes. *Ecotoxicol. Environ. Saf.* **2013a**, 96, 168-174.

Li, Y.; Niu, J.; Shen, Z.; Feng, C. Size effect of single-walled carbon nanotube on adsorption of perfluorooctanesulfonate. *Chemosphere.* **2013b**, 91, 784-790.

Lin, D.; Lie, N.; Yang, K.; Xing, B.; Wu, F. Different stabilities of multiwalled carbon nanotubes in fresh surface water samples. *Environ. Pollut.* **2010b**, 158, 1270-1274.

Lin, D.; Tian, X.; Wu, F.; Xing, B. Fate and transport of engineered nanomaterials in the environment. *J. of Environ. Qual.* **2010a**, 39(6), 1896-1908.

Linard, E.N.; van den Hurk, P.; Karanfil, T.; Apul, O.G.; Klaine, S.J. Influence of carbon nanotubes on the bioavailability of fluoranthene. *Environ. Tox. Chem.* **2015**, 34(3), 658-666.

Lotufom, G.R. Toxicity of sediment-associated PAHs to an estuarine copepod: Effects on survival, feeding, reproduction and behavior. *Mar. Environ. Res.* **1997**, 44, 146-166.

Lu, C.; Su, F. Adsorption of natural organic matter by carbon nanotubes. *Sep. Purif. Technol.* **2007**, 58, 113-121.

Ma, Y-G.; Lei, Y-D.; Xiao, H.; Wania, F.; Wang, W-H. Critical review and recommended values for the physical-chemical property data of 15 polycyclic aromatic hydrocarbons at 25°C. *J. Chem. Eng. Data.* **2010**, 55(2) 819-825.

Maldonado-Valderrama, J.; Wilde, P.; Macierzanka, A.; Mackie, A. The role of bile salts in digestion. *Adv. Colloid Interface Sci.* **2011**, 165, 36-46.

Maliszewska-Kordybach, B. Sources, concentrations, fate and effects of polycyclic aromatic hydrocarbons (PAHs) in the environment. Part A: PAHs in Air. *Pol. J. Environ. Stud.* **1999**, 8, 131-136.

Manoli, E.; Samara, C. Polycyclic aromatic hydrocarbons in natural waters: Sources, occurrences, analysis. *Trends Anal. Chem.* **1999**, 18, 417-428.

Martinez, C. R.; Iverson, B.I. Rethinking the term “pi-stacking”. *Chem. Sci.* **2012**, 3, 2191-2201.

Mauter, M.S.; Elimelech, M. Critical review: Environmental applications of carbon-based nanomaterials. *Environ. Sci. Technol.* **2008**, 42 (16), 5843-5859.

Mueller, N.C.; Nowack, B. Exposure modeling of engineered nanoparticles in the environment. *Environ. Sci. Technol.* **2008**, 42, 4447-4453.

Myers, M.H.; Henderson, M.; Black, M.C. Effects of multiwalled carbon nanotubes on the bioavailability and toxicity of diphenhydramine to *Pimephales promelas* in sediment exposures. *Environ. Tox. Chem.* **2016**, 36 (2), 320-328.

Nowack, B.; Ranville, J.F.; Diamond, S.; Gallego-Urrea, J.A.; Metcalfe, C.; Rose, J.; Horne, N.; Koelmans, A.A.; Klaine, S.J. Potential scenarios for nanomaterial release and subsequent alteration in the environment. *Environ. Tox. Chem.* **2012**, 31, 50-59.

Oleszczuk, P.; Pan, B.; Xing, B. Adsorption and desorption of oxytetracycline and carbamazepine by multiwalled carbon nanotubes. *Environ. Sci. Technol.* **2009**, 43, 967-9173.

Pan, B.; Xing, B. Critical review: Adsorption of organic chemicals on carbon nanotubes. *Environ. Sci. Technol.* **2008**, 42(24), 9005-9013.

Parks, A.N.; Chandler, G.T.; Portis, L.M.; Sullivan, J.C.; Perron, M.M.; Cantwell, M.G.; Burgess, R.M.; Ho, K.T.; Ferguson, P.L. Effects of single-walled carbon nanotubes on the bioavailability of PCBs in field-contaminated sediments. *Nanotoxicology*. **2013**, 1-7.

Peterson, E.J.; Henry, T.B. Methodological considerations for testing the ecotoxicity of carbon nanotubes and fullerenes: Review. *Environ. Tox. Chem.* **2012**, 31(1), 60-72.

Peterson, E.J.; Zhang, L.; Mattison, N.T.; O'Carroll, D.M.; Whelton, A.J.; Uddin, N.; Nguyen, T.; Huang, Q.; Henry, T.B.; Holbrook, R.D.; Chen, K.L. Potential release pathways, environmental fate, and ecological risks of carbon nanotubes. **2011**, *Environ. Sci. Technol.*, 45, 9837-9856.

Qiang, L.; Chen, M.; Zhu, L.; Wu, W.; Wang, Q. Facilitated bioaccumulation of perfluorooctanesulfonate in common carp (*Cyprinus carpio*) by graphene oxide and remission mechanism of fulvic acid. *Environ. Sci. Technol.* **2016**, 50, 11627-11636.

Radovic, L.R.; Bockrath, B. On the chemical nature of graphene edges: Origins of stability and potential magnetism in carbon materials. *J. Am. Chem. Soc.* **2005**, 127, 5917-5927.

Rajesh, C.; Majumder, C.; Mizuseki, H.; Kawazoe, Y. A theoretical study on the interaction of aromatic amino acids with graphene and single walled carbon nanotubes. *J. Chem. Phys.* **2009**, 130, 124911; doi: 10.1063/1.3079096.

Ren, X.; Chen, C.; Nagatsu, M.; Wang, X. Carbon nanotubes as adsorbents in environmental pollution management: A review. *Chem. Eng. J.* **2011**, 170, 295-410.

Riding, M.J.; Martin, F.L.; Jones, K.C.; Semple, K.T. Carbon nanomaterials in clean and contaminated soils: Environmental implications and applications. *Soil*. **2015**, 1, 1-21.

Schwarzenbach, R.P.; Gschwend, P.M.; Imboden, D.M. *Environmental Organic Chemistry*; A John Wiley & Sons, Inc. publication: Hoboken, New Jersey, **2003**.

Schwyzer, I.; Kegi, R.; Sigg, L.; Magrez, A.; Nowack, B. 2011. Influence of the initial state of carbon nanotubes on their colloidal stability under natural conditions. *Environ. Poll.* **2011**, 159, 1641-1648.

Scida, K.; Stege, P.W.; Haby, G.; Messina, G.A.; Garcia, C.D. Recent applications of carbon-based nanomaterials in analytical chemistry: Critical review. *Analytica Chimica Acta*. **2011**, 691, 6-17.

Shen, M.; Xia, X.; Zhai, Y.; Zhang, X.; Zhao, X.; Zhang, P. Influence of carbon nanotubes with preloaded and coexisting dissolved organic matter on the bioaccumulation of polycyclic aromatic hydrocarbons to *Chironomus plumosus* larvae in sediment. *Environ. Tox. Chem.* **2013**, 33(1), 1-8.

Simpson, C.D.; Mosi, A.A.; Cullen, W.R.; Reimer, K.J. Composition and distribution of polycyclic aromatic hydrocarbon contamination in surficial marine sediments from Kitimat Harbor, Canada. *Sci. Total Environ.* **1996**, 181, 265-278

Stankovich, S.; Dikin, D.A.; Piner, R.D.; Kohlhaas, K.M.; Kleinhammes, A.; Jia, Y.; Wu, Y.; Nguyen, S.T.; Ruoff, R.S. Synthesis of graphene-based nanosheets via chemical reduction of exfoliated graphite oxide. *Carbon*. **2007**, 45, 1558-1565.

Su, Y.; Yan, X.; Pu, Y.; Xiao, F.; Wang, D.; Yang, M. Risks of single-walled carbon nanotubes acting as contaminant-carriers: Potential release of phenanthrene in Japanese Medaka (*Oryzias latipes*). *Environ. Sci. Technol.* **2013**, 47, 4704-4710.

Sun, H.; Ruan, Y.; Zhu, H.; Zhang, Z.; Yu, L. Enhanced bioaccumulation of pentachlorophenol in carp in the presence of multi-walled carbon nanotubes. *Environ. Sci. Pollut. Res.* **2013b**, 21 (4): 2865-2875.

Sun, Y.; Yang, S.; Zhao, G.; Wang, Q.; Wang, X. Adsorption of polycyclic aromatic hydrocarbons on graphene oxides and reduced graphene oxides. *Chem. Asian. J.* **2013a**, 8, 2755-2761.

Tachikawa, H.; Kawabata, H. Electronic states of defect sites of graphene model compounds: A DFT and direct molecular orbital-molecular dynamics study. *J. Phys. Chem. C*. **2009**, 113, 7603-7609.

Tournus, F.; Charlier, J.C. Ab initio study of benzene adsorption on carbon nanotubes. *Phys. Rev. B*. **2005**, 71, 165421; DOI: 10.1103/PhysRevB.71.165421.

Tournus, F.; Latil, S.; Heggie, M.I.; Charlier, J.C. Pi-stacking interaction between carbon nanotubes and organic molecules. *Phys. Rev. B*, **2005**, 72, 75431-75436.

Towell, M.G.; Browne, L.A.; Paton, G.I.; Semple, K.T. Impact of carbon nanomaterials on the behavior of ¹⁴C-phenanthrene and ¹⁴C-benzo-[a] pyrene in soil. *Environ. Pollut.* **2011**, 159, 706-715.

Tukikene, A. Responses of fish to polycyclic aromatic hydrocarbons (PAHs). *Ann. Zool. Fennici*. **1995**, 32(3), 295-309.

Turco, R.F.; Bischoff, M.; Tong, Z.H.; Nies, L. Environmental implications of nanomaterials: are we studying the right thing? *Biotechnol.* **2011**, 22, 527-532.

van der Oost, R.; Beyer, J.; Vermeulen, N.P.E. Fish bioaccumulation and biomarkers in environmental risk assessment: A review. *Environ. Toxicol. Pharmacol.* **2003**, 13, 57-149.

Velzebor, I.; Peeters, E.T.H.M.; Koelmans, A.A. Multiwalled carbon nanotubes at the environmentally relevant concentrations affect the composition of benthic communities. *Environ. Sci. Technol.* **2013**, 47, 7475-7482.

von der Kammer, F.; Ferguson, P.L.; Holden, P.A.; Masion, A.; Rogers, K.R.; Klaine, S.J.; Koelmans, A.A.; Horne, N.; Unrine, J.M. Analysis of engineered nanomaterials in complex matrices (environment and biota): General considerations and conceptual case studies. *Environ. Tox. Chem.* **2012**, 31, 31-49.

Wang, J.; Chen, Z.; Chen, B. Adsorption of polycyclic aromatic hydrocarbons by graphene and graphene oxide nanosheets. *Environ. Sci. Technol.* **2014**, 48, 4817-4825.

Wang, L.; Forner, J.D.; Hou, L.; Zhang, C.; Kan, A.T.; Tomson, M.B.; Chen, W. Contaminant-mobilizing capability of fullerene nanoparticle (nC60): Effect of solvent-exchange process in nC60 formation. *Environ. Tox and Chem.* **2012**, 32(2), 329-336.

Wang, X, Lu J, and Xing B. Sorption of organic contaminants by carbon nanotubes: Influence of adsorbed organic matter. *Environ. Sci. Technol.* **2008**, 42, 3207-3212.

Wang, X, Tao S, and Xing B. Sorption and competition of aromatic compounds and humic acid on multiwalled carbon nanotubes. *Environ. Sci. Technol.* **2009**, 43, 6214-6219.

Wang, Z.; Zhao, J.; Song, L.; Mashayekhi, H.; Chefetz, B.; Xing, B. Adsorption and desorption of phenanthrene on carbon nanotubes in simulated gastrointestinal fluids. *Environ. Sci. Technol.* **2011**, 45, 6018-6024.

Xia, X.; Chen, X.; Zhao, X.; Chen, H.; Shen, M. Effects of carbon nanotubes, chars, and ash on bioaccumulation of perfluorochemicals by *Chironomus plumosus* larvae in sediment. *Environ. Sci. Technol.* **2012**, 46, 12467-12475.

Xia, X.; Zhou, C.; Huang, J.; Wang, R.; Xia, N. Mineralization of phenanthrene sorbed on multiwalled carbon nanotubes. *Environ. Tox. Chem.* **2013**, 32, 894-901.

Xia, X-R.; Monteiro-Riviere, N.A.; Riviere, J.E. An index for characterization of nanomaterials in biological systems. *Nat. Nanotechnol.* **2010**, 5, 671-675.

Yan., Z.; Lu, G.; Sun, H.; Ma, B. Influence of multiwalled carbon nanotubes on the effects of roxithromycin in crucian carp (*Carassius auratus*) in the presence of natural organic matter. *Chemosphere.* **2017**, 178, 165-172.

Yang, K.; Xing, B. Adsorption of organic compounds by carbon nanomaterials in aqueous phase: Polyani Theory and its application. *Chem. Rev.* **2010**, 110, 5989-6008.

Yang, K.; Zhu, L.; Xing, B. Adsorption of polycyclic aromatic hydrocarbons by carbon nanomaterials. *Environ. Sci. Technol.* **2006**, 40, 1855-1861.

Zhang, L.; Wang, L.; Zhang, P.; Kan, A.T.; Chen, W.; Tomson, M.B. Facilitated transport of 2,2',5,5'-Polychlorinated Biphenyl and phenanthrene by fullerene nanoparticles through sandy soil columns. *Environ. Sci. Technol.* **2011a**, 45, 1341-1348.

Zhang S, Shao T, and Karanfil T. The effects of dissolved natural organic matter on the adsorption of synthetic organic chemicals by activated carbons and carbon nanotubes. *Water Res.* **2011b**, 45, 1378-1386.

Zhang, S.; Shao, T.; Bekargolu, S.S.K.; Karanfil, T. The impacts of aggregation and surface chemistry on carbon nanotubes on the adsorption of synthetic organic contaminants. *Environ. Sci. Technol.* **2009**, 43, 5719-5725.

Zhang, W.; Wang, C.; Li, Z.; Lu, Z.; Li, Y.; Yin, J.; Zhou, Y.; Gao, X.; Fang, Y.; Nie, G.; Zhao, Y. Unraveling stress-induced toxicity properties of graphene oxide and the underlying mechanism. *Adv. Mater.* **2012**, 24, 5391–5397.

Zhang, Y.; Tao, S. Global atmospheric emission inventory of polycyclic aromatic hydrocarbons (PAHs) for 2004. *Atmos. Environ.* **2009**, 43, 812-819.

Zhao, J.; Wang, Z.; White, J.C.; Xing, B. Graphene in the aquatic environment: Adsorption, dispersion, toxicity, and transformation. *Environ. Sci. Technol.* **2014a**, 48, 9995-10009.

Zhao, J.; Wang, Z.; Zhao, Q.; Xing, B. Adsorption of phenanthrene on multilayer graphene as affected by surfactant and exfoliation. *Environ. Sci. Technol.* **2014b**, 48, 331-339.

Zhou, W.; Shan, J.; Jiang, B.; Wang, L.; Feng, J.; Guo, H.; Ji, R. Inhibitory effects of carbon nanotubes on the degradation of 14C-2,4-dichlorophenol in soil. *Chemosphere.* **2013**, 90, 527-534.

Zhu, D.; Pignatello, J.J. Characterization of aromatic compound sorptive interactions with black carbon (charcoal) assisted by graphite as a model. *Environ. Sci. Technol.* **2005**, 39, 2033-2041.

Zindler, F.; Glomstad, B.; Altin, D.; Liu, J.; Jenssen, B.M.; Booth, A.M. Phenanthrene bioavailability and toxicity to *Daphnia magna* in the presence of carbon nanotubes with different physicochemical properties. *Environ. Sci. Technol.* **2016**, 50, 12446-12454.

CHAPTER TWO

BIOAVAILABILITY OF CARBON NANOMATERIAL-ADSORBED POLYCYCLIC AROMATIC HYDROCARBONS TO *PIMPHALES PROMELAS*: INFLUENCE OF ADSORABTE MOLECULAR SIZE AND CONFIGURATION

2.1 Introduction

Among the numerous applications for carbon nanomaterials (CNMs), CNMs' high adsorption affinity for organic contaminants (OCs) has led to increasing interest in such materials for pollution remediation (Apul and Karanfil, 2015; Ren et al., 2011). However, due to CNMs' unique physicochemical characteristics, they interact with OCs in a distinctly different way than natural colloids. Considerable uncertainty exists pertaining to CNMs' potential to facilitate transport of adsorbed contaminants and likewise alter bioavailability of adsorbed contaminants in the environment (Zhang et al., 2011; Hofmann and von der Kammer, 2009; Baun et al., 2008; Klaine et al., 2008). Adsorption capacity and rate of desorption from CNMs are considered the most influential properties driving contaminant transport and likely influence bioavailability of CNM-adsorbed molecules (Hofmann and von der Kammer, 2009; Wang et al., 2011).

Several studies have found that CNM type and OC properties significantly impact bioavailability of CNM-adsorbed contaminants, though findings are not conclusive (Wang et al., 2011; Towell et al., 2011; Xia et al., 2012). Xia et al. (2012) found the bioaccumulation of aliphatic perfluorochemicals (PFCs) in *C. plumosus* was mainly driven by PFC structure rather than type of CNM. Similarly, the bioavailability and toxicity of phenanthrene adsorbed to five different types of carbon nanotubes (CNTs) in *D. magna* was not significantly different despite differences in CNTs' surface area, functionalization and diameter (Zindler et al., 2016). Conversely, studies have observed phenanthrene to become more bioaccessible as CNMs surface

curvature decreases and with increased dispersion (Wang et al., 2011; Xia et al., 2012; Su et al., 2013; Apul et al., 2012a). The bioaccumulation of several classes of aromatic OCs, including polycyclic aromatic hydrocarbons (PAHs), polychlorinated biphenyls (PCBs), and polybrominated diphenyl ethers (PBDEs) in benthic invertebrates was more effectively moderated when sediment was amended with CNTs than black soot; this was attributed to higher adsorption affinity for OCs by CNTs (Ferguson et al., 2008). Although without inclusion of adsorption data it was not possible to discern how carbonaceous material type contributed to differences in OC bioaccumulation. While the bioavailable fraction of CNM-adsorbed contaminants is often assumed to be directly related to the un-adsorbed OC concentration in the system, bioaccumulation enhancement of diuron and ionizable pentachlorophenol indicates this may not necessarily be the case (Schwab et al. 2012; Sun et al. 2013a). By examining how OC-CNM interactions and adsorption behavior is linked with resulting bioavailability of the adsorbed contaminant, a more holistic understanding of how CNMs may act as a “contaminant carrier” can be established.

Although CNTs are essentially graphene sheets rolled into tubes and graphene has become increasingly popular, few studies exist investigating the influence of graphene on bioavailability of adsorbed contaminants. Adsorption of OCs by graphene and CNTs is largely driven by hydrophobic forces and π - π bonding (Chen et al., 2007; Zhao et al., 2014), but due to different interactions with adsorbates, graphene and CNTs can have different adsorption mechanisms (Apul et al., 2013; Wang et al., 2014). To the best of our knowledge, no study exists examining how such differences in adsorption interactions of graphene and CNTs may differentially affect bioavailability of adsorbed contaminants. Therefore, the main objectives of this study were to (i) compare adsorption of four OCs by exfoliated graphene (GN) and multi-walled carbon nanotubes (MWCNTs), (ii) investigate the role of OC physicochemical characteristics on adsorption interaction differences between the two materials, and (iii) compare

the impact of GN and MWCNT on OC bioavailability to *Pimphales promelas* as a function of adsorption behavior, in environmentally relevant conditions. PAHs were selected as a model class of OCs for this study because they are ubiquitous in the environment, on the EPAs priority pollutant list, and have a wide range of physicochemical properties.

2.2 Materials and Methods

2.2.1 Chemicals and Particles

Four polycyclic aromatic hydrocarbons (PAHs) were used in this study: naphthalene (NAP), 99+% purity, from Alfa Aesar; phenanthrene (PHEN), 97% purity, and anthracene (ANT), 99% purity from ACROS Organics; and fluoranthene (FLU), 98% purity, from ULTRA Scientific. Physicochemical properties of PAHs are presented in Appendix A (Table A1). Stock solutions were prepared in HPLC grade methanol. Multi-walled carbon nanotubes (MWCNTs) were purchased from Nanostructured & Amorphous Materials (Houston, TX) and mechanically exfoliated graphene (GN) was prepared at Clemson University. Suwannee River natural organic matter (NOM) collected from near the Suwannee River Visitor's Center (Fargo, GA) had a dissolved organic carbon concentration of 64 mg C/L, determined using a Shimadzu total organic carbon analyzer and had a specific ultraviolet absorbance ($SUVA_{254}$) value of $4.08 \text{ L mg}^{-1}\text{m}^{-1}$. All solutions were prepared in moderately hard water following the U.S. Environmental Protection Agency standard recipe; 96 mg/L NaHCO_3 , 60 mg/L CaSO_4 , 60 mg/L MgSO_4 , 4 mg/L KCl in 18 mega-ohm Millipore Milli-Q water.

2.2.2 CNM Characterization

Manufacturer, Nanostructured & Amorphous Materials (Houston, TX), supplied the outer diameter (25nm), length (5-30 μm) and purity ($> 95\%$) of the purchased multi-walled carbon nanotubes (MWCNTs). Mechanically exfoliated graphene was prepared at Clemson University. Morphological characteristics, i.e. diameter, length, and thickness, were verified or determined via transmission electron microscopy (Hitachi HD-9500 or H-7600) in conjunction with image

analysis software (Image Pro) and are summarized in Appendix B (Table B1; Figure B1). Structural and electronic properties of MWCNT and GN were also assessed using Raman spectroscopy (Figure B2). Nitrogen adsorption of the CNMs was performed with a physisorption analyzer (Micromeritics) at 77K after CNM adsorption of dissolved organic carbon, as all experiments conducted in this work were done in the presence of 2 mg C/L natural organic matter. Surface area, pore volume and pore size distribution of the CNMs were calculated from the nitrogen adsorption isotherms with the use of the Brunaur-Emmett-Teller (BET) equation, the Barrett-Joyner-Halendea (BJH) equation, and the density functional theory model (DFT), respectively (Zhang et al. 2009).

2.2.3 Suspension of CNM

Pristine MWCNTs and GN were suspended in 2 mg C/L NOM at a concentration of 10 mg/L following previously published methods (Linard et al., 2015). CNMs were sonicated for 1 hour at 60 watts using a 0.5 microtip affixed Branson model 450 digital sonifier. Mass based calibration curves of MWCNTs and GN in solution are supplied in Appendix B (Figure B3); concentration was measured via visible light absorbance at 800 and 660 nm for MWCNT and GN solutions respectively, using a Molecular Devices Spectramax 190 microplate spectrophotometer (Hyung and Kim, 2008; Lotya et al. 2008). CNM solutions were diluted to ~1.5 mg/L in 2 mg C/L NOM background solution for all adsorption and bioavailability assays. Absorbance measurements of CNM solutions at beginning and end of each experiment showed little change in concentration, indicating a stable solution.

2.2.4 Adsorption Isotherms

Adsorption experiments were run in triplicate following the batch approach previously published (Linard et al., 2015). Briefly, 10 mL glass centrifuge tubes containing either 1.5 mg/L MWCNT or GN suspension were spiked with each PAH individually, sealed with aluminum-foil-lined Teflon screw caps and allowed to come to equilibrium on a rotary tumbler at room

temperature ($25^{\circ}\text{C} \pm 1^{\circ}\text{C}$) for 96 hours (preliminary tests showed that equilibrium was reached within 48 hours). PAH stock solutions used to spike experimental vials were prepared so that the volume percentage of methanol was 0.1% to avoid co-solvent effects. Initial PAH concentrations of NAP, PHEN, ANT and FLU ranged from 5-1000, 5-400, 0.25-40, and 1-200 $\mu\text{g/L}$, respectively. Vials without CNMs were identically prepared to serve as positive controls; controls for the entire system were spiked with methanol only. A combination of centrifugation and fluorescence quenching techniques were used to quantify the un-adsorbed PAH concentration in the system. After equilibrium was reached vials with and without CNM were centrifuged (Eppendorf 5804 R) at $\sim 1500 \times g$ for 1 hour to sediment any CNM agglomerates that may have formed during tumbling. The remaining supernatant was analyzed in black polystyrene 96-well plates with Molecular Devices Gemini fluorescence microplate reader at excitation/emission wavelengths 276/330, 252/399, 250/363, and 280/440 for NAP, ANT, PHEN and FLU respectively. PAHs act as π -donors when interacting with graphitic materials and when adsorbed no longer are in an excited state. Therefore, fluorescence of CNM-adsorbed PAHs is statically quenched and the remaining unbound PAH concentration in the aqueous solution could be determined via fluorescence intensity (Singh et al. 2011; Debnath et al. 2010; Kukkonen and Pellinen, 1994). Analysis of a methanol rinse of positive control vials showed minimal loss of PAHs due to sorption to vial walls. CNM sorption of all PAHs was calculated as differences in aqueous PAH concentration between positive controls and CNM samples using fluorescent standard curves developed for each PAH in the background solution containing 2 mg C/L NOM. Temperature, pH, and ionic strength were controlled across each experiment and reflected minimal change.

Experimental data was log-transformed and fit with the Freundlich model where q_e represents the solid-phase concentration of the PAH adsorbed to CNM (mg PAH /g CNM) and C_e is the equilibrium aqueous phase concentration of the PAH (mg/L).

Freundlich model (FM):

$$q_e = K_f C_e^n \quad (2.1)$$

where K_f ((mg PAH/ g CNM)/(mg PAH/L)), the Freundlich constant, reflects adsorption capacity of the CNM for the specific PAH and the dimensionless Freundlich exponent n is an indicator of surface heterogeneity and adsorption intensity. The goodness of model fit was analyzed by the correlation coefficients (R^2) and residual root mean square error (RMSE).

2.2.5 Organismal Care

Pimphales promelas (fathead minnows), the standard test organism recommended for toxicity testing by the EPA, were cultured at the Clemson University Institute of Environmental Toxicology (CU-ENTOX) in a recirculating system with a water turnover rate of 3-4 times a day (hardness = 100-120 mg/L as CaCO_3 ; alkalinity = 40-60 mg/L as CaCO_3 ; pH = 7.5-8.0). Temperature was maintained at $25^\circ\text{C} \pm 1^\circ\text{C}$ with a 16/8 h light/dark photoperiod and fish were fed a Tetramin mix to satiation daily during culturing and acclimatizing periods. Mature fish that were greater than or equal to 1 g wet weight were transferred to Clemson Cherry Farm Fish Facility for acclimatization and experiments. Water at the Cherry Farm Fish Facility was supplied by Lake Hartwell (SC) via a flow-through system where water was sand filtered and UV sterilized.

To minimize the effect of feeding on bile release during exposures, test organisms were starved for the 24 h leading up to exposures and starved throughout the duration of exposures (Vuorinen et al., 2006; Linard et al. 2015). As exposures were static and non-aerated, *P. promelas* were stocked below 1 g biomass/L in solution and full water changes were made every 4 hours. Water quality and fish behavior was monitored throughout the duration of the experiment. Mortality was rare (<5%) and random across all treatments and controls, indicating that concentrations of neither CNMs nor PAHs used during this study were at a level to cause an adverse effect on organisms. All exposures were prepared using a background solution

consisting of moderately hard water containing 2 mg C/L NOM (hardness = 100 mg/L as CaCO_3 ; alkalinity = 60 mg/L as CaCO_3 ; pH = 8.0).

2.2.6 Bioavailability Assays

All exposures were conducted for 16 h in static, non-aerated conditions with full water renewals every 4 h. Assays for the influence of MWCNT and GN on PAH bioavailability to *P. promelas* were replicated four times where each aquarium was stocked with ~4 fish per treatment. Response of fish from each aquarium were pooled to represent a single measurement unit per treatment per replicate. The prepared treatments for each PAH were 1) *control*, consisting of background solution only; 2) *PAH only*, a positive control consisting of PAH-spiked background solution (i.e. 10 $\mu\text{g/L}$ of NAP, PHEN and FLU; 5 $\mu\text{g/L}$ of ANT); and 3) *PAH and CNM*, consisting of the same PAH-spiked background solution with either ~1.5 mg/L of suspended MWCNT or GN. Solutions for each treatment were tumbled in 4L amber glass containers on a rotary tumbler to reach equilibrium prior to fish exposure. Water samples from each exposure were collected at the beginning and end of each water renewal; analysis of water samples verified the treatment PAH concentrations throughout duration of the exposure. At the end of each exposure, fish were euthanized, the gallbladder harvested, and the collected bile analyzed for PAH metabolites to determine the bioavailable fraction of PAH in the system.

Bioavailability is defined as the total amount of PAH that is taken up by the organism from the system and biotransformed (Arnot and Gobas, 2006; Torreiro-Melo et al 2014); including aqueous and CNM-adsorbed PAH exposure. PAHs taken up by fish are quickly biotransformed into water-soluble metabolites in the liver and concentrated in the gallbladder for later excretion (Beyer et al. 2010). Dose-response relationships, shown in Appendix C, had a linear correlation between PAH exposure and bile fluorescence intensity (Figure C1); therefore, change in bile fluorescence was directly related to change in PAH bioavailability. Extracted bile was diluted, vortexed, and centrifuged. The supernatant was analyzed via fixed wavelength

fluorescence (FF) analysis at discrete excitation and emission wavelength pairs for each PAH (Beyer et al., 2010; Aas et al 2000). PHEN, ANT, and FLU metabolites were detected using a Molecular Devices Gemini fluorescence microplate reader at excitation/emission wavelengths of 250/363, 252/399, and 280/440 nm, respectively; NAP metabolites were detected via HPLC with a UV-fluorescence detector 276/330 nm.

2.2.7 Bile Analysis

After an exposure and fish were euthanized, harvested *P. promelas* gallbladders were stored in amber microcentrifuge tubes in a -80°C freezer until processed. Bile was drained from defrosted gallbladders, diluted to 1:15 with 150 µl of Millipore Milli-Q water, vortexed and then centrifuged for 2 mins at 14000 rpm. An aliquot of each bile sample was further diluted with 50:50 MeOH: H₂O solution to an overall dilution of 1:50 for fish exposed to ANT and FLU and to an overall dilution of 1:200 for fish exposed to PHEN. Fluorescence of ANT, FLU and PHEN metabolites were analyzed in a black 96-well plate using a Molecular Devices Gemini fluorescence microplate reader at excitation/emission wavelengths of 252/399, 280/440, and 250/363, respectively. Due to the background fluorescence of various components in the bile occurring at similar excitation/emission wavelengths used to detect NAP metabolites, bile samples from NAP exposures were analyzed via an HPLC with a UV-fluorescence detector. NAP bile samples were similarly processed with the following changes: bile was initially diluted to 1:5 with 50 µl of Millipore Milli-Q water; after vortex and centrifugation same as previously described, bile was diluted with 360 µl MeOH to an overall dilution of 1:50. Excitation/ emission wavelengths were 276/330 nm with peaks appearing at 9-10mins. For all bile samples, an aliquot of 25 µl of bile sample was collected for a protein assay after the first initial dilution with Millipore Milli-Q water. The Pierce™ bicinchoninic acid (BCA) protein assay was used to determine total protein content in all bile samples using a Molecular Devices Spectramax 190 UV microplate reader to measure absorbance at 562 nm of the samples and a bovine serum

albumin (BSA) standard curve. Protein content in fish bile can give indications of the state of the individuals' health and is commonly used for bile fluorescence normalization if the organisms feeding history is unknown (Vuorinen et al., 2006). Distribution of total protein content from all individual fish had a normal distribution, suggesting good health in all fish used. Further, protein normalization of bile fluorescence data did not adequately reduce the coefficient of variance and or explain the normality and variance issues observed in the data set. For these reasons and considering that the feeding states of the test organisms were controlled, bile fluorescence data were presented without protein normalization, similar to previously published work (Linard et al., 2015).

2.2.8 Statistical Analysis

JMP Pro 12 software, SAS Institute Inc., was used to perform all statistical tests. Adsorption isotherms were fit with the non-linear Freundlich model. Multiple regression was used to assess and compare the influence of PAH physicochemical characteristics on adsorption of PAHs by CNMs. Linear regression and correlation coefficients (R^2) were used to assess goodness of fit of predicted fish responses to actual response in fish exposures and CNM bioavailability assays. Analysis of variance (ANOVA) followed by Student's T test was used to compare the response of fish across all treatments for a single PAH; linear squared contrasts were used to compare differences between treatments across the different PAHs. Two-tailed mean hypothesis testing was used to determine whether bioavailability indices differed from 1 for each PAH-CNM combination. Student's T test was used to compare bioavailability indices to one another across all PAHs. Shapiro-Wilk's test was used to test normality of bile fluorescence residuals; Brown and Forsythe test was used to test homogeneity of variance within treatments. Unless otherwise denoted, the significance level of all tests was set at 0.05.

2.3 Results and Discussion

2.3.1 Influence of CNM Type on Adsorption

Adsorption isotherms of PAHs by MWCNT and GN in the presence of 2 mg C/L NOM on a mass and surface basis are represented in Figure 2.1 with the corresponding Freundlich parameters in Table 2.1. Following methods by Zhu et al. (2005), adsorption (q_e) of the PAHs by GN was plotted against the adsorption of the PAHs by MWCNT at the same experimental concentration to form a distribution curve (Figure 2.2). To help conceptualize differences in GN/MWCNT distribution among the four PAHs, lines at 0.33, 1 and 3 are provided on Figure 2.2 to represent GN/MWCNT distribution coefficients ($K_{GN/MWCNT}$) where $q_{GN} = 0.33 q_{MWCNT}$, $q_{GN} = q_{MWCNT}$, or $q_{GN} = 3q_{MWCNT}$, respectively. On a mass basis, distribution coefficients of PHEN and FLU fall along 0.33 distribution line (Figure 2.2 [A]) though NAP and ANT fall closer to the distribution line equal to one. Further comparison of the Freundlich K_F values confirms that MWCNT adsorption capacity for FLU and PHEN was significantly greater (p-value <0.0001) than that of GN; adsorption of ANT and NAP by the two adsorbents was not significantly different (Table 2.1). Except for FLU, normalization of the adsorption isotherms by CNM surface area did not collapse the isotherms onto the distribution line equaling one. Instead, GN appeared to adsorb NAP, PHEN and ANT three times greater than MWCNT (Figure 2.2 [B]). This may be due to greater π - π interactions between PAHs' aromatic rings and the flat surface of GN compared with MWCNTs' curved surface. Several studies have suggested that surface curvature affects the stacking arrangement of adsorbates and causes a lower binding energy (Rajesh et al., 2009; Tournus et al., 2005; Apul et al., 2012a; Dindayalane and Leszczynski, 2010). Interestingly, it has also been observed that the presence of a non-aromatic ring, as in FLU, can hinder molecules contact with a flat graphitic surface leading to weaker binding (Bjork et al., 2010).

Table 2.1. Freundlich isotherm model parameters for adsorption of PAHs by GN and MWCNTs in the presence of NOM.

<i>Compound</i> <i>d</i>	<i>Adsorbent</i> <i>t</i>	K_F (95% CI) (mg/g)/(mg/L) <i>n</i>	$K_{F,SSA}$ (95% CI) (mg/m ²)/(mg/L) <i>n</i>	<i>n</i> (95% CI)	RMSE	<i>R</i> ²
NAP	GN	43.4 (40.0-46.8)	2547.0 (2346.8-2750.0)	0.71 (0.61-0.83)	0.174	0.986
NAP	MWCNT	53.6 (48.4-58.9)	529.3 (478.1-581.5)	0.84 (0.69-1.04)	0.297	0.947
PHEN	GN	16.8 (12.1-23.1)	985.6 (709.6-1353.4)	0.49 (0.34-0.67)	0.228	0.938
PHEN	MWCNT	49.6 (36.6-68.7)	490.3 (361.1-678.7)	0.56 (0.42-0.74)	0.163	0.973
ANT	GN	47.2 (24.7-103.3)	2768.6 (1451.3-6062.6)	0.64 (0.49-0.83)	0.219	0.974
ANT	MWCNT	48.1 (25.3-101.1)	475.4 (248.2-998.4)	0.52 (0.38-0.69)	0.265	0.972
FLU	GN	30.3 (24.3-38.7)	1776.9 (1417.1-2269.7)	0.49 (0.41-0.59)	0.088	0.993
FLU	MWCNT	88.5 (63.5-124.1)	874.0 (627.5-1225.5)	0.40 (0.30-0.51)	0.263	0.957

NAP = naphthalene; PHEN = phenanthrene; ANT = anthracene; FLU = fluoranthene; GN= exfoliated graphene; MWCNT = multiwalled carbon nanotube; CI = confidence interval; SSA = specific surface area; $K_{F,SSA}$ = K_F normalized to specific surface area; RMSE = root mean square error

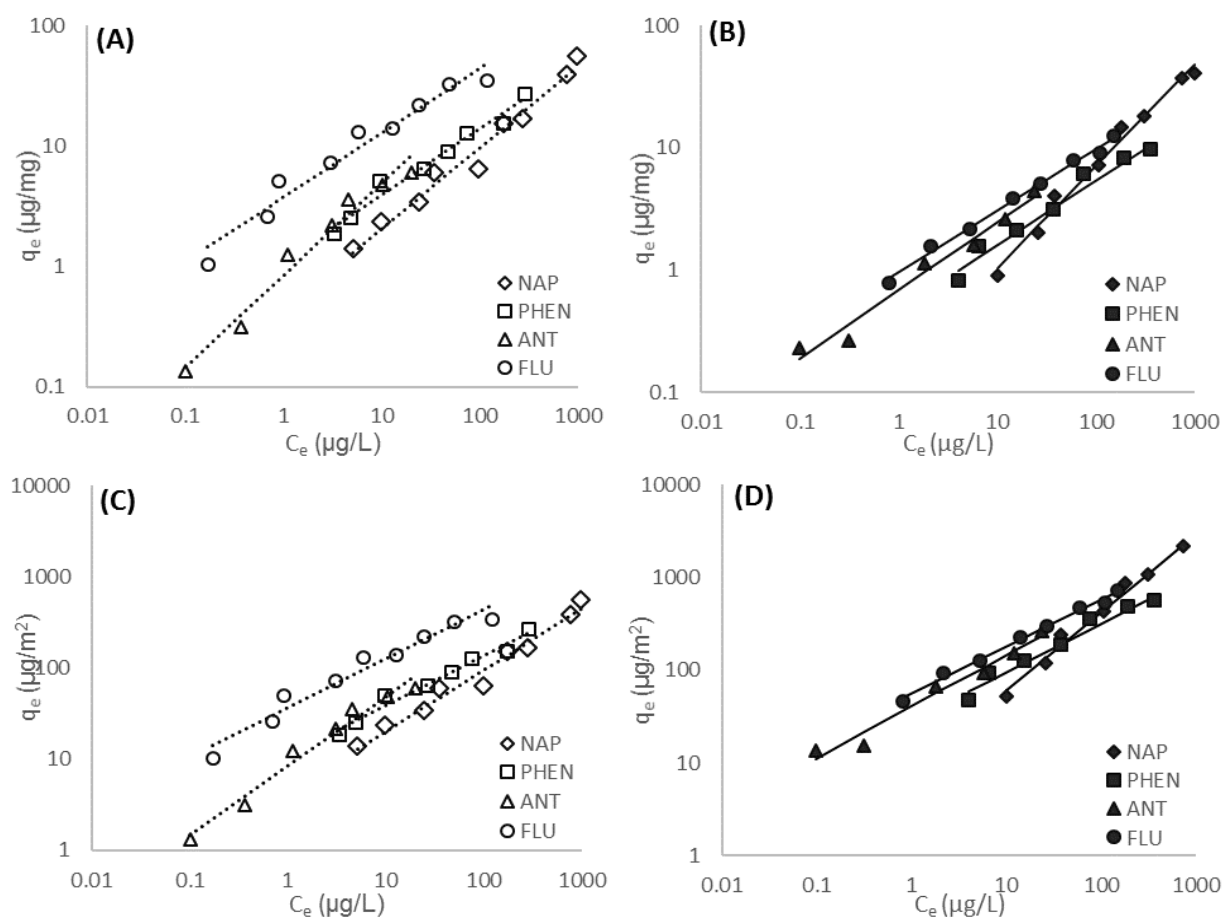


Figure 2.1. Adsorption isotherms of PAHs by MWCNT and GN on a mass and surface area basis. Isotherms were plotted in logarithmic scale where adsorption by A) MWCNT and B) GN were plotted on a mass basis; adsorption isotherms of C) MWCNT and D) GN on a surface area basis. Dashed lines represent fit of Freundlich model of PAHs adsorbed to MWCNT; solid lines represent fit of Freundlich model of PAHs adsorbed to GN.

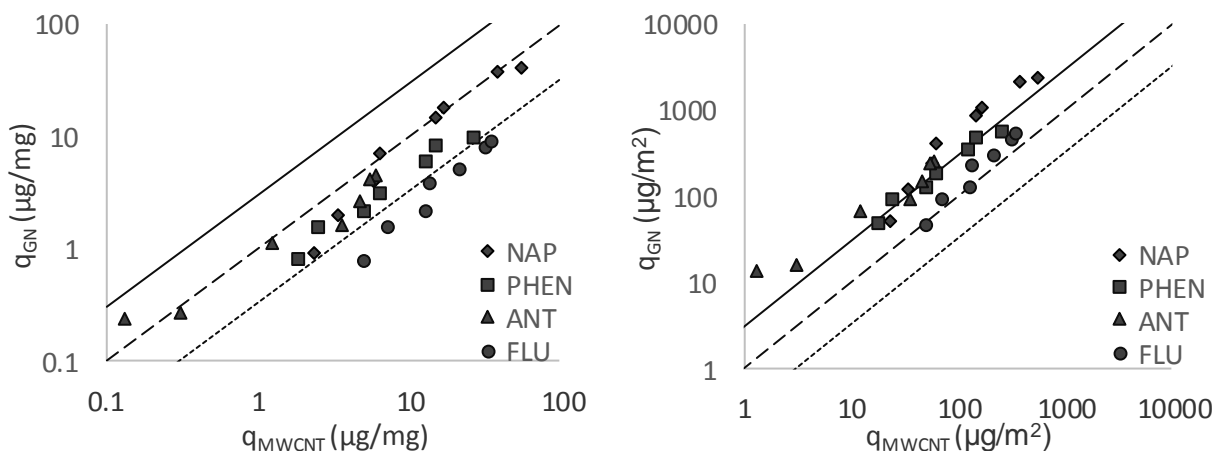


Figure 2.2. Distribution of PAH adsorption between GN and MWCNT on a mass and surface area basis. The adsorption (q_e) of each PAH on GN at a given experimental concentration plotted against the adsorption of the PAH on MWCNT at the same experimental concentration represents the graphene-multi walled carbon nanotube distribution on a unit (A) mass and (B) surface area.

To further investigate differences in adsorption of PAHs by MWCNT compared with GN, the GN/MWCNT distribution coefficient ($q_{\text{GN}}/q_{\text{MWCNT}} = K_{\text{GN/MWCNT}}$) as a function of various PAH physicochemical properties across all equilibrium concentrations was analyzed via regression analysis on a surface area basis (Figure 2.3). Analysis of covariance (ANCOVA) was used to assess differences in the partition coefficients ($K_d = q_e/C_e$) of PAHs for GN and MWCNT as a function of PAH physicochemical properties to account for contrasting simple effects. There was a strong negative correlation between $K_{\text{GN/MWCNT}}$ and PAH resonance energy, polarizability, molecular size and octanol-water partition coefficient ($\text{Log } K_{\text{ow}}$), where the distribution coefficient between GN and MWCNT approached one with increases in these parameters (Figure 2.3). Considering that resonance energy and polarizability are indicators of π -donor strength (Zhu et al., 2005), while molecular size and $\text{Log } K_{\text{ow}}$ are indicative of PAHs hydrophobicity suggests that as π - π interactions and hydrophobic forces increase, the differences in adsorption

between MWCNT and GN are minimized. Further, the influence of PAH resonance energy, polarizability, molecular size and hydrophobicity were significantly more influential on the adsorption of PAHs by MWCNTs (K_{MWCNT}) than by GN (K_{GN}) (p-values: 0.009, 0.011, 0.012 and 0.016, respectively), indicating that π - π interactions and hydrophobic forces are the key mechanisms driving adsorption of PAHs by MWCNTs, but are only moderately responsible for the adsorption of PAHs by GN.

Adsorption of PAHs by MWCNT and GN was also considered as a function of chemical reactivity and stability, where lower HOMO-LUMO gaps and lower ionization energy were considered indicative of greater molecular reactivity (Radovic and Bockrath, 2005). Although there was no correlation between $K_{\text{GN/MWCNT}}$ and PAHs' HOMO-LUMO gap or ionization potential (Figure 2.3 [E, F]), a notable negative correlation existed between K_{GN} and PAHs' HOMO-LUMO gap (R^2 : 0.93; p-value: 0.0003) and ionization energy (R^2 : 0.68; p-value: 0.0018), indicating that adsorption of PAHs by GN was higher when molecules were more reactive. In contrast, adsorption of PAHs to MWCNT appeared to be much less influenced by PAHs molecular reactivity as indicated by the low correlation of K_{MWCNT} with PAHs HOMO-LUMO gap (R^2 : 0.56; p-value: 0.003) and ionization potential (R^2 : 0.27; p-value: 0.18). This may be attributed to differences in CNM morphology; surface curvature of MWCNTs create a diversity of C-C bond lengths and alters the distribution of HOMO and LUMO π -orbitals on the graphitic surface unlike those in existence on the planar surface of graphene or graphite (Zhu et al., 2005). Such differences affect electronic properties and adsorption site distribution on the two materials, thus can cause adsorbates to interact with the CNMs in a different manner (Dindayalane and Leszczynski, 2010). These findings are in line with previous studies that found electrostatic interactions contributed to stabilizing adsorption of planar molecules by flat graphitic surfaces, which may not be as prevalent for CNTs (Zhu et al., 2005; Bjork et al 2010). Overall, the specific interactions PAHs have with the available adsorption sites present seem to

be more influenced by the PAHs physicochemical characteristics and CNM morphology rather than CNM surface area.

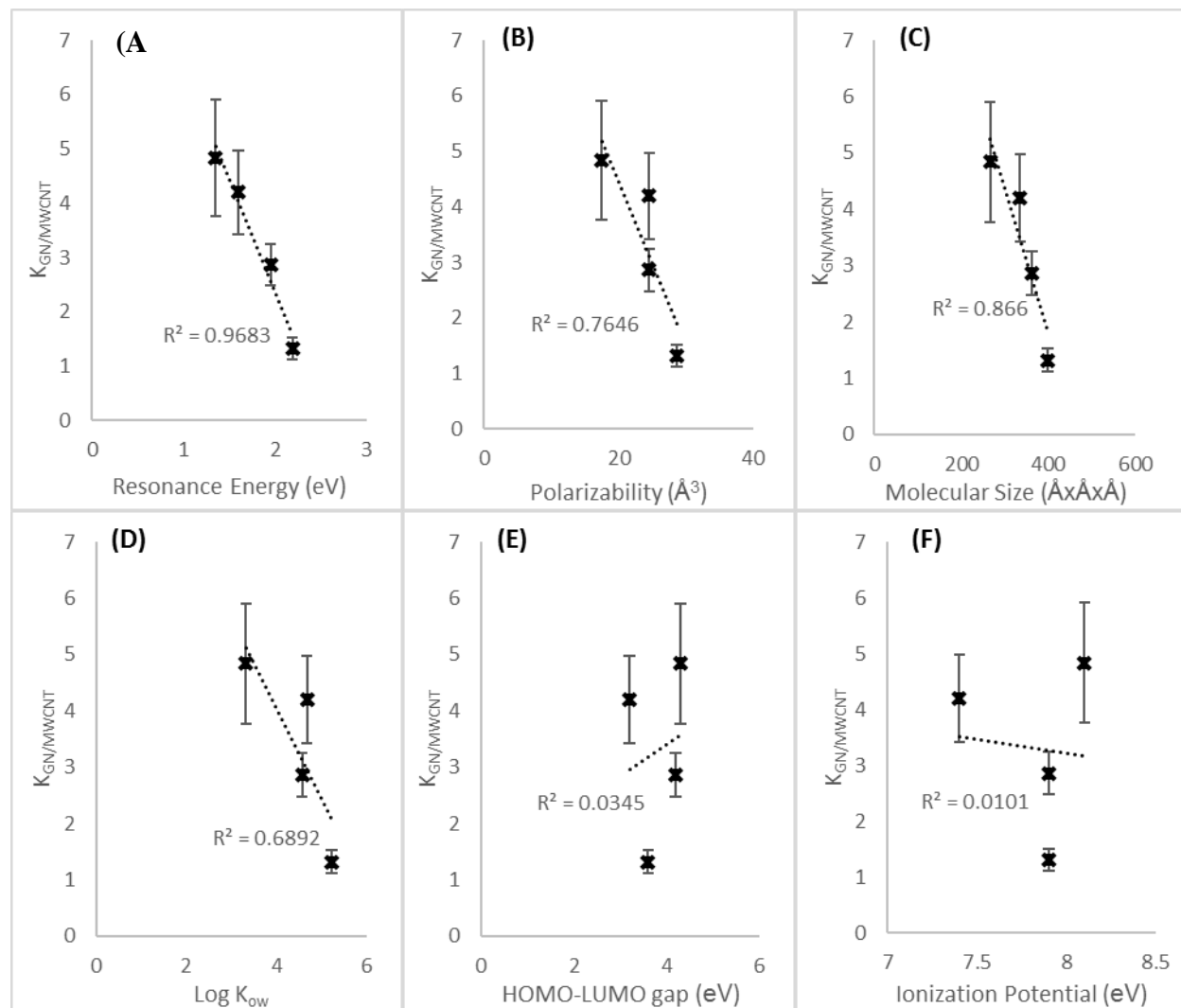


Figure 2.3. Relationship between surface area normalized GN/MWCNT partition coefficient ($K_{GN/MWCNT} = q_e \text{ GN} / q_e \text{ MWCNT}$) and selected PAH physicochemical properties: A) resonance energy; B) polarizability; C) molecular size; D) octanol-water partition coefficient; E) HOMO-LUMO gap; F) ionization potential. Represented PAH physicochemical characteristic values were collected from the literature and chemical databases and are listed in table 2. Error bars represent 95% confidence interval of $K_{GN/MWCNT}$ across all equilibrium concentrations used.

2.3.2. Influence of PAH Properties on Adsorption

Adsorption capacity can be described empirically by Freundlich K_F values and as distribution coefficients at single concentration points ($K_d = q_e/C_e$, where q_e is the concentration of PAH adsorbed per unit CNM and C_e is the equilibrium aqueous concentration of the PAH). The adsorption isotherms of PAHs by MWCNT and GN were well fit by the Freundlich model where similar trends in K_F and n values were observed for both CNM types. The Freundlich exponent n , where low values are indicative of greater surface heterogeneity and adsorption intensity (Brooks et al., 2012), similarly decreased for both materials as PAH polarizability and resonance energy increased. This suggests that as PAH π -donor strength increased there was also an increase in adsorption intensity to both CNMs (Zhu et al., 2005). Following previously established trends, PAH uptake by MWCNT and GN increased with increasing hydrophobicity (Apul et al. 2013). Adsorption of FLU by MWCNT [K_F value: 88.5 in $(\text{mg/g})(\text{mg/L})^n$] was nearly two times greater than that of ANT, PHEN, and NAP, all of which had similar adsorption capacities [K_F values: 48.1, 49.6, and 53.6 in $(\text{mg/g})(\text{mg/L})^n$ respectively] (Table 2.1). Interestingly, adsorption capacity of NAP and ANT by GN [K_F values: 43.4 and 47.2 in $(\text{mg/g})(\text{mg/L})^n$, respectively] was significantly larger than FLU and PHEN [K_F values: 30.3 and 16.8 in $(\text{mg/g})(\text{mg/L})^n$, respectively], suggesting that beyond hydrophobicity, PAH morphology may influence adsorption interactions (Table 2.1). The hydrophobic effect was suppressed by normalizing the adsorption coefficient (K_d) by the PAHs' octanol-water partition coefficient (K_{ow}). The normalized adsorption coefficient (K_d/K_{ow}) plotted against equilibrium concentrations of each of the PAHs showed higher adsorption of NAP over the other three PAHs by both CNMs (Figure 2.4 [A & B]). This is attributed to the ability of NAP to better access available adsorption sites over larger PAH molecules (Wang et al. 2014; Sun et al 2013b). K_d/K_{ow} as a function of equilibrium concentration also revealed that MWCNT adsorption of NAP and ANT had similar slopes (slopes: -0.32 to -0.24, respectively) that were significantly smaller than that of FLU and

PHEN (slopes: ~ -0.45 , for both) with a p-value of 0.0345. As equilibrium concentration surpassed 10% of the PAHs' solubility concentration there was an increasing divergence between the two sets of PAHs, where MWCNT had a higher adsorption affinity for NAP and ANT than FLU and PHEN (Figure 2.4 [C]). This suggests that at a higher solubility range, higher energy adsorption sites were still available for NAP and ANT, but became more limited for FLU and PHEN. Previous studies have found linear PAHs, such as NAP and ANT, can better align with MWCNTs' curved surface than angular or irregular PAHs, which may undergo steric hindrance thus are less able to access sorption sites at higher concentrations (Gotovac et al., 2007; Apul et al., 2012a; Tournus et al., 2005; Wang et al., 2014). In contrast, when adsorbed to GN, NAP K_d/K_{ow} remained relatively constant while K_d/K_{ow} values for PHEN, ANT and FLU decreased with increasing equilibrium concentrations (Figure 2.4 [B]). Preliminary analysis of Raman spectra of MWCNT and GN when PAHs are adsorbed, showed a shift in the G band position of MWCNT when NAP is adsorbed, indicating that the interaction between MWCNT and NAP is beyond physical adsorption to the surface (Table B2). This supports findings by Sun et al. (2013b) that adsorption of NAP by GN is partially driven by pore-filling mechanisms rather than adsorption just to the flat surface, such as is the case for larger PAHs.

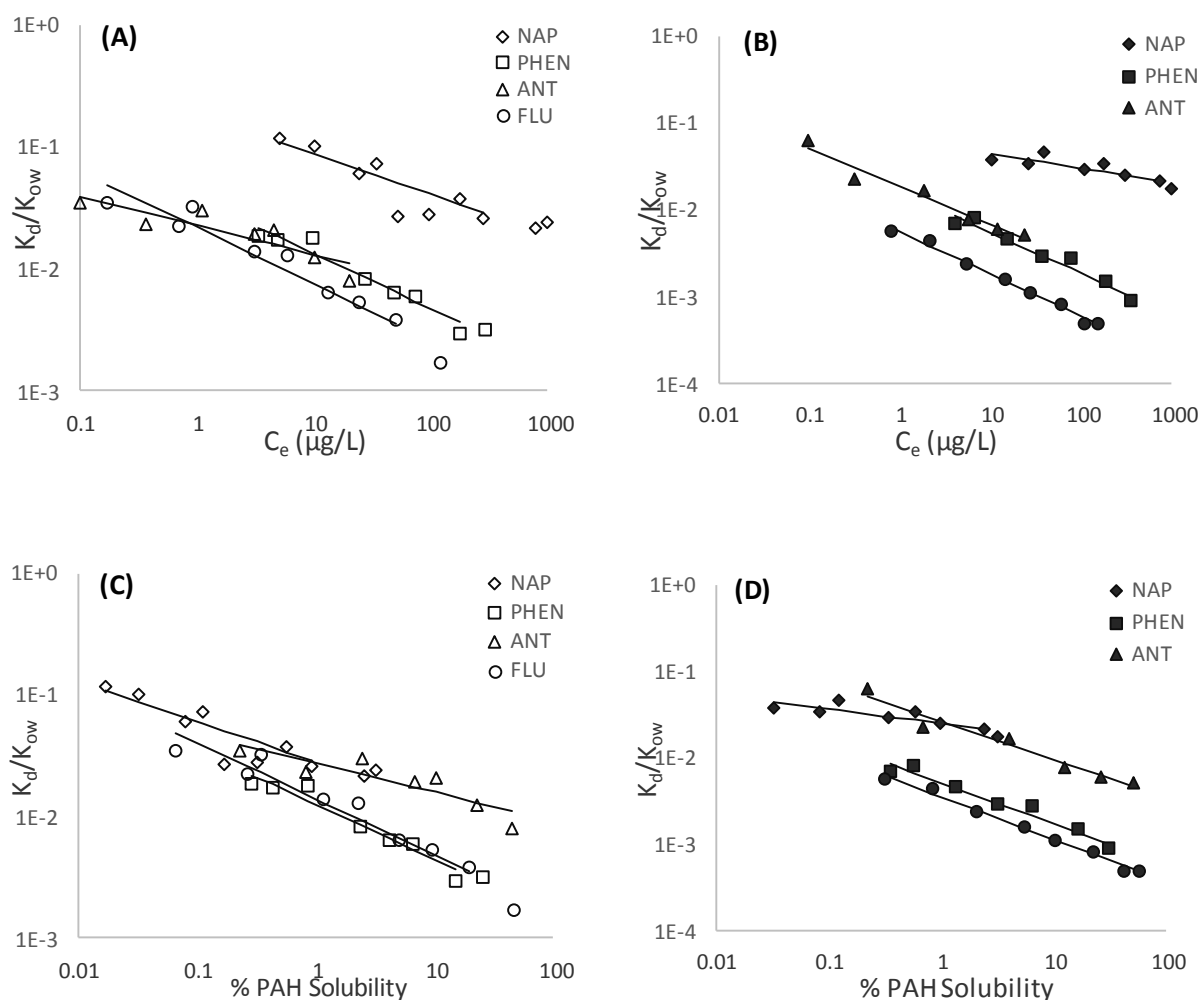


Figure 2.4. Adsorption normalized by hydrophobic character plotted as a function of equilibrium concentration. The relationship between the octanol-water partition coefficient (K_{ow}) normalized adsorption descriptor (K_d/K_{ow}) and equilibrium concentration was plotted on a mass basis (A & B) and as % PAH water solubility (C & D), of naphthalene, phenanthrene, anthracene and fluoranthene by MWCNT (open symbols) and GN (closed symbols) represented in logarithmic scale.

2.3.3 Bioavailability of PAHs Adsorbed to MWCNT and GN

Log transformation of the bile fluorescence data corrected the normality and variances issues observed in the raw data (Figure 2.5). Bile fluorescence was significantly lower in all

PAH-spiked treatments containing MWCNT compared to treatments of just PAH-spiked background solution. In PHEN, ANT, and FLU spiked MWCNT treatments, bile fluorescence was significantly higher than the response in the control treatments (p-value: 0.019, <.0001, and 0.004, respectively); in NAP spiked MWCNT treatments the response was not significantly different than the control, suggesting MWCNT-adsorbed NAP was completely un-bioavailable. In contrast, bile fluorescence in PAH-spiked treatments containing GN appeared to be significantly lower than the PAH-only treatments for only ANT spiked treatments, though this was still significantly higher than the control (p-value: 0.0015). This suggests that either a) fish are responding to the aqueous concentration (C_e) of PAH remaining in the system after adsorption equilibrium had been reached and/or b) some of the CNM-adsorbed PAH is still bioavailable.

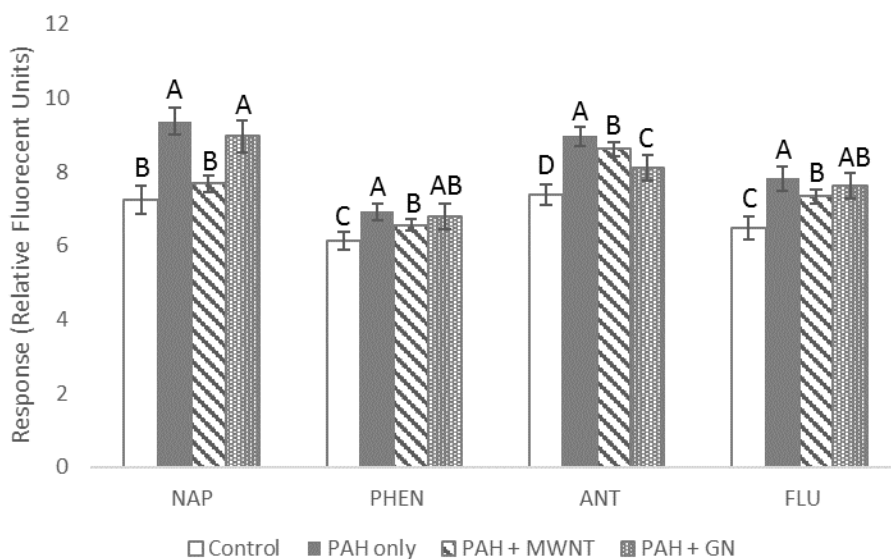


Figure 2.5. Response of *P. promelas* to PAHs in the absence and presence of CNMs.

Response of *P. promelas* to control, PAH only, PAH with multi-walled nanotubes (MWCNT) and PAH with exfoliated graphene (GN) treatments is represented as the mean bile fluorescence intensity (in natural logarithmic units). Error bars represent a 90% confidence interval of the mean. Within each PAH, levels not labeled by the same letters are significantly different based on Student's T test and least squares mean (p-value < 0.1).

The response of *P. promelas* in treatments containing MWCNT or GN as a function of PAH aqueous concentration (C_e) was further investigated by plotting the measured response of *P. promelas* against the predicted response (Figure 2.6). Aqueous concentrations of NAP, PHEN, ANT, and FLU were 4, 4, 1, and 2 $\mu\text{g/L}$ in MWCNT treatments and 4, 5, 1, and 6 $\mu\text{g/L}$ in GN treatments, respectively. The predicted response of *P. promelas* was calculated from dose-response curves established for each PAH, where bile fluorescence intensity was a function of aqueous PAH exposure. In general, the predicted bile fluorescence of *P. promelas* was within the 95% confidence envelope of actual bile fluorescence. Similar to Xia et al (2012), this suggests that the response of *P. promelas* was largely due to the un-adsorbed fraction of the PAH. The

apparent greater effectiveness of MWCNT over GN to reduce bioavailability of PHEN and FLU is attributed to the lower adsorption capacity of PAHs by GN on a mass basis. Two exceptions existed; the predicted response of *P. promelas* in NAP-spiked MWCNT treatments and ANT-spiked GN treatments was significantly higher than the actual response (p-value: <.0001 for both). This is partially attributed to the route of exposure and subsequent excretion of small PAHs, like NAP. Although the remaining aqueous fraction of most PAHs left in such a system would be taken up at the gills and the metabolites excreted into the gallbladder, exposure of NAP at the gills is likely to remain unconjugated and excreted directly via urine and, therefore, was not measured through the bile analysis technique (Tukikene, 1995). Additionally, studies have observed that linear PAHs, like NAP and ANT, have an enhanced stacking ability with the GN surface carbon rings (Chakrova-Kack et al., 2010). This type of interaction in combination with the low solubility of ANT could contribute to the large observed reduction in bioavailability.

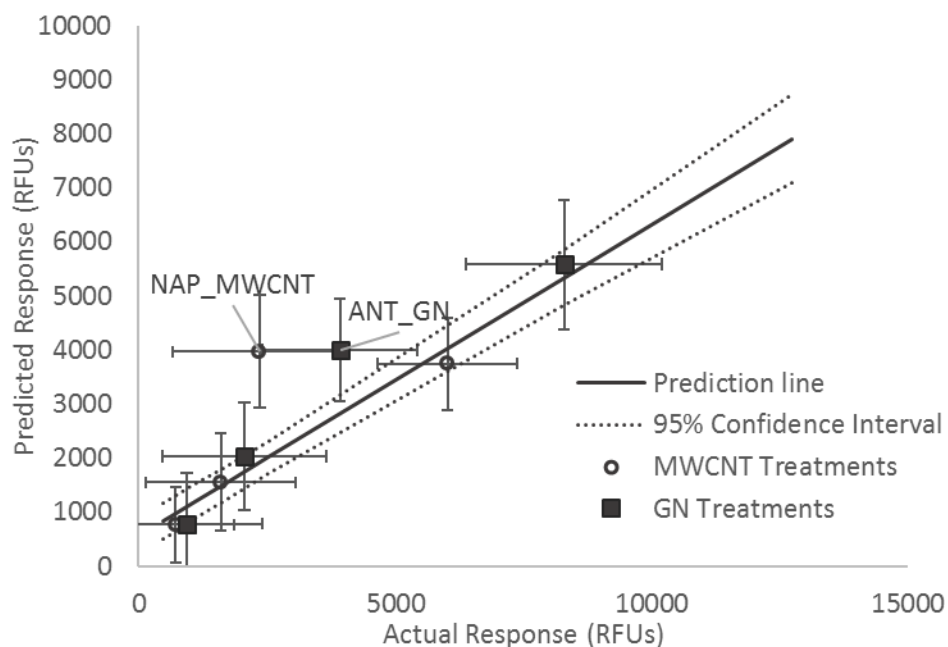


Figure 2.6. Relationship between the measured and the predicted response of *P. promelas* from each treatment. The solid line represents the relationship between the actual and predicted response of *P. promelas* to the aqueous exposure of the PAHs in control and PAH only treatments; dashed lines represent the 95% confidence interval envelope around the prediction line. Individual data points represent the mean response of *P. promelas* in PAH-spiked treatments with MWCNT (open symbols) and GN (closed symbols); error bars represent 90% confidence interval across exposure replicates. RFUs = relative fluorescent units; MWCNT = multi-walled carbon nanotubes; GN = exfoliated graphene; NAP = naphthalene; ANT = anthracene

2.3.4 Relationship Between Adsorption Behavior and Bioavailability of MWCNT and GN Adsorbed PAHs

Due to differences in fluorescence intensity between PAHs as a product of metabolite fluorescent properties, bile fluorescence comparisons are only relative among samples analyzed at the same wavelength pair. To allow for a direct comparison across different PAHs, the change

in bile fluorescence due to presence of CNMs was expressed as a proportion of bile fluorescence of fish exposed to just the PAH without CNMs present. Following methods from the literature, a bioavailability index was developed to assess how a change in PAH bioavailability relates to the observed adsorption of the PAH by CNMs in each exposure (Chen et al., 1996; Torreiro-Melo et al. 2015). The bioavailability index is expressed as follows.

$$BI = \frac{\Delta Response / Response_{PAH}}{\Delta C / C_0} \quad (2.2)$$

Where $Response_{PAH}$ = bile fluorescent intensity measured in fish from PAH-spiked treatments containing only the background solution (i.e. positive control), $\Delta Response$ = difference in bile fluorescent intensity measured in fish between PAH-spiked treatments with and without the CNM present, C_0 = original concentration of PAH spiked into the system, and ΔC = change in aqueous concentration of PAH left in the system after adsorption equilibrium was reached with either MWCNT or GN.

A bioavailability index of one, where change in bile fluorescence is the same as the change in PAH aqueous concentration due to CNM, indicates that only the un-adsorbed PAH (C_e) remains bioavailable for metabolism. A bioavailability index < 1 results when change in response was less than the measured change in PAH concentration in the system, suggesting that some of what is adsorbed is bioavailable; a bioavailability index of zero is due to a lack of change in response regardless of changes in the aqueous concentration of the PAH, indicating that all of what was adsorbed remained bioavailable. In instances where change in response was greater than the measured change in aqueous PAH concentration in the system, a bioavailability index < 0 or > 1 could result; a bioavailability index < 0 would indicate that CNMs enhance bioavailability of PAHs. A bioavailability index > 1 suggests that bioavailability of the PAH was reduced beyond what was adsorbed and indicates that the adsorbed fraction of the PAH is not bioavailable through dietary exposure. Although, it is important to note that exposure to aqueous

PAH at the gills may result in excretion of some metabolites through urine rather than bile and may be a confounding factor leading to lower response detected via bile analysis thus an index > 1 (Tukikene, 1995).

A comparison of bioavailability indices across PAHs indicates that while MWCNT reduces bioavailability of ANT, PHEN and FLU similarly, some of what was adsorbed remained bioavailable (Figure 2.7). Two-tailed mean hypothesis testing that bioavailability indices equal one indicated that 35-70%, 40-75%, and up to 90% of adsorbed ANT, FLU and PHEN, respectively, could remain bioavailable. Even with a large variation in fish response from NAP-spiked treatments containing MWCNT, data indicated that only up to 20% of adsorbed NAP could remain bioavailable. This suggests MWCNTs were more effective at reducing bioavailability of NAP than other PAHs in terms of dietary exposure. This is attributed to small-sized NAP adsorbing to both the surface of MWCNT and filling pores (Sun et al., 2013b), where it is likely less accessible for digestive components.

Assessment of GN treatments shows an average bioavailability index that is above 1 for both NAP and ANT spiked treatments, while the index was below one for PHEN and FLU treatments (Figure 2.7). Two-tailed mean hypothesis testing the null hypothesis that $BI = 1$ indicated that it is unlikely that any of GN-adsorbed NAP is bioavailable, though up to 30% of GN-adsorbed ANT could be bioavailable. 80-100% of GN-adsorbed FLU was calculated to be bioavailable and up to 100% of GN-adsorbed PHEN may remain bioavailable. Adsorption of PAHs onto GN sheets at low concentrations can alter the aggregate formations of GN nanosheets, thus leading to desorption hysteresis (Wang et al., 2014; Zhao et al., 2014). Depending on the degree of desorption hysteresis, the reduction in bioavailability can be variable. Of significant interest, the effect of GN on bioavailability of NAP and ANT was statistically similar and significantly greater than the influence of GN on PHEN and FLU bioavailability (p -value < 0.05). This is likely due to NAP and ANT having a stronger interaction

with GN than PHEN and FLU, as also was observed in the adsorption data. This is attributed to differences in the morphology of PAH molecules, which can alter the compounds stability and ability to form π - π interactions with the surface of the CNM. The linear configuration NAP and ANT molecules gives them a lower resonance energy than PHEN and FLU; this increased compound stability in linear molecules appears to be a significant contributing factor driving bioavailability of GN-adsorbed PAHs (Tournus et al., 2005; Tournous and Charlier, 2005; Li et al 2013a; Shen et al. 2013).

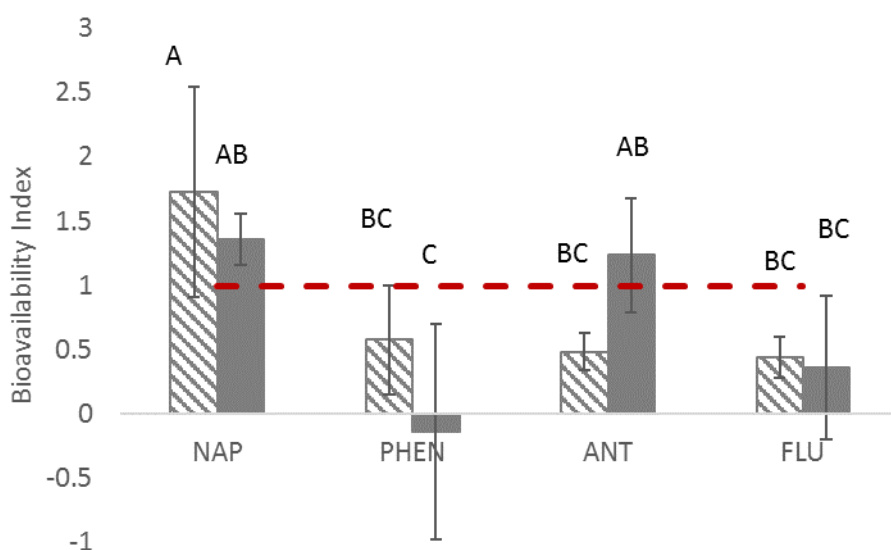


Figure 2.7. Comparison of bioavailability index across all treatments containing MWCNT (stripped bars) and GN (solid bars). Error bars represent the 95% confidence interval of the mean and levels not connected by the same letter are statistically different based on Student's T test and least squared means (p-value < 0.05). Dashed line at 1 bioavailability index represents the expected indices if only the free fraction (C_e) of PAH were bioavailable.

ANCOVA of bioavailability indices as a function of PAH physicochemical characteristics indicated that there was no interaction with CNM type, suggesting that even if differences in adsorption were observed due to interactions between CNM type and PAH

physicochemical characteristics this was not a significant factor influencing bioavailability of adsorbed PAHs (Figure 2.8). However, regression analysis of bioavailability indices from CNM exposures as a function of PAH physicochemical characteristics showed a strong negative correlation with the PAHs' π -donor strength, represented by resonance energy and polarizability, and hydrophobic character, represented by molecular size and the octanol-water partition coefficient (Figure 2.8, [A, B, C & D]). This suggests that the bioavailability of adsorbed PAHs increases with increasing π -donation capability and increasing hydrophobicity. While increasing π -donation capability and hydrophobicity increases the strength of adsorption of PAH molecules by CNM, it may also increase the bioaccumulative potential of the compounds in the organism (Bleeker and Verbuggen, 2009).

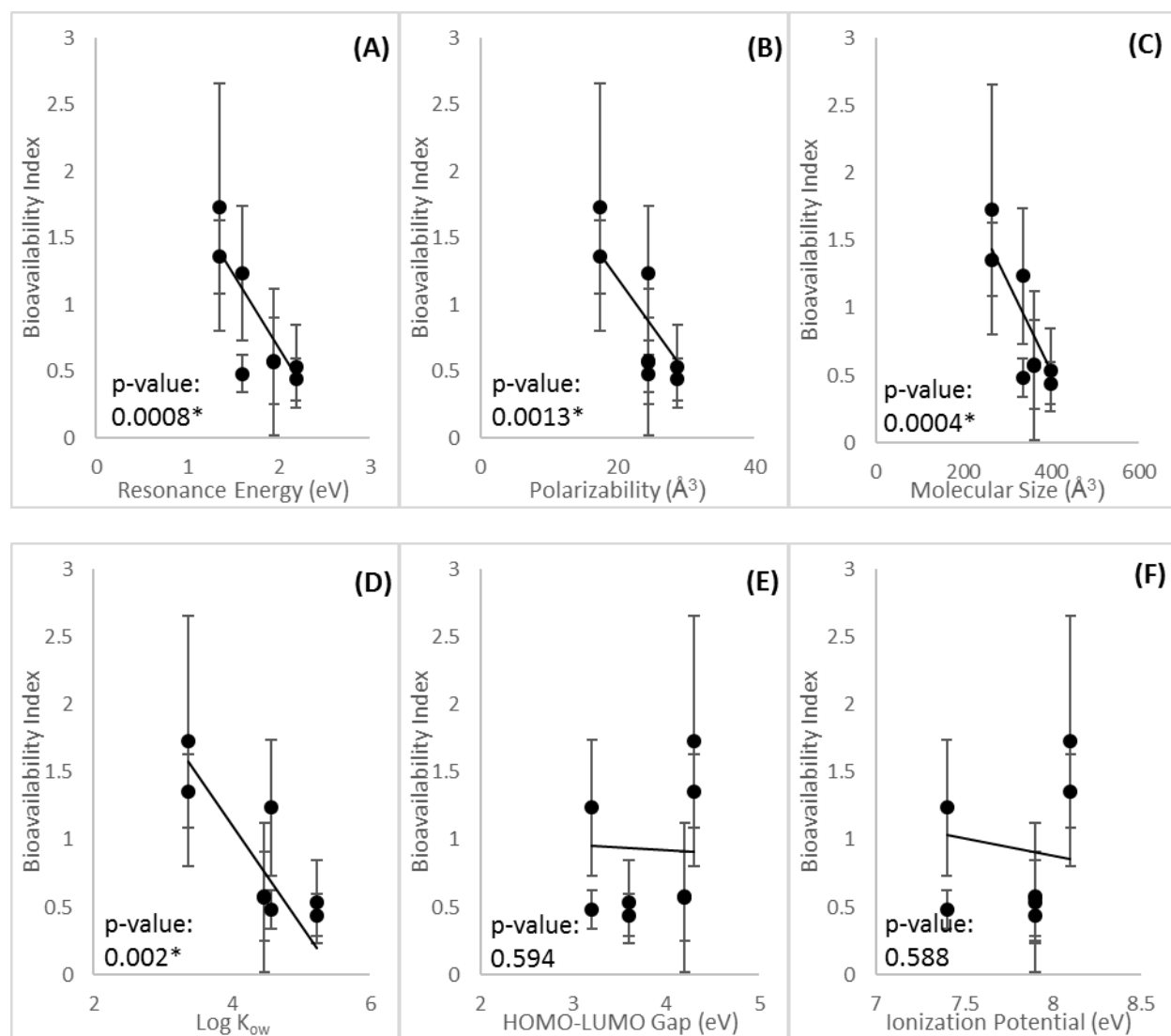


Figure 2.8. Relationship between bioavailability index from CNM exposures with PAH physicochemical characteristics. Error bars represent 95% confidence levels of the mean bioavailability indices from CNM treatments for each PAH. The listed p-value describes the effect of the PAH physicochemical characteristic on bioavailability index from all treatments containing CNM; asterisks indicate a significant relationship between the bioavailability indices and the PAH physicochemical characteristic.

To further investigate the relationship between adsorption behavior and bioavailability, the bioavailability indices were plotted as a function of calculated Freundlich model adsorption

parameters, n and K_F . While the Freundlich capacity factor (K_F) had no correlation with bioavailability indices for MWCNT, there was a moderate positive correlation for GN where higher adsorption capacity led to greater reduction in bioavailability of adsorbed PAHs (data not shown). For both MWCNT and GN, there was a significant positive correlation between the Freundlich n value and bioavailability indices (Figure 2.9 [A]). Although this appears to suggest a greater reduction in bioavailability as the adsorption process became more linear and surface more homogenous, it is important to point out that variances in the bioavailability index for each PAH increased as Freundlich exponent n approached 1. Greater variation at higher n -values suggests that with greater surface homogeneity and a narrower distribution of high energy adsorption sites, adsorption may be weaker (Brooks et al., 2012; Zhu et al. 2005). The observed trend is attributed, in part, to a concentration effect as a function of surface area coverage by the PAH molecules (Figure 2.9 [B]). The % surface area coverage can be estimated given the CNM BET surface area, concentration in solution, individual PAHs molecular surface area supplied in Table S2 and PAH concentration in solution. Although similar concentrations were used in the bioavailability assays, estimated surface area coverage on MWCNT by NAP, PHEN, ANT and FLU was 15, 25, 35, and 85% respectively, and on GN was 35, 45, 75, and ~100% respectively. At low surface area coverage there is a greater distribution of sorption sites, but as surface area coverage increases with increasing concentration, the high energy adsorption sites become filled leaving only lower energy sites available (Apul et al., 2013; Wang et al. 2014; Brooks et al., 2012). Molecules adsorbed in lower energy sites are more vulnerable to release due to competition by biomolecules present in the digestive tract or to preferring to complex with other compounds present in the aqueous phase (Van de Wiele et al., 2004). At the concentrations used, surface area coverage by small sized NAP is low so is likely less bioaccessible than the other PAHs, although it is likely that at higher concentrations the ability of CNM to reduce NAP bioavailability may not be as effective as currently observed. Overall, the interactions occurring

between the adsorbate and the surface of the CNM play a significant role in bioavailability of CNM-adsorbed PAHs although the relationship with surface heterogeneity is not well understood. Future work should examine the role of surface interactions between the CNM and the adsorbed OC as it relates to bioavailability.

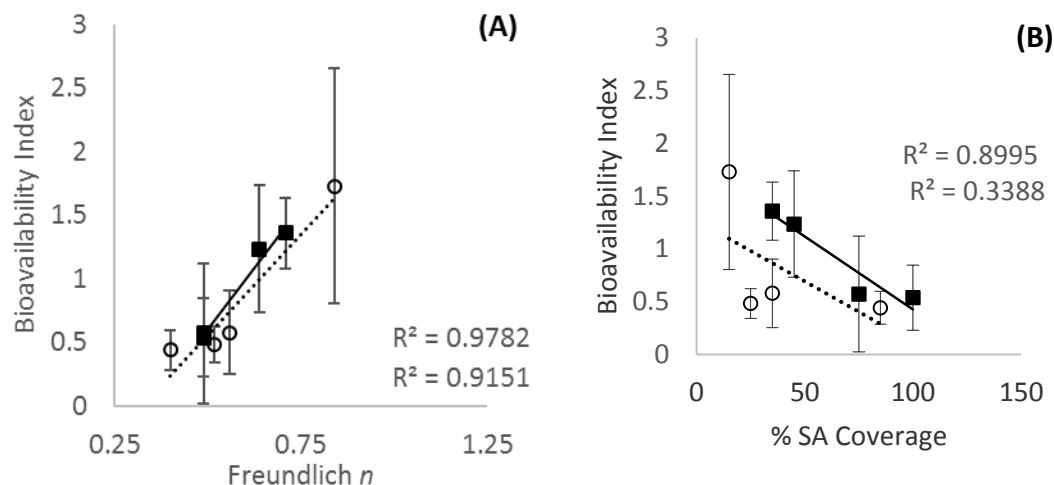


Figure 2.9. Bioavailability index as a function of (A) surface heterogeneity and (B) % CNM surface area coverage. Surface heterogeneity is represented by Freundlich exponent n and % surface area coverage by PAH molecules is based on the assumption of monolayer adsorption. Single data points represent the mean bioavailability index determined from MWCNT treatments (open circles) and GN treatments (solid squares) where error bars represent the 95% confidence interval of the mean.

2.3.5 Effect of Biological Conditions on Bioavailability

Similar to previous studies, CNMs alone were not found to be toxic to the fish though they were readily ingested and compartmentalized in the gut prior to excretion (Su et al., 2013; Peterson et al., 2009; Edgington et al., 2010; Bisesi et al., 2015) (Figure C2). While small aggregates of CNM may form at the gills, the digestive tract has been considered the primary

route of absorption of CNM-adsorbed OCs (Hou et al., 2013; de Maagd and Vethaak, 1998; Qiang et al., 2016; Su et al. 2013), where bioaccessibility and metabolism of PAHs during the digestion process is largely driven by residence time, gastrointestinal pH, and presence of bile salts (Dean and Ma, 2007). Like previously published findings of minnow gut passage time, the test organisms were observed to egest any ingested CNM material within a few hours (German et al., 2009), suggesting that the bioaccessible fraction of CNM-adsorbed PAH would be absorbed into the organism within that time (Su et al., 2013). Because *P. promelas* are from the Cyprinidae family of fish, they lack true stomachs so ingested materials are directly released into the intestine with a near neutral pH (~6.8) (Hofer et al., 1981; German et al., 2009). Even in more complex gastrointestinal fluids, desorption of OCs from CNTs has not been observed to be significantly influenced by pH or ionic strength (Wang et al., 2011). Rather the presence of bile salts, bio-surfactants released during digestion to enhance solubility and uptake of hydrophobic compounds, are largely responsible for driving desorption of OCs from ingested materials (Wang et al., 2011; Sun et al., 2013; Van de Wiele et al., 2004; Olsen and Ringo et al., 1997). The solubilizing effect of bile salts is dependent on the concentration and accessibility to the compound (Maldonado-Valderrama et al., 2011; Wang et al., 2011); in starvation conditions, such as existed in the presented work, the low level of bile salts has been shown to have little effect on OC desorption from CNTs (Wang et al. 2011; Sun et al., 2013). Although microbiota in the gut can also contribute to solubilization and metabolism of PAHs (Nayak, 2010), starvation conditions and the presence of CNMs can alter microbiota makeup making it difficult to discern their potential role in desorption of PAHs from CNM in fish (Bisesi et al., 2015; Nayak, 2010). Considering the starvation conditions used in this study and the relative similarity of *P. promelas* gut tract with the outside aqueous environment, the biological components involved in the digestion process were not likely a major contributor. However, differences in CNMs' geometry can allow for the formation of closed interstitial spaces when aggregating thus entrapping

adsorbed molecules and causing desorption hysteresis (Yang and Xing, 2007). Rather than biological components, it may be that agglomeration or physical packing of CNMs in the gut tract may significantly influence desorption and the corresponding bioavailability of adsorbed OCs.

2.4 Conclusion

In summary, the adsorption data supported studies previously concluding that hydrophobic interactions largely drive adsorption of PAHs to MWCNT and electrostatic interactions are more important for adsorption of PAHs to GN. In contrast, bioavailability appeared to be more influenced by the ability of PAH molecules to access the available adsorption sites, as a function of molecular size and morphology, rather than the type of CNM. This work supported findings by Xia et al. (2012) that found chemical characteristics of OCs to be more influential on resulting bioavailability than CNM type. Further, the current study suggested that reduction in bioavailability of CNM-adsorbed PAHs was due to desorption hysteresis occurring during dietary exposure which may be altered by the CNMs agglomeration in the gut tract. This may explain why surface heterogeneity, an indication of adsorption site distribution, and surface area coverage appeared to be important factors influencing bioavailability of CNM-adsorbed OCs. While assessing adsorption of PAHs by CNMs in aqueous solutions provided insight into the more favorable adsorption interactions to occur, the physical and chemical alterations of CNMs in an organisms' digestive system limit the ability to accurately estimate the resulting bioavailability. To better understand dietary exposure of CNM-adsorbed compounds, future studies should investigate the mechanism by which desorption hysteresis occurs in the intestinal tract and the relationship to adsorption interactions with compounds occurring in the aqueous phase prior to ingestion.

2.5 References

- Aas, E.; Beyer, J.; Goksoyr, A. Fixed wavelength fluorescence (FF) of bile as a monitoring tool for polyaromatic hydrocarbon exposure in fish: an evaluation of compound specificity, inner filter effect and signal interpretation. *Biomarkers*. **2000**, 5 (1), 9-23.
- Apul, O.; Karanfil, T. Adsorption of synthetic organic contaminants by carbon nanotubes: A critical review. *Water Res.* **2015**, 68, 34-55.
- Apul, O.G.; Shao, T.; Zhang, S.; Karanfil, T. Impact of carbon nanotube morphology on phenanthrene adsorption. *Environ. Tox. Chem.* **2012a**, 31(1), 783-788.
- Apul, O.G.; Wang, O.; Zhou, Y.; Karanfil, T. Adsorption of aromatic organic contaminants by graphene nanosheets: Comparison with carbon nanotubes and activated carbon. *Water. Res.* **2013**, 47, 1648-1654.
- Apul, O.G.; Wang, Q.; Shao, T.; Rieck, J.R.; Karanfil, T. Predictive model development for adsorption of aromatic contaminants by multi-walled carbon nanotubes. *Environ. Sci. Technol.* **2012b**, 47, 2295-2303.
- Arnot, J.A.; Gobas, F. A review of bioconcentration factor (BCF) and bioaccumulation factor (BAF) assessments for organic chemicals in aquatic organisms. *Environ. Rev.* **2006**, 14, 257-297.
- Baun, A.; Sorensen, S.N.; Rasmussen, R.F.; Hartmann, N.B.; Koch, C.B. Toxicity and bioaccumulation of xenobiotic organic compounds in the presence of aqueous suspensions of aggregates of nano-C60. *Aquat. Toxicol.* **2008**, 86, 379-387.
- Beyer, J.; Jonsson, G.; Krahn, M.M.; Arese, F. Analytical methods for determining metabolites of polycyclic aromatic hydrocarbon (PAH) pollutants in fish bile: A review. *Environ. Tox. Pharm.* **2010**, 30, 224-244.
- Bisesi, J.H. Jr.; Ngo, T.; Ponnayolu, S.; Liu, K.; Lavelle, C.M.; Afrooz, A.R.M.N.; Saleh, N.B.; Ferguson, P.L.; Denslow, N.D.; Sabo-Attwood, T. Examination of single-walled carbon nanotubes uptake and toxicity from dietary exposure: tracking movement and impacts in the gastrointestinal tract. *Nanomaterials*. **2015**, 5, 1066-1086.
- Bjork, J.; Hanke, F.; Palma, C.; Samori, P.; Cecchini, M.; Persson, M. Adsorption of aromatic and anti-aromatic systems on graphene through π - π stacking. *J. Phys. Chem. Lett.* **2010**, 1, 3407-3412.
- Bleeker, E.A.J.; Verbuggen, E.M.J. Bioaccumulation of polycyclic aromatic hydrocarbons in aquatic organisms. *RIVM report 601779002*; National Institute for Public Health and the Environment: Netherlands, **2009**.
- Brooks, A.J.; Lim, H-N.; Kilduff, J.E. Adsorption uptake of synthetic organic chemicals by carbon nanotubes and activated carbons. *Nanotechnology*. **2012**, 23, 294008; doi:10.1088/0957-4484/23/29/294008.
- Chakarova-Kack, S.; Vojvodic, A.; Kleis, J.; Hyldgaard, P.; Schroder, E. Binding of polycyclic aromatic hydrocarbons and graphene dimers in density functional theory. *New J. Phys.* **2010**, 12, 1-16

Chen, B.; Shan, X.; Qian, J. Bioavailability index for quantitative evaluation of plant availability of extractable soil trace elements. *Plant Soil*. **1996**, 186, 275-283.

Chen, W.; Duan, L.; Zhu, D. Adsorption of polar and nonpolar chemical to carbon nanotubes. *Environ. Sci. Technol.* **2007**, 41, 8295-8300.

de Maagd, P.G-J.; Vethaak, A.D. Biotransformation of PAHs and their carcinogenic effect in fish. In *The Handbook of Environmental Chemistry*; Neilson, A.H., Ed.; Springer-Verlag: Berlin, Heidelberg, **1998**; Vol. 3 (Part J); 266-308.

Dean, J.R.; Ma, R. Approaches to assess the oral bio accessibility of persistent organic pollutants: A critical review. *Chemosphere*. **2007**, 68, 1399-1407

Debnath, S.; Cheng, Q.; Hedderman, T.; Byrne, H. A comparative study of the interaction of different polycyclic aromatic hydrocarbons on different types of single walled carbon nanotubes. *J. Phys. Chem. C*. **2010**, 114 (18), 8167-8175.

Dinadayalane, T.C.; Leszczynski, J. Remarkable diversity of carbon-carbon bonds: Structures and properties of fullerene, carbon nanotubes and graphene. *Struct. Chemc.* **2010**, 21, 1155-1169.

Edgington, A.J.; Roberts, A.P.; Taylor, L.M.; Alloy, M.M.; Reppert J.; Rao, A.M.; Mao, J.; Klaine, S.J.; The influence of natural organic matter on the toxicity of multiwalled carbon nanotubes. *Environ. Tox. Chem.* **2010**, 29 (11), 2511-2518.

Ferguson, P.L.; Chandler, G.T.; Templeton, R.C.; Demarco, A.; Scrivens, W.A.; Englehart, B.A. Influence of sediment-amendment with single-walled carbon nanotubes and diesel soot on bioaccumulation of hydrophobic organic contaminants by benthic invertebrates. *Environ. Sci. Technol.* **2008**, 42: 3879-3885.

German, D.P.; Nagle, B.C.; Villeda, J.M.; Ruiz, A.M.; Thomson, A.W.; Balderas, S.C.; Evans, D.H. Evolution of herbivory in a carnivorous clade of minnows (Teleostei: Cyprinidae): Effects on gut size and digestive physiology. *Physiol. Biochem. Zool.* **2009**, 83 (1), 000-000.

Gotovac, S.; Honda, H.; Hattori, Y.; Takahshi, K.; Kanoh, H.; Kaneko, K. Effect of nanoscale curvature of single-walled carbon nanotubes on adsorption of polycyclic aromatic hydrocarbons. *Nano Lett.* **2007**, 7(3), 583-587.

Hofer, R.; Schiemer, F. Proteolytic activity in the digestive tract of several species of fish with different feeding habits. *Oecologia*. **1981**, 48, 342.

Hofmann, T.; von der Kammer, F. Estimating the relevance of engineered carbonaceous nanoparticle facilitated transport of hydrophobic organic contaminants in porous media. *Environ. Polln.* **2009**, 157, 1117-1126.

Hou, W.C.; Westerhoff, P.; Posner, J.D. Biological accumulation of engineered nanomaterials: a review of current knowledge. *Environ. Sci.: Processes Impacts*. **2013**, 15, 103-122.

Hyung, H.; Kim, J.H. Natural organic matter (NOM) adsorption to multi-walled carbon nanotubes: Effect of NOM characteristics and water quality parameters. *Environ. Sci. Technol.* **2008**, 42, 4416-4421.

Klaine, S.J.; Alvarez, P.J.J.; Batley, G.E.; Fernandes, T.F.; Handy, R.D.; Lyon, D.Y.; Mahendra, S.; McLaughlin, M.J.; Lead, J.R. Nanomaterials in the environment: Behavior, fate, bioavailability and effects. *Environ. Tox. Chem.* **2008**, 27 (9), 1825-1851.

Kukkonen, J.; Pellinen, J. Binding of organic xenobiotics to dissolved organic macromolecules: comparison of analytical methods. *Sci. Total Environ.* **1994**, 152, 19-29.

Li, Y.; Niu, J.; Shen, Z.; Feng, C. Size effect of single-walled carbon nanotubes on adsorption of perfluorooctanesulfonate. *Chemosphere.* **2013**, 91, 784-790.

Linard, E.N.; van den Hurk, P.; Karanfil, T.; Apul, O.G.; Klaine, S.J. Influence of carbon nanotubes on the bioavailability of fluoranthene. *Environ. Tox. Chem.* **2015**, 34(3), 658-666.

Lotya, M.; Hernandez, Y.; King, P.J.; Smith, R.J.; Nicolosi, V.; Karlsson, L.S.; Blighe, F.M.; De, S.; Wang, Z.; McGovern, I.T.; Duesberg, G.S.; Coleman, J.N. Liquid phase production of graphene by exfoliation of graphite in surfactant/water solutions. *J. Am. Chem. Soc.* **2008**, 131, 3611-3620.

Maldonado-Valderrama, J.; Wilde, P.; Macierzanka, A.; Mackie, A. The role of bile salts in digestion. *Adv. Colloid Interface Sci.* **2011**, 165, 36-46.

Nayak, S.K. Review Article: Role of gastrointestinal microbiota in fish. *Aquacult. Res.* **2010**, 41, 1553-1573.

Olsen, R.E.; Ringo, E. Lipid digestibility in fish: A review. *J. Lipid Res.* **1997**, 1, 199-264.

Peterson, E.J.; Pint, R.A.; Landrum, P.F.; Weber, W.J.Jr. Influence of carbon nanotubes on pyrene bioaccumulation from contaminated soils by earthworms. *Environ. Sci. Technol.* **2009**, 43, 4181-4187.

Qiang, L.; Chen, M.; Zhu, L.; Wu, W.; Wang, Q. Facilitated bioaccumulation of perfluorooctanesulfonate in common carp (*Cyprinus carpio*) by graphene oxide and remission mechanism of fulvic acid. *Environ. Sci. Technol.* **2016**, 50, 11627-11636.

Radovic, L.R.; Bockrath, B. On the chemical nature of graphene edges: Origins of stability and potential magnetism in carbon materials. *J. Am. Chem. Soc.* **2005**, 127, 5917-5927.

Rajesh, C.; Majumder, C.; Mizuseki, H.; Kawazoe, Y. A theoretical study on the interaction of aromatic amino acids with graphene and single walled carbon nanotubes. *J. Chem. Phys.* **2009**, 130, 124911; doi: 10.1063/1.3079096.

Ren, X.; Chen, C.; Nagatsu, M.; Wang, X. Carbon nanotubes as adsorbents in environmental pollution management: A review. *Chem. Eng. J.* **2011**, 170, 295-410.

Schwab, F.; Bucheli, T.D.; Camenzuli, L.; Magrex, A.; Knauer, K.; Sigg, L.; Nowack, B. Diuron sorbed to carbon nanotubes exhibits enhanced toxicity to *Chlorella vulgaris*. *Environ. Sci. Technol.* **2012**, 47: 7012-7019.

Shen, M.; Xia, X.; Zhai, Y.; Zhang, X.; Zhao, X.; Zhang, P. Influence of carbon nanotubes with preloaded and coexisting dissolved organic matter on the bioaccumulation of polycyclic aromatic hydrocarbons to *Chironomus plumosus* larvae in sediment. *Environ. Tox. Chem.* **2013**, 33(1), 1-8.

- Singh, D.K.; Giri, P.K.; Iyer, P.K. Evidence for defect-enhance photoluminescence quenching of fluorescein by carbon nanotubes. *J. Phys. Chem. C*, **2011**, 115, 24067-24072.
- Su, Y.; Yan, X.; Pu, Y.; Xiao, F.; Wang, D.; Yang, M. Risks of single-walled carbon naotubes acting as containants-carriers: potential release of phenanthrene in Japanese Medaka (*Oryzias latipes*). *Environ. Sci. Technol.* **2013**, 47, 4704-4710.
- Sun, H.; Ruan, Y.; Zhu, H.; Zhang, Z.; Yu, L. Enhanced bioaccumulation of pentachlorophenol in carp in the presence of multi-walled carbon nanotubes. *Environ. Sci. Pollut. Res.* **2013a**, 21 (4): 2865-2875.
- Sun, Y.; Yang, S.; Zhao, G.; Wang, Q.; Wang, X. Adsorption of polycyclic aromatic hydrocarbons on graphene oxides and reduced graphene oxides. *Chem. Asian. J.* **2013b**, 8, 2755-2761.
- Torreiro-Melo, A.G.; Silva, J.S.; Bianchini, A.; Zanardi-Lamardo, E.; de Carvalho, P.S.M. Bioconcentration of phenanthrene and metabolites in bile and behavioral alterations in the tropical estuarine guppy *Poecilia vivipara*. *Chemosphere*. **2014**, 132, 17-23.
- Tournus, F.; Charlier, J.C. Ab initio study of benzene adsorption on carbon nanotubes. *Phys. Rev. B*. **2005**, 71, 165421; DOI: 10.1103/PhysRevB.71.165421.
- Tournus, F.; Latil, S.; Heggie, M.I.; Charlier, J.C. Pi-stacking interaction between carbon nanotubes and organic molecules. *Phys. Rev. B*, **2005**, 72, 75431-75436.
- Towell, M.G.; Browne, L.A.; Paton, G.I.; Semple, K.T. Impact of carbon nanomaterials on the behavior of ¹⁴C-phenanthrene and ¹⁴C-benzo-[a] pyrene in soil. *Environ. Polln.* **2011**, 159, 706-715.
- Tukikene, A. Responses of fish to polycyclic aromatic hydrocarbons (PAHs). *Ann. Zool. Fennici*. **1995**, 32(3), 295-309.
- Van de Wiele, T.R.; Verstraete, W.; Siciliano, S.D. Polycyclic aromatic hydrocarbon release from a soil matrix in the in vitro gastrointestinal tract. *J. Environ. Qual.* **2004**, 33, 1343-1353.
- Vuorinen, P.J.; Keinänen, M.; Vuontisjärvi, H.; Baršienė, J.; Broeg, K.; Förlin, L.; Gercken, J.; Kopecka, J.; Köhler, A.; Parkkonen, J.; Pempkowiak, J.; Schiedek, D. Use of biliary PAH metabolites as a biomarker of pollution in fish from the Baltic Sea. *Mar. Pollut. Bull.* **2006**, 53, 479-487.
- Wang, J.; Chen, Z.; Chen, B. Adsorption of polycyclic aromatic hydrocarbons by graphene and graphene oxide nanosheets. *Environ. Sci. Technol.* **2014**, 48, 4817-4825.
- Wang, Z.; Zhao, J.; Song, L.; Mashayekhi, H.; Chefetz, B.; Xing, B. Adsorption and desorption of phenanthrene on carbon nanotubes in simulated gastrointestinal fluids. *Environ. Sci. Technol.* **2011**, 45, 6018-6024.
- Xia, X.; Chen, X.; Zhao, X.; Chen, H.; Shen, M. Effects of carbon nanotubes, chars, and ash on bioaccumulation of perfluorochemicals by *Chironomus plumosus* Larvae in Sediment. *Environ. Sci. Technol.* **2012**, 46, 12467-12475.
- Yang, K.; Xing, B. Desorption of polycyclic aromatic hydrocarbons from carbon nanomaterials in water. *Environ. Poll.* **2007**, 145, 529-537.

Zhang, L.; Wang, L.; Zhang, P.; Kan, A.T.; Chen, W.; Tomson, M.B. Facilitated transport of 2,2',5,5'-Polychlorinated Biphenyl and phenanthrene by fullerene nanoparticles through sandy soil columns. *Environ. Sci. Technol.* **2011**, 45, 1341-1348.

Zhang, S.; Shao, T.; Bekargolu, S.S.K.; Karanfil, T. The impacts of aggregation and surface chemistry on carbon nanotubes on the adsorption of synthetic organic contaminants. *Environ. Sci. Technol.* **2009**, 43, 5719-5725.

Zhao, J.; Wang, Z.; Zhao, Q.; Xing, B. Adsorption of phenanthrene on multilayer graphene as affected by surfactant and exfoliation. *Environ. Sci. Technol.* **2014**, 48, 331-339.

Zhu, D.; Pignatello, J.J. Characterization of aromatic compound sorptive interactions with black carbon (charcoal) assisted by graphite as a model. *Environ. Sci. Technol.* **2005**, 39, 2033-2041.

Zindler, F.; Glomstad, B.; Altin, D.; Liu, J.; Jenssen, B.M.; Booth, A.M. Phenanthrene bioavailability and toxicity to *Daphnia magna* in the presence of carbon nanotubes with different physicochemical properties. *Environ. Sci. Technol.* **2016**, 50, 12446-12454.

CHAPTER THREE

CHARACTERIZATION AND MODELING THE ADSORPTION- BIOAVAILABILITY RELATIONSHIP OF PAHS BY MWCNTS

3.1 Introduction

With the growing use of carbon nanomaterials (CNMs) in consumer products and inevitable release into the environment, it has become increasingly important to understand how these materials interact with various environmental components. Due to their strong adsorption affinity for organic molecules, including both natural organic matter and anthropogenic chemicals, it is not surprising that they can alter the fate and transport of organic materials in various environmental compartments (Hofmann and von der Kammer, 2009; Zhang et al., 2011; Wang et al. 2012). Of particular concern is the potential of CNMs to alter the bioavailability of adsorbed compounds to organisms (Baun et al., 2008).

The adsorption of organic contaminants by CNMs, such as carbon nanotubes and graphene, has been found to largely be reversible in aquatic systems (Yang and Xing, 2007). As such, transport of CNM-adsorbed contaminants is dependent on the strength of adsorption and the rate of desorption (Hofmann and von der Kammer, 2009). Similarly, the influence of carbon nanotubes (CNTs) on the bioavailability of adsorbed contaminants is attributed to their adsorption behavior (Ferguson et al., 2008; Xia et al., 2012). In recent years, studies have used bioconcentration and biota-sediment factors to help describe the bioavailability of CNM-adsorbed contaminants with variable success (Ferguson et al., 2008; Peterson et al., 2009). The bioconcentration factor (BCF), defined as the uptake of a chemical into the organism via absorption from just the surrounding water, assumes that only the freely dissolved fraction is bioavailable (Voutas et al. 2002; Peterson et al., 2009). For sediment ingesting organisms, the biota-sediment accumulation factor (BSAF) describes the uptake of the compound from the sediment assuming that adsorption/absorption equilibrium has been reached (Ferguson et al.,

2008). It is generally assumed that the sequestered or adsorbed fraction of contaminant is not bioavailable unless it desorbs; thus by understanding the adsorption/ desorption behavior, resulting bioavailability should be relatively predictable (Alexander, 2000; Gomez-Laho and Ortega-Calvo, 2005; Beckles et al., 2007).

The use of predictive models to estimate bioavailability of contaminants adsorbed to soil or sediment has been useful in decreasing the costs of risk assessments and providing enhanced understanding on abiotic and biotic interactions of contaminants in the environment. However, a massive amount of data is required to establish such relationships for CNMs. Although several studies exist that have examined the influence of various CNMs on the bioavailability and toxicity of a range of contaminants, there is still a gap in understanding the mechanism driving the bioavailability of CNM-adsorbed molecules. In recent years, the understanding of the adsorption behavior of carbon nanomaterials, particularly carbon nanotubes (CNTs), has drastically advanced. QSAR (quantitative structure activity relationship) and LSER (linear solvation energy relationship) models have been shown to have high accuracy in predicting the adsorption of a wide range of organic contaminants to CNTs where the adsorption descriptors are initially established from adsorption isotherms (Apul et al., 2012a; Xia et al., 2010; Zhao et al., 2014). As studies have also found good correlations between bioaccumulation of chemicals adsorbed to sediment and the experimental established adsorption/desorption isotherms (Lawrence et al., 2000), the potential to use adsorption isotherms to describe the bioavailability of CNM-adsorbed organic contaminants is promising.

In this study, a systematic approach was used to characterize the relationship between adsorption and resulting bioavailability of polycyclic aromatic hydrocarbons (PAHs) adsorbed to multi-walled carbon nanotubes (MWCNTs). The goal was to establish a more holistic understanding of the mechanisms controlling bioavailability of CNM-adsorbed organic contaminants and improve our ability to predict the biological impacts of CNMs. A suite of

seven PAHs ranging in hydrophobicity, size, ring configuration and molecular structure were used in this study to assess the influence of adsorbate physicochemical characteristics on the adsorption-bioavailability relationship. Traditional linear free energy relationships (LFER) and generalized regression modeling techniques were used to gain insight into the predominant adsorption interactions of planar aromatics by MWCNTs. Multiple linear regression analysis was used to develop a model describing the bioavailability of the MWCNT-adsorbed PAHs given the experimentally measured adsorption descriptors.

3.2 Materials and Methods

3.2.1 Materials

Seven polycyclic aromatic hydrocarbons (PAHs) were used in this study: naphthalene (NAP), 99+% purity from Alfa Aesar; acenaphthene (ACE), 99% purity, fluorene (FLO), 98% purity, and pyrene (PYR), 98% purity, from Sigma-Aldrich; phenanthrene (PHEN), 97% purity, and anthracene (ANT), 99% purity from ACROS Organics; fluoranthene (FLU), 98% purity, from ULTRA Scientific. Physicochemical properties of PAHs are presented in Appendix A (Table A1). Stock solutions were prepared in HPLC grade methanol.

Multi-walled carbon nanotubes (MWCNTs) were purchased from Nanostructured & Amorphous Materials (Houston, TX) and suspended in moderately hard water with 2 mg C/L natural organic matter (NOM) via sonication (Branson 450 digital sonifier affixed with 0.5 microtip) at 60 watts for 1 hour (Linard et al., 2015). Concentration was measured via visible light absorbance at 800 and 660 nm for MWCNT and GN solutions, respectively, using a Molecular Devices Spectramax 190 microplate spectrophotometer (Hyung and Kim, 2008; Lotya et al. 2008). Mass based calibration curves of MWCNTs in solution are supplied in Appendix B (Figure B3). The final solution ratio of MWCNT to dissolved organic carbon was 1.5 to 2 mg/L. Characterization data of MWCNT as received and after preparation with the NOM are summarized in Appendix B (Table B1). Morphological characteristics, i.e. diameter, and length

were verified or determined via transmission electron microscopy (Hitachi HD-9500 or H-7600) in conjunction with image analysis software (Image Pro) (Figure B1). For surface characterization, MWCNT solutions were centrifuged 4 hours at 1000 x g. Sedimented MWCNT were dried in a desiccator at 30°C for ~ 72 h. Nitrogen adsorption of the MWCNTs was performed with a physisorption analyzer (Micromeritics) at 77K before and after MWCNT adsorption of dissolved organic carbon. Surface area, pore volume and pore size distribution of the MWCNTs was calculated from the nitrogen adsorption isotherms with the use of Brunaur-Emmett-Teller (BET) equation, the Barrett-Joyner-Halendea (BJH) equation, and the density functional theory model (DFT) respectively (Zhang et al. 2009).

Suwannee River NOM collected from near the Suwannee River Visitor's Center (Fargo, GA) had a dissolved organic carbon concentration of 64 mg C/L, determined using a Shimadzu total organic carbon analyzer and had a specific ultraviolet absorbance (SUVA₂₅₄) value of 4.08 L mg⁻¹m⁻¹. All solutions were prepared in moderately hard water following the U.S. Environmental Protection Agency standard recipe; 96 mg/L NaHCO₃, 60 mg/L CaSO₄, 60 mg/L MgSO₄, 4 mg/L KCl in 18 mega-ohm Millipore Milli-Q water.

3.2.2 Adsorption Isotherms

Batch aqueous phase adsorption isotherms were run in triplicate for each PAH in moderately hard water (MHW) containing 2 mg C/L NOM. Glass centrifuge tubes containing 1.5 mg/L MWCNT suspension affixed with aluminum-foil-lined Teflon caps were spiked with PAH stock solution. Isotherm vials were allowed to come to equilibrium on a bench top shaker table at 200 rpm at room temperature (25°C ± 1°C) for 96 hours (preliminary tests showed that equilibrium was reached within 24-48 hours). Initial PAH concentrations of NAP, ACE, FLO, PHEN, ANT, FLU, and PYR ranged from 5-1000, 1-250, 1-200, 5-400, 0.25-40, 1-200, and 1-100 µg/L, respectively. Vials without CNMs were identically prepared to serve as positive controls; controls for the entire system were spiked with methanol only. After equilibrium was

reached, vials with and without CNM were centrifuged (Eppendorf 5804 R) at $\sim 1500 \times g$ for 1 hour to sediment any CNM agglomerates that may have formed during tumbling. The remaining supernatant was analyzed in black polystyrene 96-well plates with Molecular Devices Gemini fluorescence microplate reader at excitation/emission wavelengths 276/330, 285/330, 260/310, 250/363, 252/399, 280/440 and 270/390 nm for NAP, ACE, FLO, PHEN, ANT, FLU and PYR, respectively. Fluorescence of CNM-adsorbed PAHs is statically quenched due to PAHs acting as π -donors when interacting with graphitic materials, thus the remaining unbound PAH concentration in the aqueous solution could be determined via fluorescence intensity (Singh et al. 2011; Debnath et al. 2010; Kukkonen and Pellinen, 1994). Analysis of a methanol rinse of positive control vials showed minimal loss of PAHs due to sorption to vial walls. CNM sorption of all PAHs was calculated as differences in aqueous PAH concentration between positive controls and CNM samples using fluorescent standard curves developed for each PAH in the background solution containing 2 mg/L NOM. Temperature, pH, and ionic strength were controlled across each experiment and reflected minimal change.

3.2.3 Isotherm Modeling

Experimental isotherm data were fit with four non-linear models that have been commonly used to investigate the adsorption behavior of PAHs by CNMs, activated carbon and black carbon (Kah et al., 2011). The equations and parameters are presented in Table 3.1. The Freundlich model (FM) assumes a heterogenous distribution of adsorption sites, whereas the Langmuir model (LM) assumes a homogenous distribution of adsorption sites with a finite number sites. Like the LM, the dual-Langmuir model (DLM) also assumes a finite number of adsorption sites with a maximum adsorption capacity although two types of adsorption sites are considered (i.e. high and low-energy) (Kah et al., 2011; Yang et al., 2006). The Polyani-Manes model (PMM) assumes that adsorption is related to the distance the molecule is from the adsorbent surface (i.e. adsorption space) and the attractive forces between the adsorbate and

adsorbent (i.e. adsorption potential) (Yang et al., 2006). The goodness of model fit was analyzed by the correlation coefficients (R^2) and residual root mean square error (RMSE).

Table 3.1. Nonlinear sorption models used to fit adsorption isotherms of all PAHs to MWCNTs.

Model	Equation	Parameters
Freundlich (FM)	$q_e = K_F * C_e^{1/n}$	$K_F[(\text{mg/g})/(\text{mg/L})^{1/n}]$, Freundlich affinity coefficient; $1/n$, Freundlich exponential coefficient
Langmuir (LM)	$q_e = (q_{\max} * K_L * C_e) / (1 + K_L * C_e)$	$K_L(\text{L/mg})$, Langmuir affinity coefficient; $q_{\max}(\text{mg/g})$, maximum adsorbed capacity
Polyani-Manes (PMM)	$\log q_e = \log q_{\max} + a * (C_{\text{sw}}/V_s)^b$ $C_{\text{sw}} = RT * \ln(C_s/C_e)$	$q_{\max}(\text{mg/g})$, maximum adsorbed capacity; $C_{\text{sw}}(\text{J/mol})$, effective adsorption potential; $C_s(\text{mg/L})$, adsorbate water solubility $V_s(\text{cm}^3/\text{mol})$, molar volume of solute; $a[(\text{cm}^3)^{b+1}/(\text{mol J}^b)]$ and b , fitting parameters; $R [8.314 \text{ J/(K mol)}]$, universal gas constant; $T(\text{K})$, absolute temperature
Dual-Langmuir (DLM)	$q_e = [(q_{\max 1} * K_{L1} * C_e)/(1 + K_{L1} * C_e)] + [(q_{\max 2} * K_{L2} * C_e)/(1 + K_{L2} * C_e)]$	$q_{\max 1}(\text{mg/g})$ and $q_{\max 2}(\text{mg/g})$, maximum adsorbed capacity of site population 1 and 2; $K_{L1}(\text{L/mg})$ and $K_{L2}(\text{L/mg})$, affinity coefficient of site populations 1 and 2

*For all models, q_e (mg/g) and C_e (mg/L) represent the adsorbed concentration and aqueous concentration, respectively, of PAH at equilibrium.

3.2.4 LFER Modeling

Single point adsorption descriptors, $\text{Log } K_d$ (i.e. q_e/C_e) can be described by linear free energy relationship (LFER) model in the form:

$$\text{Log } K_d = c + rR_i + p\pi_i + a\alpha_i + b\beta_i + vV_i \quad (3.1)$$

Where R_i , π_i , α_i , β_i , and V_i are the molecular descriptors for the i th adsorbate from the list of PAHs used in this study. c is the regression constant, R is the excess molar refractivity calculated from refractive index using the Lorenz-Lorentz expression (Pacak, 1988), π is polarizability, α is hydrogen bond donating ability (i.e. acidity), β is hydrogen bond accepting ability (i.e. basicity) and V is the molecular volume, reflective of London dispersion (Xia et al., 2010). These parameters are summarized in Appendix A (Table A1); hydrogen bond donating

ability was not included, because this value was zero for all PAHs (Schwarzenbach et al., 2003). The coefficients [r, p, b, v] of the LFER model were determined via multiple linear regression analysis using JMP Pro 12 software. The parameter value size is reflective of the relative contribution of the different molecular interactions occurring between the adsorbate and adsorbent (Xia et al., 2010). LFER models are concentration dependent, thus different models were developed for the dependent variable ($\text{Log } K_d$) at two concentrations, 1% and 10% PAH water solubility denoted as $\text{Log } K_{0.01}$ and $\text{Log } K_{0.1}$, respectively. Individual model parameters were assessed to determine if the true coefficient was significantly different from zero using an alpha value of 0.05. Parameters were considered to have a significant influence on the dependent $\text{Log } K_d$ value when p-values were less than 0.05 and variance inflation factor (VIF) values were <10 .

Training data sets were obtained from the experimental adsorption isotherms and were internally validated using prediction error sum of squares (PRESS) values that operate by using a Leave-One-Out technique. The models were externally validated using the experimental obtained adsorption descriptors from later described bioavailability assays. The goodness of fit was measured via correlation coefficient (R^2), root mean squared error (RMSE), and PRESS values, where smaller PRESS values indicated a stronger predictability by the model than larger values (Apul et al., 2012). Multicollinearity among the independent variables was evaluated by the VIF where variables with VIF values > 10 indicated too high of correlation between the variables to distinguish the influences each independent variable has on the dependent variable (Belsley et al., 1980).

3.2.5 Bioavailability Assays

Adult *Pimphales promelas* (fathead minnows) weighing greater than or equal to 1 g wet weight were randomly selected from an established culture at Clemson University Cherry Farm Fish Facility for bioavailability assays. Test organisms were allowed to acclimatize for a

minimum of 7 days in the exposure aquaria where temperature was maintained at $25^{\circ}\text{C} \pm 1^{\circ}\text{C}$ with a 16/8 h light/dark photoperiod. Fish were fed a Tetramin mix to satiation daily during the acclimatizing period and starved 24 hours prior to and during exposures to minimize the effect of feeding variation between individuals (Vuorinen et al., 2006; Linard et al. 2015). All exposures were static, non-aerated and conducted for a total of 16 hours in a background solution of moderately hard water containing 2 mg C/L NOM (hardness = 100 mg/L as CaCO_3 ; alkalinity = 60 mg/L as CaCO_3 ; pH = 8.0). Water quality and fish behavior were monitored throughout the duration of the experiment with full water changes every 4 hours. Mortality was rare (<1%) and random across all treatments and controls, indicating that concentrations of neither MWCNTs nor PAHs used during this study were at a level to cause an acute adverse effect for the organisms.

All exposures were run in replicates with ~4 fish per aquaria where the average response per tank per treatment was considered a single measurement unit. Fish were exposed to a range of concentrations in the background solution to establish dose-response relationships for each PAH which are shown in Appendix C (Figure C1). Preliminary tests comparing the response of fish in control treatments with and without MWCNT solution were not different indicating that the change in response was directly related to the change in PAH concentration taken up by the organism. Therefore, bioavailability assays consisted of three distinct treatments: 1) *control*, consisting of background solution only; 2) *PAH only*, the background solution spiked with a predetermined concentration of each PAH; and 3) *PAH and MWCNT*, identically prepared to “*PAH only*” treatments with the addition of 1.5 mg/L of suspended MWCNT. Treatments 2 and 3 were conducted at two different concentrations for each PAH at a relative “low” and “high” Log K_d (i.e. 5 and 40 $\mu\text{g/L}$ NAP; 10 and 100 $\mu\text{g/L}$ ACE; 20 and 80 $\mu\text{g/L}$ FLO; 10 and 70 $\mu\text{g/L}$ PHEN; 2.5 and 15 $\mu\text{g/L}$ ANT; 5 and 25 $\mu\text{g/L}$ FLU; 2.5 and 15 $\mu\text{g/L}$ PYR). Solutions for each treatment were tumbled in 4L amber glass containers on a rotary tumbler to reach equilibrium

prior to fish exposure. Water samples from each exposure were collected at the beginning and end of each water renewal; analysis of water samples verified the treatment PAH concentrations throughout duration of the exposure.

At the end of each exposure, fish were euthanized, the gallbladder harvested, and the collected bile analyzed for PAH metabolites to determine the bioavailable fraction of PAH in the system. Due to highly efficient metabolism of PAHs by fish, the bioaccumulation potential of these compounds in traditionally monitored tissues such as muscles is typically low and are instead concentrated in the gallbladder for later excretion (Beyer et al., 2010; Bleeker & Verbuggen, 2009). Because most PAHs have distinct fluorometric properties, metabolites can be easily detected and identified at discrete excitation/emission wavelengths in complex matrices like bile (Beyer et al., 2010; Aas et al., 2000). Collected bile was less than 10 μ l and for fish exposed to FLO, PHEN, ANT, FLU and PYR was initially diluted to 1:15 with Millipore Milli-Q water; bile from fish exposed to NAP and ACE was only diluted to 1:5 with Millipore Milli-Q water. Bile samples from fish exposed to NAP or ACE were further diluted with 100% MeOH to a final dilution of 1:50 and analyzed via an HPLC (Waters-Breeze) with a UV-fluorescence detector. Bile samples from fish exposed to the other five PAHs were diluted with a 50:50 MeOH:H₂O solution and analyzed in a black 96-well plate using a Molecular Devices Gemini fluorescence microplate reader (i.e. final dilution of bile containing metabolites of FLO or PHEN = 1:300; ANT or FLU = 1:200; and PYR = 1:800). The following excitation/emission wavelengths were used to detect NAP, ACE, FLO, PHEN, ANT, FLU and PYR metabolites, respectively, 276/330, 285/330, 260/310, 250/363, 252/399, 280/440, and 270/390.

Dose-response relationships showed a linear correlation between PAH exposure and bile fluorescence intensity for the concentrations used (Figure C1); therefore, change in bile fluorescence was directly related to change in PAH bioavailability. As such, concentration of the PAH in the bile could be calculated as PAH equivalents using calibration curves of PAHs in the

same background solution used to analyze the bile fluorescence (Torreiro-Melo et al 2015). Calibration curves, where relative fluorescence units (RFUs) as a function of PAH concentration, are expressed as linear equations summarized in Appendix C (Table C1). The average bile fluorescence observed in fish exposed to the PAHs was corrected by subtracting the average bile fluorescence of the control fish from the same replicate. The corrected bile response in RFUs was then converted to the PAH equivalent concentration using the developed calibration curves and correcting for the dilutions made to analyze the samples.

Using the PAH equivalent concentration calculated in bile samples allowed for a bile bioconcentration factor (BCF_{bile}) to be established. BCF_{bile} were calculated as the ratio between the concentration of PAH in the bile (PAH_{bile}) compared to the concentration of the PAH in water concentration (PAH_{water}) as represented by the following equation (Torreiro-Melo et al., 2015):

$$BCF_{bile} = \frac{PAH_{bile}}{PAH_{water}} \quad (3.2)$$

3.2.6 Statistical Analysis and Model Development

All statistical tests and model development were performed using JMP Pro 12 software, SAS Institute Inc. Multiple regression techniques were used to characterize the influence of PAH physicochemical characteristics and concentration effects on adsorption of PAHs by MWCNTs. Linear regression and linear squared contrasts were used to compare predicted fish responses to actual fish responses in bioavailability assays. Analysis of variance (ANOVA) followed by Student's T test were used to compare response of fish across all treatments for a single PAH; linear squared contrasts were used to compare differences between treatments across the different PAHs. Analysis of covariance (ANCOVA) was used to assess the influence of categorical covariants, structure and aromatic character, on bioavailability. Two-tailed mean hypothesis testing was used to determine if bioavailability indices differed from 1 for each

PAH_MWCNT combination. Shapiro-Wilk's test was used to test normality of bile fluorescence residuals; Brown and Forsythe test was used to test homogeneity of variance within treatments. Unless otherwise denoted, the significance level of all tests was set at 0.05.

Multiple linear regression techniques were used to develop a model that describes the relationship between bioavailability (i.e. the concentration of PAH taken up into the bile as compared with the total system PAH concentration) and adsorption ($\text{Log } K_{\text{MWCNT}}$). Data from the 42 independent bioavailability assays were randomly and evenly split into a training and validation data set. The bioavailability model was developed from the training data set. Adaptive least absolute shrinkage and selection operator (A-LASSO) allowed for simultaneous estimation and variable selection by using a regularization parameter such that coefficients associated with non-informative variables are penalized and shrunk towards zero as the model is optimized. The advantage of A-LASSO is that by using adaptive weights to penalize coefficients differently and using different regularization for each coefficient, overfitting the model is avoided (Zou, 2006). Individual selected parameters were assessed to determine if the true coefficient was significantly different than zero; coefficients with a p-value less than 0.05 were considered significant. The degree of collinearity among the independent variables was evaluated by the variation inflation factor (VIF). Variables with VIF values greater than 10 were considered evidence of multicollinearity issues, and these variables were omitted. Correlation among the independent variables used in the model (i.e. multicollinearity) can lead to issues in terms of the values and variance associated with the estimated coefficients for each independent variable. Specifically, it reduces the ability to accurately determine the influences that each independent variable has on the dependent variable (Belsley et al., 1980).

Overall evaluation of the developed models and the selected variables was evaluated using the adjusted R-squared value, Bayesian information criterion (BIC), and K-fold cross validation R-squared. Smaller BIC values indicate the model that has the best balance between a

better fit and the number of independent variables. Adjusted R-squared also gives information on the best number of independent variables to use to fit the data (Anderson-Sprecher, 1994). K-fold cross validation involves the division of the sample set into k subsets where all but one of k subsets is used as training data to develop a model and predict the subset left out. The higher the average R-squared computed across each of these trials left out subsets indicates a higher prediction accuracy of the model. An additional measure of cross-validation of the model was done using the prediction error sum of squares (PRESS), where each data point is removed from the data set and then predicted using the model refitted in its absence. A change of less than 10% in the sum of squares (SSE) and RMSE from all the resulting prediction errors compared to the full models SSE and RMSE is indicative of good predicting capabilities of the full model (Tarpey, 2000). PRESS was also used to compare between multiple model candidates, where the lower PRESS values suggest higher prediction capabilities (Apul et al., 2013). The predictive precision of the model for the validation data set was evaluated by the correlation coefficient (R^2) and RMSE.

3.3 Results and Discussion

3.3.1 Adsorption Isotherm Modeling.

The single-solute adsorption isotherms were fit with the nonlinear isotherm models, Freundlich (FM), Langmuir (LM), Polanyi-Manes (PMM), and dual-Langmuir models (DLM) (Figure 3.1). The respective fitting parameter estimates are given in Table 3.2. In most cases, all the nonlinear models appeared to fit the experimental data well with R^2 values typically between 0.90 and 0.98. However, it was observed that LM and DLM model estimation deviated substantially from the experimental data at low concentrations (Figure 3.1B and 3.1D). Given the deviation of LM and DLM fits of the experimental data, the adsorption process was not characterized by a monolayer formation on a homogenous surface (i.e., LM) and it was not limited to just high and low-energy adsorption sites (i.e., DLM) (Yang et al., 2006). FM and

PMM fits of the experimental data yielded similar R^2 values that were generally higher than LM or DLM for all PAHs except for FLO. The slightly better fit of FLO experimental data by LM was not statistically different from FM or PMM fits. It is not surprising that the FM and PMM similarly fit the experimental adsorption data, as the models become the same with the PMM fitting parameter $b = 1$ (Yang et al., 2006). Figure 3.1A shows that the curvature of the isotherms is still observed even when on a logarithmic scale indicating that though the FM fits the data well, it oversimplifies the adsorption behavior of PAHs to MWCNTs over a wide concentration range (Kah et al., 2011). Similar to Yang et al. (2006), the data appear to be best fit by the PMM; even with three fitting parameters the PMM had lower RMSE values for all the isotherms than FM (Table 3.2).

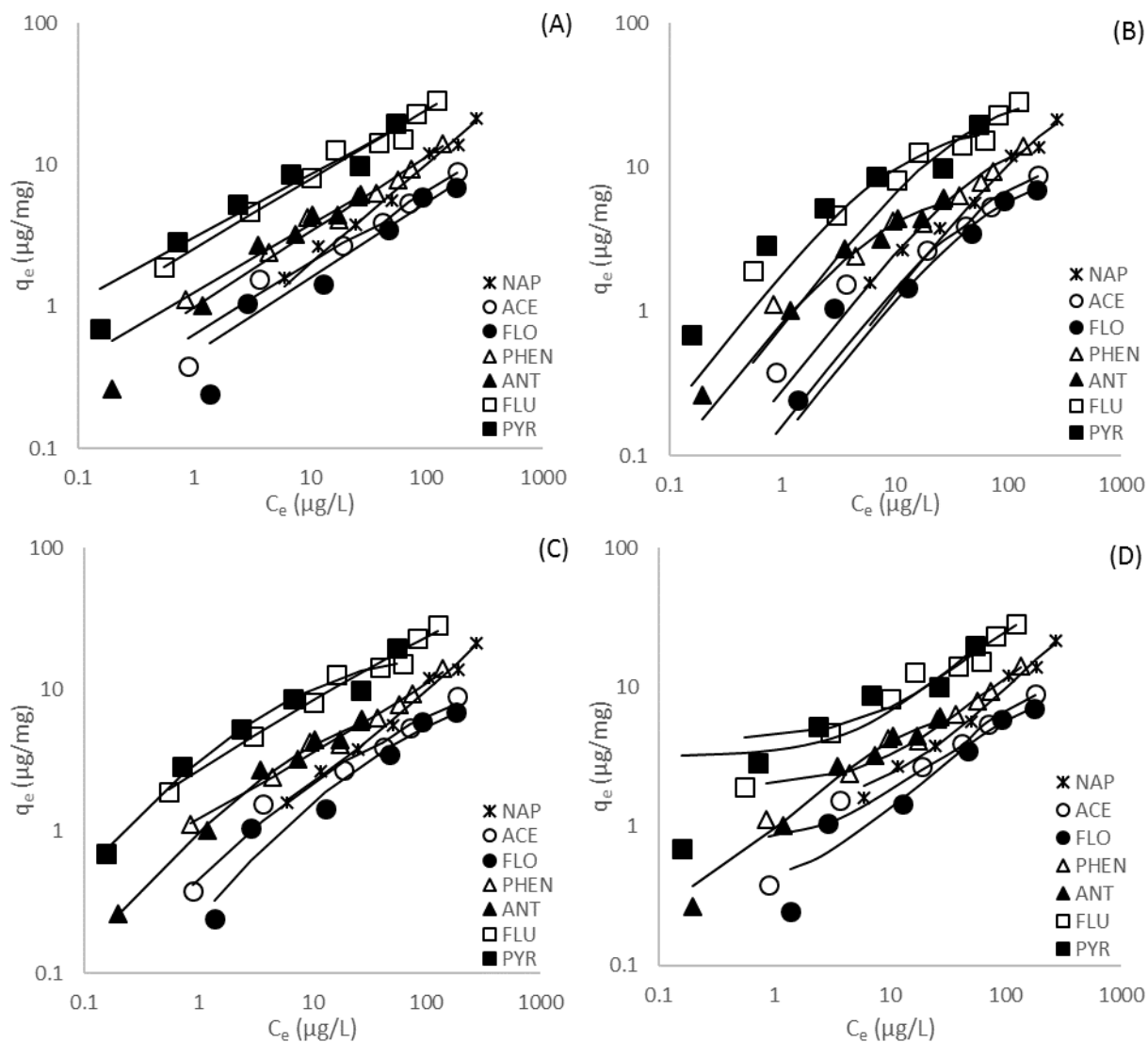


Figure 3.1. Adsorption isotherms of PAHs fit with the A) Freundlich model, B) Langmuir model C) Polyani-Manes model, and D) Dual-Langmuir model. C_e = the equilibrium aqueous concentration; q_e = the adsorbed concentration per mg MWCNT

Table 3.2. Fitting parameters of nonlinear models to adsorption isotherms of PAHs on MWCNT

Freundlich Model (FM)						
	K _F (mg/g)/(mg/L) ^{1/n}	1/n	RMSE	R ²		
naphthalene	51.19±6.70	0.70±0.07	1.24	0.976		
acenaphthene	20.79±1.12	0.50±0.022	0.215	0.996		
fluorene	18.31±2.90	0.53±0.068	0.494	0.975		
phenanthrene	38.87±3.87	0.533±0.036	0.586	0.982		
anthracene	34.27±8.766	0.479±0.0599	0.424	0.966		
fluoranthene	74.98±13.82	0.489±0.0665	2.17	0.950		
pyrene	65.89±20.53	0.444±0.086	1.96	0.933		
Langmuir Model (LM)						
	q _{max}	K _L	RMSE	R ²		
naphthalene	43.69±14.17	3.14±1.63	1.49	0.970		
acenaphthene	12.22±1.75	13.27±4.20	0.597	0.981		
fluorene	10.13±1.43	13.10±4.28	0.438	0.984		
phenanthrene	19.53±3.57	14.703±5.305	1.14	0.951		
anthracene	7.36±0.906	126.57±40.513	0.436	0.962		
fluoranthene	33.94±7.08	24.13±12.6	3.18	0.909		
pyrene	19.7±4.47	101.297±73.42	2.86	0.868		
Polyani-Manes Model (PMM)						
	Log q _{max}	a	b	RMSE	R ²	
naphthalene	4.44±4.7	-0.33±1.45	0.51±0.66	0.054	0.977	
acenaphthene	1.11±0.24	-1.06e-4±3.65e-4	1.929±0.672	0.088	0.975	
fluorene	0.995±0.4	-1.47e-4±8.68e-4	1.9±1.18	0.171	0.976	
phenanthrene	1.71±0.34	-0.035±0.050	0.842±0.27	0.048	0.983	
anthracene	0.799±0.06	-1.36e-3±1.27e-3	1.523±0.20	0.056	0.968	
fluoranthene	1.53±0.112	-7.78e-3±9.3e-3	1.11±0.25	0.066	0.943	
pyrene	1.21±0.102	-1.38e-4±3.10e-4	1.973±0.479	0.105	0.867	
Dual Langmuir Model (LM)						
	Q _{max1}	KL ₁	Q _{max2}	KL ₂	RMSE	R ²
naphthalene	73.7±101.3	1.29±2.53	1.40±2.91	-2.66e6±1.08e11	1.64	0.970
acenaphthene	13.36±2.7	8.254±4.62	0.7532±0.755	-2.66e6±8.13e9	0.514	0.930
fluorene	10.51±2.3	0.01±7.34e-3	0.345±0.956	-2.66e6±3.31e10	0.527	0.973
phenanthrene	31.21±13.5	4.53±3.27	1.897±0.81	-2.66e6±3.74e9	0.584	0.958
anthracene	7.46±1.3	106.37±87.54	0.22±1.18	-7.42e5±6.28e8	0.301	0.902
fluoranthene	61.75±57.3	5.024±7.64	4.178±3.15	-2.66e6±4.33e9	3.024	0.924
pyrene	80.18±328.3	4.58±23.558	3.13±2.89	-2.66e6±1.64e9	3.257	0.906

It has been suggested that the PMM is appropriate for describing both pore filling and adsorption to the surface of MWCNTs, which is supported by both FM and PMM fitting the

experimental data well (Yang et al., 2006). Commonly, a correlation curve has been used to assess the ability of PMM to describe the adsorption process, where adsorbed volume (q_v) is plotted as a function of adsorption potential that has been normalized by the adsorbate's molar volume (C_{sw}/V_s). For a single adsorbent, correlation curves should be the same for all adsorbates under the assumptions i) adsorption sites are accessible to all the adsorbates such that no molecular sieving is occurring and ii) only the adsorbates' molar volume will affect adsorption irrespective of other physicochemical properties (Yang et al., 2006; Yang and Xing, 2010). The correlation curves of NAP and ANT significantly deviated from those of ACE, FLO, PHEN, FLU and PYR, which largely fell on a single curve (Figure 3.2). This indicates that though size of the adsorbate molecules is important in influencing adsorption, it does not fully describe the differences in adsorption behavior between the different PAHs. In an attempt to collapse the correlation curves onto a single line, normalizing factors related to the adsorbate's properties such as polarizability, hydrogen bond donating or accepting, etc. have been used to adjust or replace the molar volume term (Manes et al. 1998; Crittenden et al. 1999). In many cases even such adjusting factors were not enough to obtain a single correlation curve (Yang and Xing, 2010). Similarly, the correlation curves of the PAHs in the study could not be collapsed onto a single line by adjusting molar volume nor normalizing the adsorption potential with the PAHs physicochemical properties such as H-bond accepting, polarizability, refractive index, etc (data not shown).

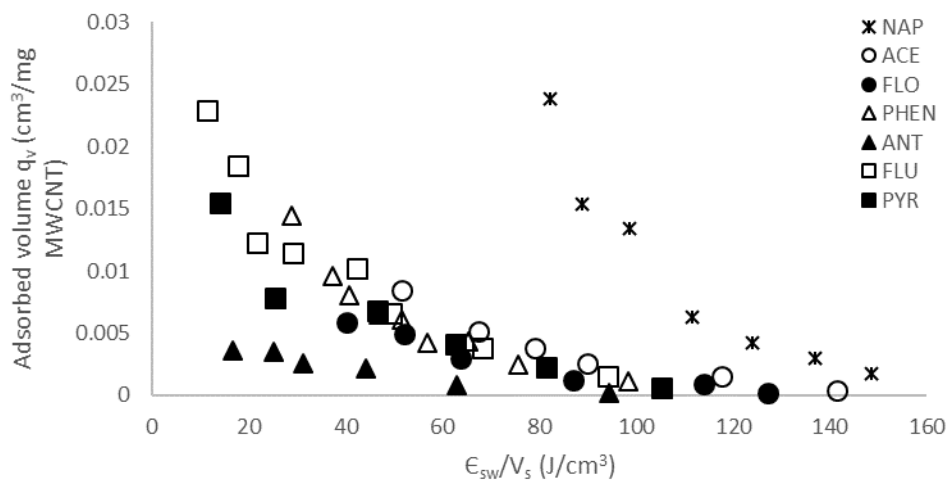


Figure 3.2. Correlation Curve of PAHs adsorbed to MWCNTs. q_v = the adsorbed volume of PAH and ϵ_{sw}/V_s = adsorption potential normalized by PAH molecular volume.

The fitting parameters of the PMM influence the shape of the isotherms and can provide some insight into the observed adsorption behavior (Yang and Xing, 2010) (Table 3.1). The maximum adsorption capacity of the adsorbent, represented by $\text{Log } q_{\max}$, is related to the adsorbent's properties and the available adsorption sites. The fitting parameter b has been suggested to relate to adsorption potential energy and describe the distribution of adsorption site energy (Yang and Xing, 2010). Adsorption potential, the energy required to remove the adsorbate from the attractive forces of the adsorbent's surface, is related to the distance of the adsorbate from the adsorbent surface and access to adsorption sites (Kah et al., 2011; Yang et al., 2006). The curvature of adsorption isotherms increase as the value of b increases beyond 1 and has been suggested to describe the transition of sorption occurring at a greater fraction of high energy adsorption sites compared to a greater fraction of adsorption occurring at the low energy sites (Yang and Xing, 2010). When $b=1$ the log-log plot of the adsorption isotherms is linear and the PMM becomes the same as the FM. Available adsorption space and ability of adsorbates to access the adsorption sites can be variable due to differences in adsorbate size and molecular

configuration (Yang and Xing, 2010; Apul et al., 2013). NAP had the highest $\text{Log } q_{\text{max}}$ (4.44) and lowest b value (0.51), supporting previous findings that the small size of NAP allowed it to better access high energy adsorption sites at higher equilibrium concentrations than other larger PAHs and indicated a pore filling mechanism (Wang et al., 2014; Sun et al. 2013). While there was no apparent correlation between fitting parameter b and the PAHs' physicochemical properties, b values were above 1 for all the PAHs except NAP and PHEN. The higher b values of ~ 2 for ACE, FLO and PYR, indicated lower adsorption energy and a decrease in adsorption at higher equilibrium concentrations (Yang and Xing, 2010). It may be that the bulkiness of PYR and the presence of non-aromatic rings in ACE and FLO affected the ability of these PAHs to access the adsorption space at the MWCNT's surface as well as the other PAHs (Yang and Xing, 2010; Bjork et al., 2010), although this needs to be further investigated. Due to the apparent difference in adsorption mechanisms NAP undergoes compared with the other PAHs, NAP adsorption data were excluded when assessing relationships between $\text{Log } q_{\text{max}}$ and PAHs physicochemical characteristics. Unlike Yang et al. (2006), no correlation was observed between PAH molecular size (\AA^3) or surface area and $\text{Log } q_{\text{max}}$, although a positive correlation did exist between PAH bulk molar volume (cm^3/mol) and $\text{Log } q_{\text{max}}$ ($R^2 = 0.85$). This may indicate a difference between the adsorbed phase and the respective bulk phase influenced adsorbed capacity (Yang et al., 2006). Both size and configuration of molecules influence their solid-phase density and as such they may orientate differently when in adsorbed phase vs bulk phase (Yang and Xing, 2010). Further, solubility can also influence adsorption capacity and cause isotherm curvature (Kah et al., 2011). This is likely why ANT had the lowest $\text{Log } q_{\text{max}}$; of the PAHs studied, ANT had the lowest solubility of $45\mu\text{g/L}$, which was quickly approached in the adsorption isotherms. Overall, assessment of the PMM model fitting suggests that isotherm curvature represented by the fitting parameter b , appears to be influenced by a combination of molecular size, configuration and the differences in bulk phase vs adsorbed phase.

3.3.2 Adsorption Mechanisms.

In Figure 3.3, single point adsorption descriptors (K_d) decreased with increasing equilibrium concentrations (C_e) further indicating a heterogenous adsorption process where the high energy sites were occupied first with strong affinity (Wang et al., 2014). Although Wang et al. (2014) observed that the equilibrium concentration (C_e) at which the isotherm transitioned from linear to nonlinear was related to a “turning point”, where single point K_d values ceased to increase with increasing C_e , this was not observed in the present study. However, the residuals of actual q_e plotted against model predicted q_e became significantly larger and more varied after surpassing 10 $\mu\text{g PAH/mg MWCNT}$ (Figure 3.4A). A similar trend was observed when the residuals were plotted against the estimated % surface area coverage of MWCNT by the PAH molecules, where there appeared to be a distinct threshold and the variation in residuals drastically increased after 50% surface area coverage had been reached (Figure 3.4B). Surface area coverage (%) was calculated assuming flat surface adsorption and the formation of a monolayer using the BET measured surface area of the MWCNTs (98m²/g) and the PAHs’ molecular area (Table A1). When the residuals were plotted against equilibrium concentration on a mass basis and as the concentration related to the PAHs water solubility, no trend or apparent threshold in residual variability was observed (Figure 3.4C and 3.4D). This suggests that the deviation of the model fit is related to the amount of PAH adsorbed as it relates to surface area coverage of the MWCNT.

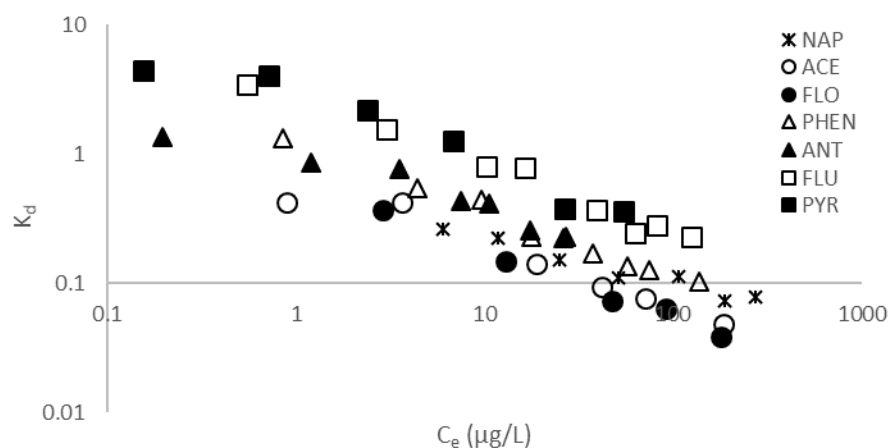


Figure 3.3. The relationship between single point adsorption descriptors (K_d) with the equilibrium concentration (C_e) of the PAHs by MWCNTs in log-log plot.

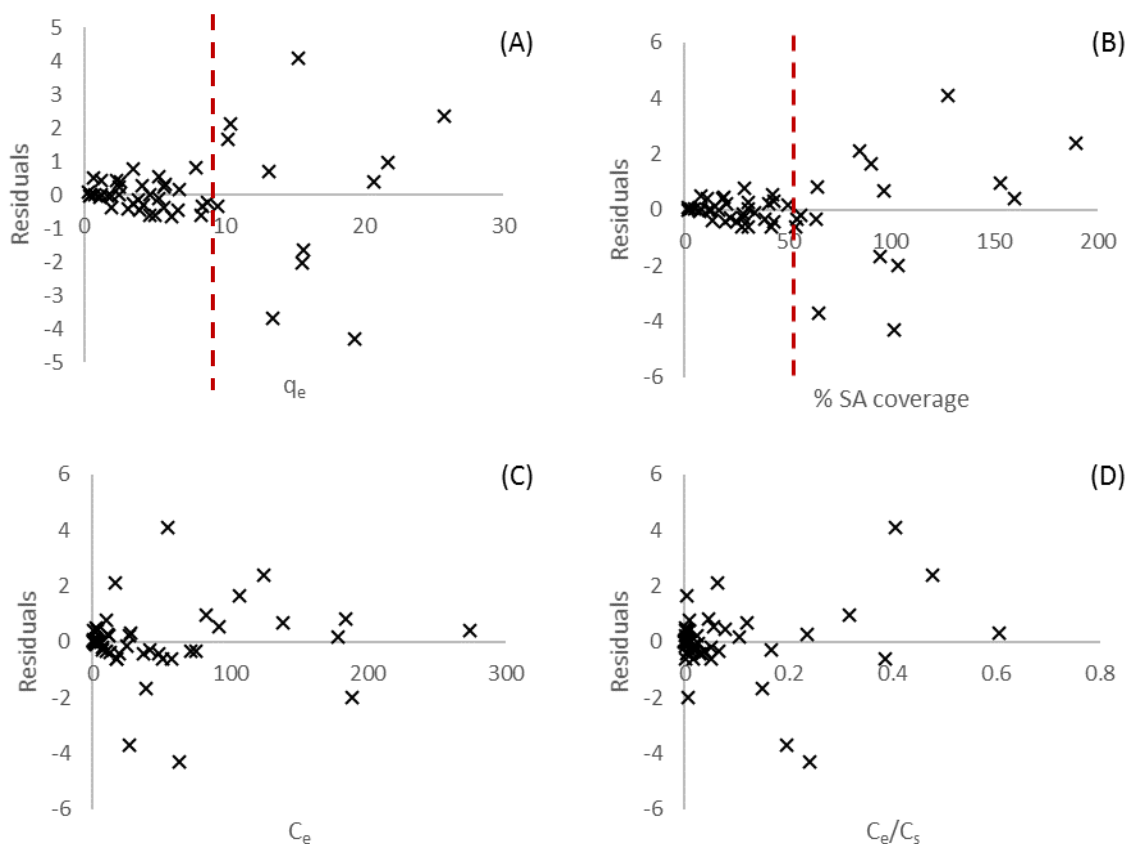


Figure 3.4. Residuals of predicted q_e vs actual q_e . Residuals are plotted against (A) adsorbed concentration (q_e), (B) % surface area coverage, (C) equilibrium concentration (C_e) and (D) relative solute concentrations (C_e/C_s) where C_s is the water solubility of individual PAHs. The red lines represent the apparent threshold where residual variation increases.

Adsorption isotherm curvature was further investigated by fitting the isotherms with the Freundlich model in two stages, above and below the isotherm transition point. In contrast to findings by Wang et al. (2014), there was little observed change in the model fit or the model parameters, indicating that the adsorption affinity above and below the point of isotherm curvature was not significantly different. The fitting parameters and goodness of fit of FM above and below the transition point are summarized in Appendix D, Table D1. The one exception is that the Freundlich $1/n$ value significantly decreased from the first stage of adsorption to the second stage (from 0.88 to 0.45; p -value = 0.0355) for ANT. Although Wang et al. (2014) attributed the change in FM $1/n$ value to a change in surface heterogeneity of the adsorbent due to adsorption of a greater concentration of the PAH, in this case it is more likely a product of the solubility limit being reached (Kah et al., 2011). ANCOVA was used to compare the isotherms of the different PAHs in log-log plots above and below the isotherm curvature point. Adsorption isotherms below the isotherm transition point were linear and had significantly different intercepts (p -value < 0.0001), although the slopes were the same indicating a similar adsorption mechanism for all the PAHs before the transition point. Above the transition point, only the isotherm of NAP had a distinctly different slope (p -value: 0.0360) compared with the other PAHs, where adsorption of NAP remained relatively linear while the other PAH isotherms became nonlinear. This supports that most of the PAHs are undergoing the same adsorption process, likely surface adsorption, while NAP may also be undergoing pore filling (Wang et al., 2014; Sun et al; Yang et al., 2006).

Regression analysis was used to assess the relationship of the isotherm transition point as a function of Freundlich model fitting parameters and PAH physicochemical characteristics. Due to the high adsorption capacity (K_F value), of the smallest PAH, NAP, there was not a well-defined correlation between K_F values and the equilibrium concentration at the transition point (C_e). However, the Freundlich exponent ($1/n$) was positively correlated with the equilibrium

concentration (C_e) at the isotherm transition point ($R^2 = 0.68$; p-value = 0.0234) and negatively correlated with PAH molecular surface area ($R^2 = 0.76$; p-value = 0.011). Additionally, the equilibrium concentration at which the isotherms changed slope was strongly correlated ($R^2 = 0.93$) with PAHs molecular surface area, where the smaller the molecule surface area the greater the concentration reached before the isotherm curvature point (Figure 3.5.A). The positive correlation between the adsorption descriptor calculated at the transition point (i.e. $\text{Log } K_d$) and molecular surface area, indicates that the PAH molecules have the same face-to face attachment orientation on the surface of MWCNT (Figure 3.5.B). As such, the larger molecules have a higher volume adsorption capacity and greater surface area coverage than the smaller molecules (Yang and Xing 2010). The relationship of the isotherm transition point with the FM fitting parameters indicates that though the adsorption sites were more heterogenous for the larger molecules, a greater equilibrium concentration was reached before the isotherm transitions to nonlinear for smaller molecules. Overall, the transition from linear to nonlinear adsorption is attributed to a concentration effect largely due to surface area coverage, where the high energy adsorption sites become saturated first (Yang and Xing, 2010; Wang et al., 2014). It is important to note that molecular size, configuration and solubility likely influence how PAHs adsorb and cover MWCNT surface.

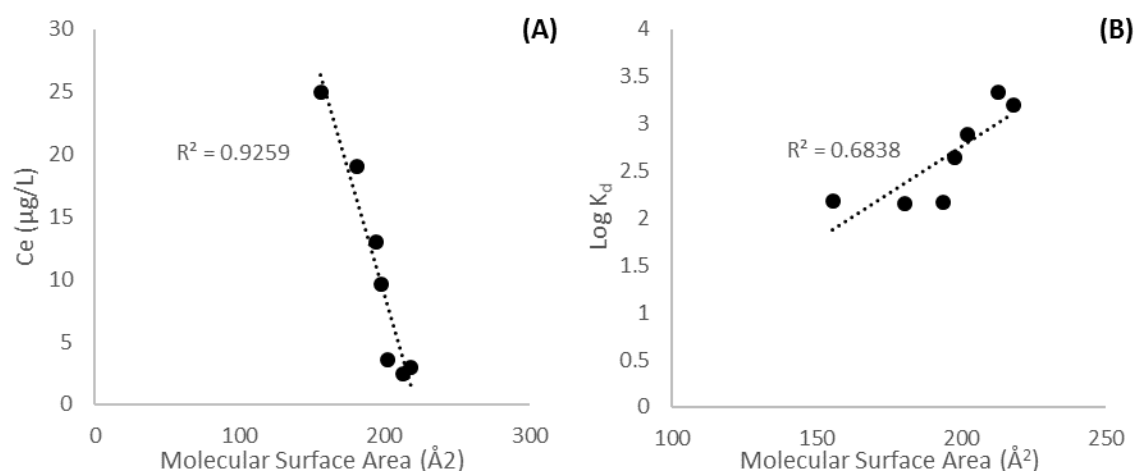


Figure 3.5. The relationship between PAH molecular surface area and (A) the equilibrium concentration and (B) calculated adsorption descriptor ($\text{Log } K_d$) at the isotherm curvature point.

3.3.3 Influence of Adsorbate Properties on Adsorption.

Multiple linear regression was used to initially assess the relationship between single point adsorption descriptors (K_d) and PAH physicochemical characteristics. The surface area coverage effect was taken into consideration by assessing this relationship at K_d values above and below the isotherm curvature point at $\sim 10\%$ and $\sim 40\%$ surface area coverage, respectively. In general, there was a stronger correlation observed between $\text{Log } K_d$ values and the PAH's physicochemical characteristics at lower surface area coverage (Figure 3.6). At low surface area coverage, $\text{Log } K_d$ was significantly influenced (i.e. $p\text{-value} < 0.05$) by PAH physicochemical characteristics in the following order: resonance energy $>$ hydrophobicity ($\text{Log } K_{ow}$) $>$ molecular surface area $>$ polarizability \geq HOMO-LUMO gap at low coverage with correlation coefficients (R^2) of 0.88, 0.81, 0.74, 0.65, and 0.63 respectively. At higher surface area coverage, resonance energy, hydrophobicity, and molecular surface area were still significant factors contributing to adsorption, but with lower correlation coefficients (R^2) of 0.77, 0.62, and 0.54, respectively. There is no longer a significant correlation between polarizability nor HOMO-LUMO gap and

Log K_d . Polarizability of PAHs gives an indication of π -electron density (Zhu et al., 2005) while HOMO-LUMO gap of PAHs gives an indication of molecular stability due to electron delocalization, a product of molecular structure and aromatic character (Aihara, 1999; Ruiz-Morlaes, 2002; Ormsby and King, 2004). Yang and Xing (2010) have previously suggested that interactions between CNTs and PAHs beyond hydrophobic effects are responsible for a nonlinear isotherm. It may be that at lower concentrations or surface area coverage of MWCNT surface by PAHs, the specific interactions between the PAH molecules and MWCNT surface are more influential in the adsorption process, whereas when adsorption sites begin to be filled at higher concentrations and adsorption affinity is lower, nonspecific hydrophobic effects become the main driver of adsorption.

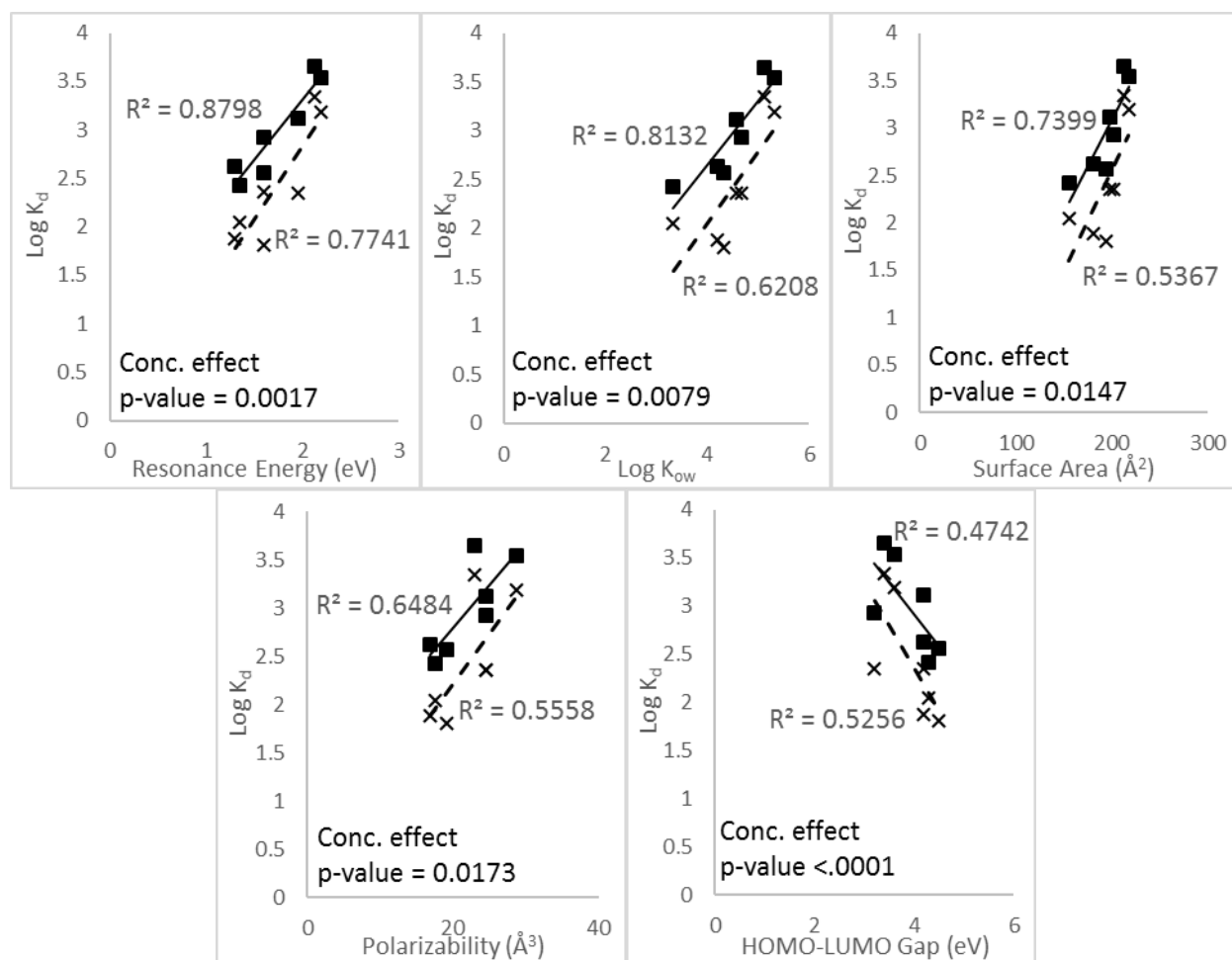


Figure 3.6. The relationship between single point adsorption descriptors (K_d) and PAH physicochemical characteristics. This is shown at ~ 10% (filled squares; solid line) and ~40% (X; dashed line) surface area coverage.

The hydrophobic effect was suppressed by expressing the equilibrium concentration (C_e) in the adsorption isotherms as the equivalent concentration that would exist in an inert solvent (i.e. C_{ow}) where $C_{ow} = C_e \cdot K_{ow}$ (K_{ow} = octanol-water partitioning coefficient) (Brooks et al., 2012). This normalized differences in PAH's water solubility and hydrophobicity that can influence their interaction with the adsorbent surface (Brook et al., 2012). Except for NAP, the adsorption isotherms of the other PAHs largely collapsed onto a single line, confirming the hydrophobic interactions were a main mechanism driving adsorption of PAHs by MWCNTs

(Figure 3.7). The greater adsorption of NAP, once normalized, compared with the other PAHs, support previous findings that the adsorption of NAP by MWCNTs is likely undergoing an additional interaction with the MWCNT, such as pore filling (Sun et al. 2013, Brooks et al., 2012; Wang et al., 2014; Yang et al., 2006).

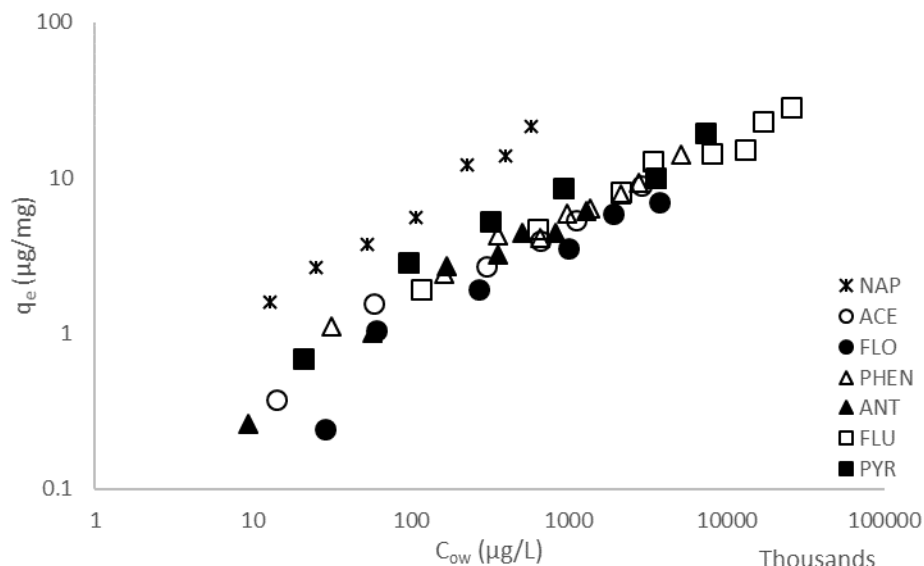


Figure 3.7. Log-log plot of PAH adsorption by MWCNT as a function of equilibrium concentration normalized for hydrophobicity. The equilibrium concentration has been normalized for hydrophobic effect as follows: $C_{ow} = C_e \cdot K_{ow}$ (C_e = aqueous equilibrium concentration; K_{ow} = octanol-water partitioning coefficient).

To further investigate the influence the PAH's morphology on surface adsorption to MWCNT, ANCOVA was used to compare the hydrophobic effect normalized adsorption isotherms in log-log form, where the covariants were *structure* (i.e. linear vs nonlinear vs clustered) and *aromatic character* (i.e. alternate and non-alternate PAHs where non-alternate is defined as PAHs having a non-aromatic ring present in the structure). NAP was not included in this analysis as it was apparent that NAP was not just undergoing surface adsorption like the other PAHs. In terms of structure, "linear" PAHs were specifically represented by FLO and

ANT, “non-linear” represented by ACE and PHEN, and “clustered” represented by FLU and PYR. Both structure and aromatic character appeared to be significantly influential on adsorption of PAHs by MWCNT (p-value = 0.0007 and 0.0003, respectively). By analyzing the influence of structure on alternate and non-alternate PAH groupings separately, it became clear that for alternate PAHs, the apparent influence of structure was actually due to the number of aromatic rings present (p-value 0.021), where adsorption increased with increasing number of aromatic rings. For non-alternate PAHs, the number of aromatic rings was not a significant factor, though structure was (p-value 0.0118). Comparison between similarly structured PAHs with the same number of rings, showed that alternate PAHs had a greater adsorption at the same equilibrium concentration than non-alternate PAHs (p-value = 0.0017). However, this trend was only significantly observed at a 0.05 alpha value for linear PAHs (0.0069), although at a 0.1 alpha value it was also observed for the non-linear and clustered PAHs (p-value = 0.081 and 0.0874, respectively). This is attributed to the linear non-alternate PAH, FLO, having a non-aromatic ring separating the aromatic rings preventing any cycling of electrons, whereas the non-alternate non-linear and clustered PAHs, ACE and FLU, respectively, both had two aromatic rings side by side in the structure allowing for some electron cycling and increased stability which led to similar adsorption (Aihara, 1999; Krygowski and Ciesielski, 1995; Suresh and Gadre 1999). Overall, adsorption of PAHs by MWCNTs increased as the number of un-interrupted aromatic rings present increased (p-value < .0001), demonstrating that adsorption was largely driven by the molecule’s π system and degree of electron delocalization (Pan and Xing, 2008; Apul and Karanfil, 2015; Keiluweit and Kleber, 2009). In non-alternate PAHs, the degree to which the five-membered ring disrupts or alters the cyclic conjugation of delocalized electrons depends on the molecule’s topography and how the six-membered aromatic ring are connected (Gutman et al., 2009). As such, it is not surprising that the impact of structure on the molecule’s stability and

π - π interactions with the MWCNT surface was greater for non-alternate PAHs than alternate ones.

3.3.4 Linear Free Energy Relationship (LFER)

A number of studies have successfully characterized and predicted adsorption of organic contaminants to CNTs by using quantitative activity structure relationships (QSAR), linear solvation energy relationships (LSER), or linear free energy relationships (LFERs). These techniques are advantageous in having input parameters that are related to the adsorbates' physicochemical characteristics that are easier to obtain than the input parameters required for thermodynamic models (Apul et al., 2012). LFER and LSER model parameters are based on the molecular interactions occurring during adsorption between the adsorbate and the adsorbent surface, thus giving insight into the relative contribution of four types of molecular interactions, i.e. London dispersion, hydrogen-bond acidity and basicity, polarizability, and molecular force of lone-pair electrons (Xia et al., 2010). However, LSER and LFER models are concentration dependent due to the change in adsorption with increasing equilibrium concentration, so the predictive models have to be developed for discreet concentration ranges where the adsorption isotherm is linear (Zhao et al., 2014; Apul et al. 2012). As such, the number of data points (i.e. n) used to develop the predictive models depended on the number of $\text{Log } K_d$ values that fell on the line about the mean of $\text{Log } K_{0.01}$ and $\text{Log } K_{0.1}$. For this study, multiple linear regression of LFER descriptors [r , p , b , v] against the $\text{Log } K_d$ values, showed that with the inclusion of all the parameters, none of the parameters were considered statistically significant at an alpha value of 0.05. Further multicollinearity issues existed where VIF values were greater than 10 for R , representative of lone-pair electron molecular force, and β , adsorbate hydrogen bond basicity (Xia et al., 2010). Therefore, only the estimates for descriptors [p , b , v] were included in the fitting of LFER models with $\text{Log } K_d$. The JMP outputs, ANOVA and parameter estimates for the

LFER models are provided in Appendix E. Below the fitting equations to the training set of Log $K_{0.01}$ and Log $K_{0.1}$ are presented.

$$\text{Log } K_{0.01} = (0.20 \pm 0.84) + (0.13 \pm 0.03) p + (9.16 \pm 2.84) b - (0.02 \pm 0.010) v \quad (3.3)$$

$$(n = 14; R^2 = 0.86)$$

$$\text{Log } K_{0.1} = (0.83 \pm 0.71) + (0.13 \pm 0.02) p + (7.79 \pm 2.22) b - (0.02 \pm 0.005) v \quad (3.4)$$

$$(n = 16; R^2 = 0.80)$$

The b term, hydrogen bond accepting, was the most influential descriptor in the LFER equation, possibly indicating that the tendency of the MWCNT to donate protons to the PAHs is greater than that of water (Xia et al., 2010; Zhao et al., 2014). The potential of PAHs to form a hydrogen bond with MWCNT is largely dependent on the oxidation of MWCNTs surface and the solution pH; with changing pH, oxidized MWCNTs can become a hydrogen bond donor (Apul and Karanfil, 2015; Schwarzenbach et al., 2003). The second most significant term is polarizability; the positive correlation indicates the importance of π - π interactions between the PAHs and MWCNT (Xia et al., 2010). Surprisingly, molar volume was the least influential term though it has commonly been found to be the most influential descriptor in LSER models (Apul et al., 2012; Xia et al., 2010; Zhao et al., 2014), and was negatively correlated with adsorption. Further, molar volume was only a statistically significant term for Log $K_{0.1}$ at the 95% level of significance. This may indicate that hydrophobic effects, represented by V , are more important in the adsorption process at higher concentrations where the available adsorption sites have a lower energy and competition with other molecules for the available adsorption sites becomes greater (Yang and Xing, 2010; Wang et al., 2014).

To investigate the influence of PAH physical characteristics, such as structure (i.e. linear vs nonlinear vs clustered) and aromatic character (i.e. alternate vs non-alternate), the developed LFER models were modified by including these categorical terms in the models. The addition of the aromatic character term did not improve the model predictability at either concentration. On

the other hand, at both concentrations (i.e. Log $K_{0.01}$ and Log $K_{0.1}$) the correlation coefficient significantly increased with the addition of a structure term ($R^2 = 0.97$ and 0.95 , respectively). The fitting equations of the modified models for the training set of Log $K_{0.01}$ and Log $K_{0.1}$ are presented below. JMP output results are in Appendix E.

$$\begin{aligned} \text{Log } K_{0.01} = & (1.81 \pm 0.71) + (0.11 \pm 0.02) p + (7.03 \pm 1.63) b - \\ & (0.02 \pm 0.007) v + \text{Match } (St) \begin{bmatrix} \text{linear} \rightarrow -0.34 \\ \text{nonlinear} \rightarrow -0.06 \\ \text{clustered} \rightarrow 0.40 \end{bmatrix} \end{aligned} \quad (3.5)$$

($n = 14$; $R^2 = 0.97$)

$$\begin{aligned} \text{Log } K_{0.1} = & (1.76 \pm 0.60) + (0.09 \pm 0.02) p + (8.18 \pm 1.23) b - \\ & (0.02 \pm 0.006) v + \text{Match } (St) \begin{bmatrix} \text{linear} \rightarrow -0.28 \\ \text{nonlinear} \rightarrow -0.07 \\ \text{clustered} \rightarrow 0.35 \end{bmatrix} \end{aligned} \quad (3.6)$$

($n = 17$; $R^2 = 0.95$)

Structure (St) of the PAHs became the second most significant term in the modified model after hydrogen bond accepting capability. In particular, clustered PAHs had the strongest adsorption, although this is likely due to the “clustered” PAHs also being the most hydrophobic with the most benzene rings in this set of data. This also suggests that PYR and FLU “bulkiness” does not inhibit adsorption by MWCNT. Additional studies with larger PAHs would be necessary to see whether there is a threshold of molecule “bulkiness” that would be too great for the attractive forces between the PAH and the MWCNT surface to overcome, thus leading to adsorption inhibition. Another difference in the modified model 3 is that the molecular volume term is now significantly different than zero at the 95% significance level ($p\text{-value} = 0.021$) though it was still negatively correlated with the adsorption descriptor. This conflicts with previously established studies and may indicate that for PAHs, specific interactions with the MWCNT surface beyond hydrophobic effects are important drivers of adsorption (Apul et al., 2012; Xia et al., 2010). The PRESS value for the modified LFER models also became lower than the original models (i.e. 1.46 and 0.6 for Log $K_{0.01}$ and Log $K_{0.1}$, respectively), indicating that by

including a PAH structure term the model predictability increased. Each of the above described models was externally validated by plotting the predicted Log K values obtained from the models against the experimentally obtained Log K values independently measured from the bioavailability assays (Figure 3.8). For the original (i.e. model 3.3 & 3.4) and the modified (i.e. model 3.5 & 3.6) LFER models, Log $K_{0.01}$ and Log $K_{0.1}$ values were plotted on the same figure to show the distribution around the prediction line at the two different concentrations tested (Figure 3.8). Prediction accuracy was good for all the models, although there was a more even distribution of the compounds around the prediction line for the modified LFER model (Figure 3.8.B) compared with the original LFER model fits, where more distinct clusters of points seemed to occur. It is important to note that the limited amount of data input and by using compounds all from the same class with a narrow range of descriptors used, the relative significance of each descriptor in the developed LFER models may be affected. As such, the results from the presented LFER models should be considered cautiously. From previous data analysis of adsorption isotherms and findings from many other studies, it is clear that molar volume is highly influential on the adsorption process of organic molecules by MWCNT. For future analysis of these data using LFERs it would be better to incorporate a larger and wider range of data. Finally, while the incorporation of a structure term may not be beneficial in predicting the adsorption of other organic compounds by MWCNT, the modified LFER models did provide insight into how the physical morphology of planar molecules may influence the adsorption interactions.

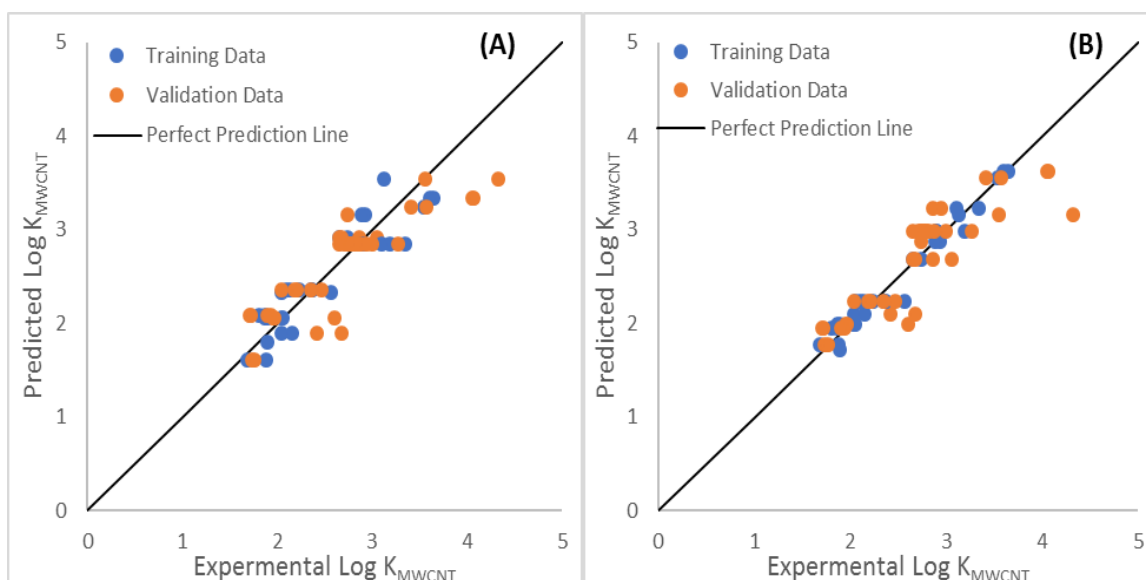


Figure 3.8. Plot of experimental training and external validation single point adsorption descriptors (Log K_d) against predicted values from developed LFER models. Data from Log $K_{0.01}$ and Log $K_{0.1}$ are plotted together where (A) is the original LFER models (i.e. eqns 3.3 & 3.4) and (B) is the modified LFER models (i.e. eqns 3.5 & 3.6).

3.3.5 Bioavailability of PAHs adsorbed to MWCNT.

P. promelas response, represented by bile fluorescence, was non-normal and had unequal variances in the raw data. Several transformations of the data were tried, showing similar trends regardless of how it was transformed enhancing confidence in the observed trends and indicating that statistically significant trends observed were not just a product of the transformation process. Log transformation was the mildest transformation that stabilized the normality and variance issues. Log transformed bile fluorescence data are depicted in Figure 3.9. The fish were exposed to two different concentrations of PAHs with the same concentration of ~ 1.5 mg/L MWCNT, to account for the observed concentration effect on the adsorption process. The “low” and “high” concentration selected for each PAH were approximately an order of magnitude different, where the “low” concentration corresponded with the larger Log K_d values obtained in the experimental adsorption isotherms, and the “high” concentration corresponded with the smaller Log K_d values.

The average Log K_d values calculated using the measured aqueous (C_e) and adsorbed (q_e) concentrations from the exposure treatments are listed in Table 3.3 along with the average measured and predicted response in bile fluorescence (RFUs).

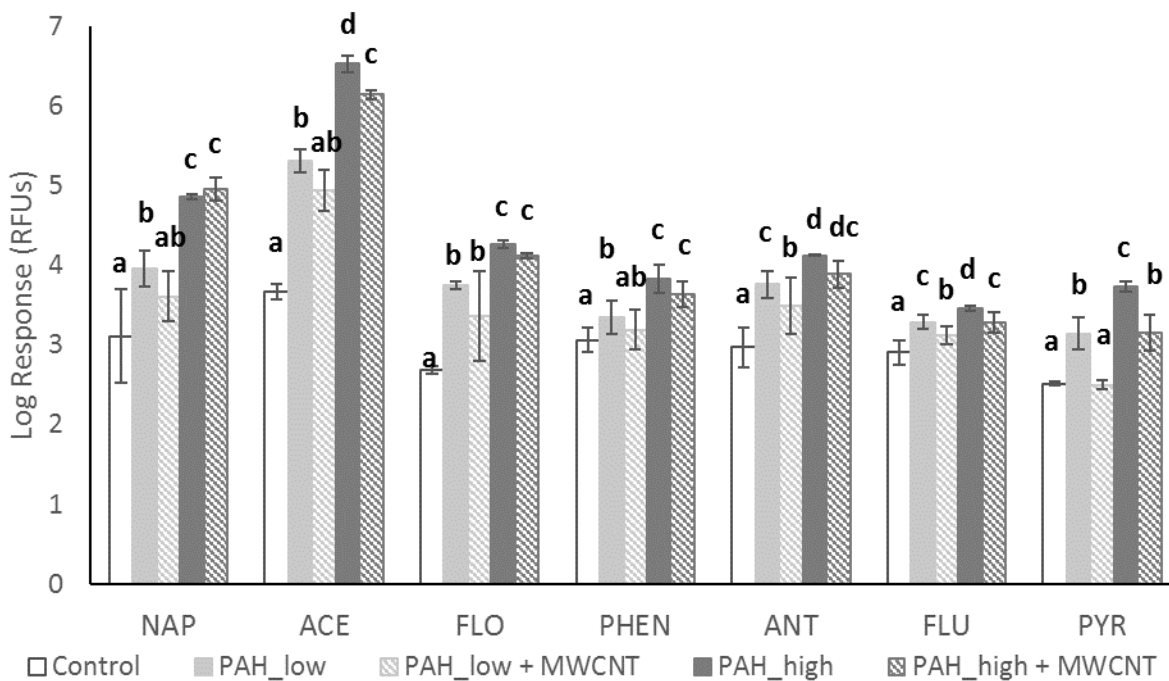


Figure 3.9. Response of *P. promelas* in PAH bioavailability assays with and without MWCNT present. Mean bile fluorescence (Log RFUs) of fish in response to the following treatments: control, PAH at low concentration, PAH at low concentration with MWCNT, PAH at high concentration, and PAH at high concentration with MWCNT was compared. Error bars represent the standard deviation about the mean. Within each PAH, levels not connected by the same letter are significantly different based on Student's T test and least squared means (p-value < 0.05).

The response of fish in the *PAH only* treatments was dose-dependent and for all of the PAHs fell within the 95% confidence envelope of the prepared dose-responses (Figure C1). At the “low” PAH-spiked treatments there was a decrease in response of *P. promelas* to most of the PAHs due to the presence of MWCNT. Compared with responses in the *PAH only* treatments,

the reduction in response to MWCNT-adsorbed FLO was not statistically significant; for NAP, ACE and PHEN the response reduction was significant at an alpha level of 0.1 (i.e. p-value = 0.09, 0.06, and 0.07, respectively); and for ANT, FLU and PYR the reduction was statistically significant at a 95% confidence level (i.e. p-value = 0.018, 0.01, and 0.004, respectively). At the higher PAH concentration, MWCNT still significantly reduced the bioavailability of FLU and PYR at a 0.05 significance level (i.e. p-value = 0.001 and 0.006, respectively), while ACE and ANT were only significantly reduced at a 0.1 alpha value (i.e. p-value = 0.06 and 0.09, respectively). However, when spiked at a “high” concentration, the bioavailability of NAP, FLO and PHEN in treatments with MWCNT was not significantly different from the *PAH only* treatments.

The response of *P. promelas*, in MWCNT treatments, was predicted using the established dose-response relationships and the aqueous PAH concentration measured in the bioavailability assays. T-tests were used to compare the predicted and actual response of the fish; the difference and associated p-values are presented in Table 3.3. At the “low” concentration, there was no significant difference between the observed bile fluorescence and the predicted response, indicating that the response, at this concentration range, appeared to be strongly associated with the un-adsorbed/ aqueous concentration of PAH left in the system. Similarly, at the “high” concentration, the predicted response and actual response of fish to ANT, FLU and PYR in MWCNT treatments was not significantly different. However, at the “high” concentration, the predicted response of fish exposed to NAP, ACE, FLO and PHEN was significantly different than the actual response, indicating that the equilibrium concentration (C_e) measured in the water was not an accurate estimate of the bioavailable fraction for these PAHs (Table 3.3). This is attributed to opposing forces of both the concentration effect on adsorption affinity and the strength of specific molecular interactions between individual PAHs and the MWCNT surface (Wang et al., 2014; Xia et al., 2010). PAHs that have a greater interaction with MWCNT, such as

ANT, FLU and PYR, seemed to be able to overcome the concentration effect on adsorption affinity and the bioavailable fraction was still well described by the aqueous PAH concentration even at higher equilibrium concentrations.

In general, the degree of change in bioavailability of PAHs due to the presence of MWCNT did decrease as adsorption affinity decreased (i.e. exposure $\text{Log } K_d$). With the exception of ACE at the “high” concentration, there appeared to be little influence of MWCNT on PAH bioavailability when the corresponding exposure $\text{Log } K_d$ was less than or approximately equal to 2. For PAHs that maintained a $\text{Log } K_d$ greater than 3 in exposures, the reduction in bioavailability due to the presence of MWCNT was statistically significant at the 95% confidence level and the measured response was directly correlated with the aqueous PAH concentration. This may indicate that there is an adsorption affinity “threshold”; when values are at or above this value, the bioavailable fraction of the MWCNT adsorbed molecules can be accurately represented by the un-adsorbed/aqueous concentration in the system (Voutsas et al., 2002; Peterson et al., 2009). Interestingly, at the “low” concentration exposures, bioavailability of PAHs in MWCNT treatments were all reduced to some extent as long as the exposure $\text{Log } K_d$ value was greater than the $\text{Log } K_d$ value associated with the isotherm transition point. This further supports that the influence of MWCNT on bioavailability becomes limited once the adsorption process transitions from linear to nonlinear. This is attributed to a decrease in adsorption affinity due to the decrease in the number and energy level of available adsorption sites with increasing concentration (Wang et al., 2014). Similarly, if the attachment orientation of molecules change from planar to end by end to access the decreasing number of sites at higher equilibrium concentrations, the strength of their interaction with the MWCNT surface will change (Zhao et al., 2014, Xia et al., 2010). This change in adsorption strength and attachment orientation may allow for easier desorption of the PAHs as they pass through the organism’s gut tract.

Table 3.3. Actual and predicted responses in RFUs \pm 95% confidence interval for *P. promelas* in PAH-spiked treatments containing MWCNT.

<i>Treatment</i>	<i>Log K_{MWCNT}</i>	<i>Actual Response (RFUs \pm CI)</i>	<i>Predicted Response^a (RFUs \pm CI)</i>	<i>Difference (Actual-Predicted \pm CI)</i>	<i>Difference p-value</i>
<i>NAP_{low_MWCNT}</i>	2.53	4967 \pm 96	7102 \pm 4211	-2135 \pm 7494	0.56
<i>NAP_{high_MWCNT}</i>	1.96	93773 \pm 195	63365 \pm 5929	30408 \pm 11849	<.0001*
<i>ACE_{low_MWCNT}</i>	2.42	95567 \pm 73306	139744 \pm 88282	-44177 \pm 686756	0.89
<i>ACE_{high_MWCNT}</i>	1.85	1401380 \pm 26905	3166715 \pm 1047998	-1765334 \pm 686756	0.0001*
<i>FLO_{low_MWCNT}</i>	2.01	33167 \pm 4704	5000 \pm 825	-1683 \pm 2626	0.19
<i>FLO_{high_MWCNT}</i>	1.71	13350 \pm 1287	17383 \pm 2600	-4033 \pm 2626	0.006*
<i>PHEN_{low_MWCNT}</i>	2.98	1768 \pm 658	2340 \pm 434	-572 \pm 1132	0.31
<i>PHEN_{high_MWCNT}</i>	2.14	4540 \pm 2004	6331 \pm 3186	-1791 \pm 1729	0.04*
<i>ANT_{low_MWCNT}</i>	3.11	3893 \pm 2627	4427 \pm 1729	-534 \pm 1679	0.52
<i>ANT_{high_MWCNT}</i>	2.62	8102 \pm 4278	9952 \pm 299	-1849 \pm 2374	0.12
<i>FLU_{low_MWCNT}</i>	3.67	1370 \pm 262	1423 \pm 237	-53 \pm 276	0.70
<i>FLU_{high_MWCNT}</i>	2.89	1988 \pm 363	2141 \pm 129	-153 \pm 218	0.17
<i>PYR_{low_MWCNT}</i>	4.22	318 \pm 60	54 \pm 18	263 \pm 1008	0.58
<i>PYR_{high_MWCNT}</i>	3.10	1526 \pm 1060	2477 \pm 781	-951 \pm 1008	0.06

^aPredicted responses were determined given the measured aqueous PAH concentration and the established dose-response relationships (Figure C1).

*Difference between actual and predicted response is significantly different ($\alpha=0.05$)

3.3.6 Characterizing the Relationship Between Bioavailability and Adsorption.

To assess the bioavailability of MWCNT-adsorbed PAHs as a function of adsorption behavior and PAH physicochemical characteristics, a bioavailability index was developed (Linard et al., 2017). This normalized the change in response, representative of bioavailability, by the change in PAH concentration in the system, thus allowing comparisons to be made across the different PAHs. The bioavailability index (*BI*) was calculated for each exposure using equation 2.2 and depicted in Figure 3.10.

$$BI = \frac{\Delta Response / Response_{PAH}}{\Delta C / C_n} \quad (2.2)$$

Where $Response_{PAH}$ = bile fluorescent intensity measured in fish from PAH-spiked treatments containing only the background solution (i.e. positive control), $\Delta Response$ = difference in bile fluorescent intensity measured in fish between PAH-spiked treatments with and without the

MWCNTs present, C_0 = original concentration of PAH spiked into the system, and ΔC = change in aqueous concentration of PAH left in the system after adsorption equilibrium was reached with MWCNT.

Two-tailed mean hypothesis testing showed that, with the exception of FLO, the bioavailability indices at the “low” PAH concentration treatments were statistically similar across all PAHs and not significantly different from 1, where $BI=1$ is indicative of the change in response mimicking the change in PAH water concentration. In the “high” PAH concentration treatments, NAP BI was significantly lower than 1 (p-value = 0.018), suggesting an enhancement of bioavailability beyond the equilibrium concentration. It may be that the pore-filling mechanism of NAP has opposing effects on bioavailability of adsorbed NAP; i) at low concentrations NAP molecules adsorbed into the pores of MWCNT are not bioaccessible to solubilizing compounds in the organism’s gut tract whereas ii) at higher concentrations, when NAP molecules are primarily adsorbing to the surface of the MWCNT, NAP easily desorbs when ingested (Wang et al., 2011; Maldonao-Valderrama et al., 2011). Additionally, the BI index of both ACE and FLO at the “higher” concentration treatments were also significantly greater than 1 (i.e. p-value <.0001 and 0.041, respectively). While this suggests that the change in bioavailability was greater than the observed change in aqueous concentration of the PAHs, it is important to note that variance of BI across the different PAHs was not equal. Variance in BI for individual PAHs decreased with increasing $\text{Log } K_d$ ($R^2 = 0.73$, p-value = 0.003), where the smaller PAHs with lower adsorption affinities (i.e. NAP, ACE, and FLO) generally had the largest variation in response. This further supports previously reported findings that the accuracy in which the un-adsorbed concentration of PAH in the system also describes the bioavailable fraction was related to the strength of the interaction between the PAH and adsorbent.

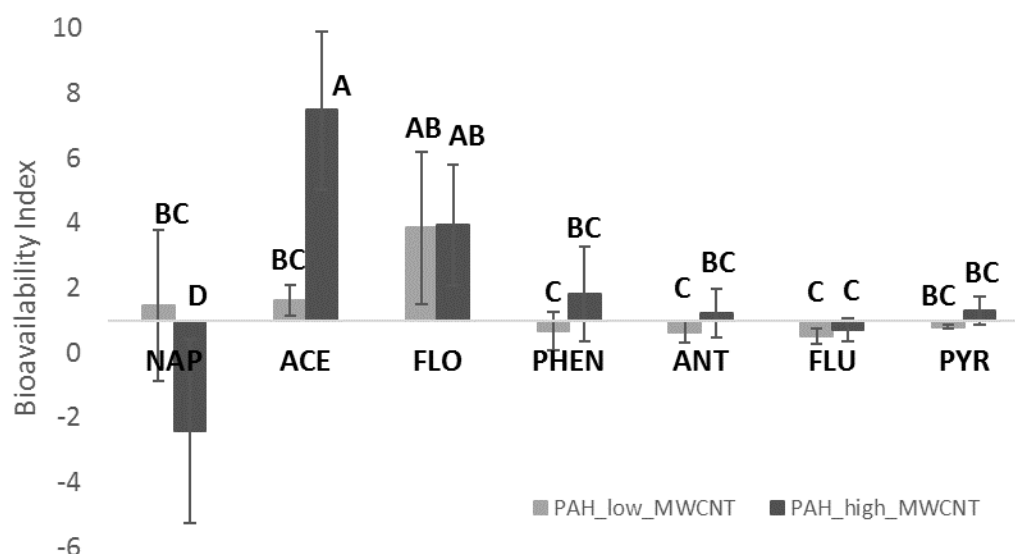


Figure 3.10. Comparison of bioavailability index across all PAHs at the “low” and “high” concentrations. Error bars represent the standard deviation of the mean and levels not connected by the same letter are statistically different based on Student’s T test and least squared means (p-value < 0.05).

Regression analysis was used to assess the relationship between BI and adsorption isotherm parameters from the Freundlich (FM) and Polyani Manes (PMM) models. In most cases the correlations between BI and the model parameters were weak and provided limited insight into the relationship between bioavailability and adsorption behavior. However, there was a significant negative correlation between FM $1/n$ values and % response reduction (i.e. p-value = 0.0177) that became stronger at higher concentrations (i.e. $R^2 = 0.84$, p-value = 0.0004). A box and whisker plot is depicted in Figure 3.11 to show the relative trend of decreasing % response reduction across all concentrations with increasing $1/n$ values. Exposure to NAP had the highest variation due to the drastically different response by fish in the low and high concentration exposures and was the cause of unequal variances when comparing % response reduction across all the PAHs. Exclusion of NAP bioavailability data, showed a stronger negative correlation between % response reduction and $1/n$ values (p-value = 0.009). This, in conjunction with the

observed negative correlation between adsorption (i.e. $\text{Log } K_d$) and $1/n$ values ($p\text{-value} = 0.0138$), indicates that the influence of MWCNT on the bioavailability of adsorbed PAHs was related to surface heterogeneity and strength of interaction. FM $1/n$ values have been considered representative of adsorption intensity, where the lower the value the greater the surface heterogeneity and the higher the adsorption energy (Brooks et al., 2012; Zhu et al., 2005). As such, weaker adsorption leads to decreased ability of MWCNT to reduce PAH bioavailability and increased the response variability.

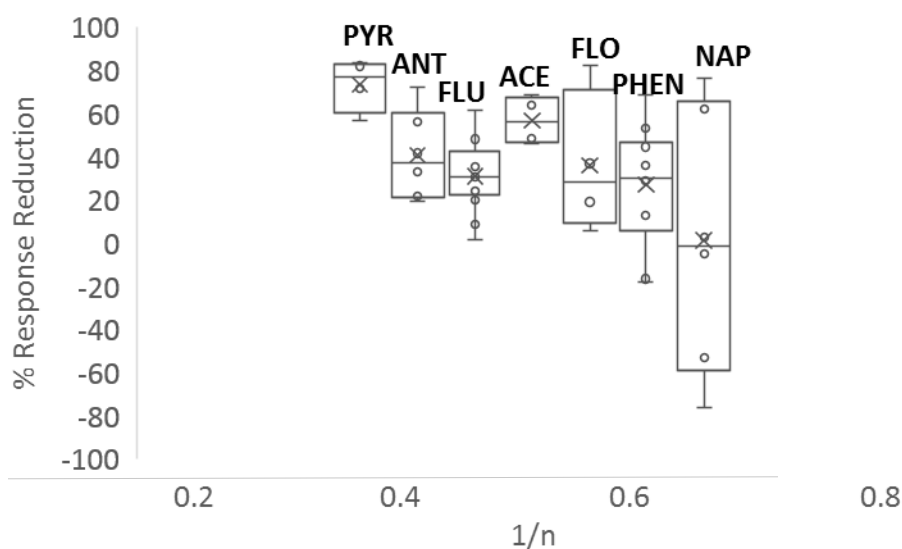


Figure 3.11. Descriptive boxplot of % response reduction to each of the PAHs due to the presence of MWCNT at all concentrations. Boxplots are in order of increasing Freundlich exponent $1/n$ for each PAH and depict the data variation within upper and lower quartiles about the median. Limits of the box display the relative variation in samples for each PAH, and whiskers indicate the variability outside the upper and lower quartiles.

The influence of PAH physicochemical characteristics on bioavailability were also assessed via regression analysis. Of all the PAH physicochemical characteristics listed in Table A1, BI was found to only be significantly correlated with polarizability and resonance energy,

both indicators of π -donor strength (p-values = 0.016 and 0.043, respectively) (Zhu et al., 2005). Considering that increases in adsorbate π -donor strength lead to increased π - π interactions between PAHs and carbon nanomaterials, it is not surprising that BI would be negatively correlated with polarizability and resonance energy as it approaches 1 (Zhu et al. 2005; Linard et al., 2017). This supports previously discussed findings, that the relationship between adsorption affinity and bioavailability is not just driven by concentration effects, but also by the specific interactions occurring between the PAH and the MWCNT surface.

Adsorption results indicated that PAH morphology was influential to the adsorption process. To investigate how PAH morphology may also influence the resulting bioavailability of MWCNT-adsorbed PAHs, regression analysis of BI across the entire suite of PAHs was conducted as well as T-test comparisons within discreet PAH pairs. T-test comparisons of BI were made within the following pairs of chemically similar PAHs to assess the influence of structure (i.e. linear vs nonlinear): (1) ACE and FLO and (2) PHEN and ANT. Similarly, T-test comparisons of BI were made within the pairs (3) ACE and PHEN, (4) FLO and ANT, and (5) FLU and PYR, to assess the influence of aromatic character (i.e. alternate vs non-alternate) when the PAHs pairs had similar number of rings and molecular structure. ANOVA across pairs (3), (4), and (5) also allowed for PAH structural comparisons (i.e. nonlinear, linear, and clustered, respectively) yet differ in aromatic character, being either fully aromatic (i.e. alternate) or containing a non-aromatic ring (i.e. non-alternate).

It was not surprising that there was no significant difference observed in BI of PAHs in pairs (1), (2) and (5). The PAHs within each of these pairs were chemically similar to one another and their adsorption isotherms were nearly identical. However, when comparing combined BI of pair (1) to pair (2), pair (2) had a significantly lower BI (p-value = 0.004) that was equal to 1. Similar trends were also observed when T-test comparisons of BI between PAHs within pairs (3) and (4) were conducted. In pair (3) PHEN had a significantly lower BI than ACE

at a 90% significance level (i.e. p -value = 0.058) and in pair (4) ANT had a significantly lower BI value than FLO (p -value = 0.038). This suggests that while structure did not influence bioavailability, aromatic character was influential particularly for smaller compounds. The lack of difference in BI between FLU and PYR (i.e. pair 5), is likely due to these larger PAHs having greater adsorption affinity than the other smaller PAHs tested. When comparing the BI of the smallest PAH, NAP, with ACE and FLO there was no statistical difference, although NAP BI was closer to 1 than ACE and FLO. Overall, these results indicate that the bioavailability of small and non-alternate PAHs adsorbed to MWCNT is not as well correlated with adsorption descriptors as alternate PAHs. This is attributed to alternate PAHs having greater adsorption affinity than non-alternate PAHs, due to greater stability and stronger π - π interactions (Krygowski and Ciesielski, 1995; Schwarzenbach et al., 2003). However, as PAHs become larger with increasing hydrophobic and π system properties, the differences due to a non-aromatic ring in terms of both MWCNT adsorption and resulting bioavailability are not observable.

3.3.7 Development of Predictive Bioavailability Model.

Initial analysis of the relationship between bioavailability and adsorption of MWCNT-adsorbed PAHs indicated that there was a significant influence of $\text{Log } K_d$ (p -value = 0.005) on BI . The relationship appeared to be nonlinear where BI plateaued at 1 after $\text{Log } K_d$ values surpassed 2.5. Although the developed BI normalizes the change in response to the change in aqueous water concentration, it does not account for partitioning of PAHs into the organism, which can vary due to molecular hydrophobicity and size (Torreiro-Melo et al, 2015). Therefore, bile bioconcentration factors (BCF_{bile}) were developed for each PAH from the established dose-responses listed in Appendix C and were used to assess the relative absorption of PAHs into the test organisms (Table C1). Two-tailed T-test showed that besides ACE and PYR, the calculated $\text{Log } \text{BCF}_{\text{bile}}$ values were significantly lower than those listed in the literature and those calculated

using the PAH Log K_{ow} values. This is partially attributed to BCF being calculated as it relates to the concentration of PAHs measured in the bile rather than measured in lipids or calculated assuming bioaccumulation in the lipids. Lipid content varies depending on the species of fish and can result in different BCF values (Bleeker and Verbuggen, 2009; Mackay., 1982; Arnot and Gobas, 2006). Further, PAHs, particularly those used in this study, are quickly metabolized in fish and are considered to have low bioaccumulative potential so BCF_{bile} measurements provide a more accurate measure of PAH uptake by fish (Torreiro-Melo et al., 2015; Beyer et al., 2010; Bleeker & Verbuggen, 2009).

For the development of an adsorption-bioavailability model, the relationship between distribution coefficient of PAH from water to MWCNT and the partitioning coefficient of PAH into bile was established. The freely dissolved PAH concentration in the system was related to the total PAH concentration in the system as follows (Voutsas et al., 2002):

$$\frac{C_e}{C_0} = \frac{1}{[1 + K_{iMWCNT} * C_{MWCNT}]} \quad (3.7)$$

Where C_e is the measured water concentration; C_0 it the total PAH concentration in the system; K_{iMWCNT} is the distribution coefficient of PAH from water to the MWCNT and is equivalent to the single point adsorption descriptors (i.e. $K_d = q_e/C_e$) and C_{MWCNT} is the concentration of MWCNT in the system. For the PAH-bile distribution coefficient, the response of fish was first converted to PAH equivalent concentration using the dose-response relationships and calibration curves listed in Appendix C. There was a strong positive correlation ($R^2 = 0.92$) between the developed Log BCF_{bile} and the measured partition coefficient of PAH from water into bile from the *PAH only* treatments (i.e. $K_{ibile} = \left(\frac{PAH_{bile}}{C_n} \right)$ where C_0 is the concentration of PAH measured in the water from *PAH only* treatments) (Figure C3). This shows that the uptake of PAHs from exposure treatments can be represented by a single BCF_{bile} value for each PAH and is representative of the expected absorption of PAHs if all of the PAH present in the system was

bioavailable. Assuming steady state had been reached in the system, the partitioning coefficient of PAH from the MWCNT into the bile can be expressed in the following form:

$$K_{\text{bileMWCNT}} = \frac{C_g * K_{\text{bile}}}{C_g * K_{\text{MWCNT}}} = \frac{BCF}{K_d} \quad (3.8)$$

The PAH concentration measured in the water and bile as a ratio of *MWCNT: PAH only* treatments was plotted as a function of the single point adsorption descriptors (Log K_d) from each exposure (Figure 3.12). The water ratio (i.e. C_e/C_0) showed the expected sigmoidal curve where it was near one at low Log K_d values, and plateaued at a near zero value for high Log K_d (Voutsas et al., 2002). The bile ratio (i.e. $C_{\text{bile_MWCNT}}/C_{\text{bile_PAH}}$) was also negatively correlated with Log K_d ($R^2 = 0.79$), but did not match the same sigmoidal trend. Instead at high Log K_d values, representative of greater adsorption affinity, the bile ratios deviated and were found to be higher than the water ratios. This indicates that even with high adsorption, some fraction of the adsorbed PAH remained bioavailable and bioavailability could not be completely reduced. This may be due to a dilution effect, where the concentration of freely dissolved PAH in the gut tract is lower than that of the outside aqueous environment, thus desorption of PAHs from the ingested MWCNT is promoted as a new equilibrium is established (Yang and Xing, 2007).

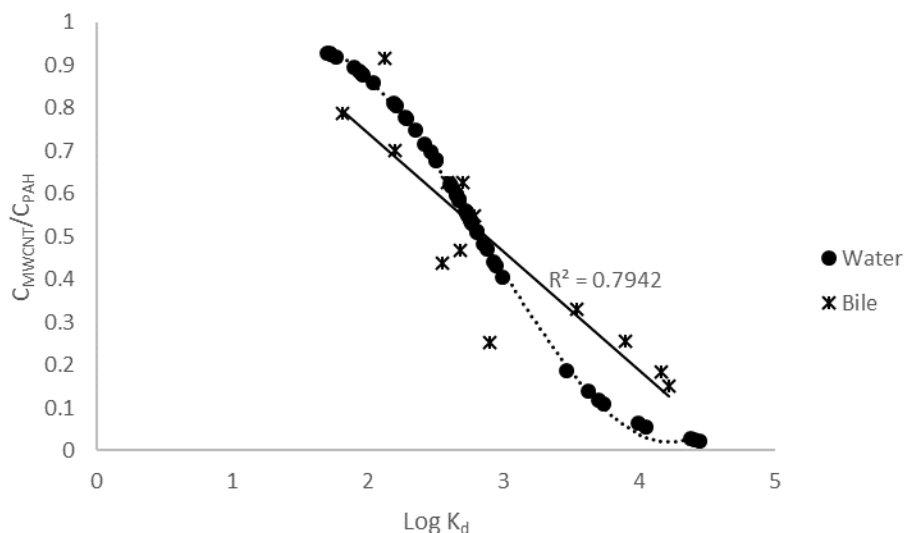


Figure 3.12. Relationship between the ratio of concentration in the MWCNT treatments to the PAH only treatments in water and bile, as a function of the adsorption descriptor (Log K_d). The correlation coefficient (R^2) show the linear regression fit of the bile ratio as a function of Log K_d .

Generalized regression was used to develop a model describing bioavailability as the ratio of the PAH concentration measured in the bile to the concentration adsorbed to MWCNTs i.e. the partition coefficient of PAH between MWCNT and bile ($C_{\text{bile}}^{\text{ex}}/C_{\text{MWCNT}} = K_{\text{bileMWCNT}}$). Data from the 42 individual exposure assays were randomly divided in half to make up the training and validation data set. Below the fitting equation of the selected model is presented; the JMP output results are listed in Appendix F.

$$\text{Log}(K_{\text{bileMWCNT}}) = (2.55 \pm 0.45) + (0.63 \pm 0.15) \text{Log BCF} - (0.52 \pm 0.11) \text{Log } K_d \quad (3.9)$$

$$(n = 21, R^2 = 0.68)$$

The tested input parameters consisted of PAH physicochemical characteristics, including aromatic character and structure, adsorption descriptor parameters, equilibrium concentration, and the determined BCF values from the dose-response relationships. Of these various indices,

A-LASSO identified that only BCF and adsorption descriptors (i.e. Log K_d) were appropriate for estimating Log ($K_{bileMWCNT}$). The fitting equation of the training set had a correlation coefficient of 0.68 and no correlation was observed between the variables ($VIF < 10$). The PRESS value of the training data set was 2.93 with an RMSE of 0.37, while the PRESS value of the validation data set was higher at 5.49 with an RMSE of 0.50. Although the prediction accuracy of the validation set was not as strong as that of the training set, the bile_MWCNT distribution coefficient values (Log $K_{bileMWCNT}$) were evenly distributed about the perfect prediction line (Figure 3.13). This indicated moderate accuracy of the above model in describing bioavailability as a function of the absorption of PAHs into the organism via water exposure and the adsorption affinity of PAHs by MWCNT.

Log BCF is the most significant term of the model, indicating that bioavailability is largely dependent on the bioaccumulative potential of the PAH by the organism. However, the negative contribution of Log K_d describes how the bioavailable fraction of PAH will decrease with increasing adsorption affinity. Overall, the resulting distribution of PAH between MWCNT and bile ($K_{bileMWCNT}$) is dependent on whether adsorption affinity of PAHs by MWCNT or bioaccumulative potential is greater. In the experimental vs actual prediction plot of Log $K_{bileMWCNT}$ values, the validation data set seemed to deviate from the perfect prediction line at lower values. This is attributed to the influences from Log K_d and Log BCF being similar in magnitude causing greater variation in the distribution of the PAH between MWCNT and uptake into the organism. Several studies have also suggested that the lack of uniform desorption can cause difficulty in describing bioavailability of adsorbed compounds with just the use of adsorption/desorption models (Beckles et al., 2007; Lawrence et al., 2000). Inclusion of a term accounting for desorption behavior of PAHs from MWCNTs may improve the fit of the model. Because fish were starved in this study, thus having low levels of solubilizing digestive components like bile salts, it is unlikely that the digestive process contributed much to the

observed relationship or desorption of PAHs differently than expected in water (German et al., 2009; Wang et al., 2011; Su et al., 2013). However, future studies should focus on investigating this relationship in different digestive conditions where food material or digestive components may provide an additional component for PAHs to associate with thus altering the partitioning of PAHs from MWCNTs into the organism.

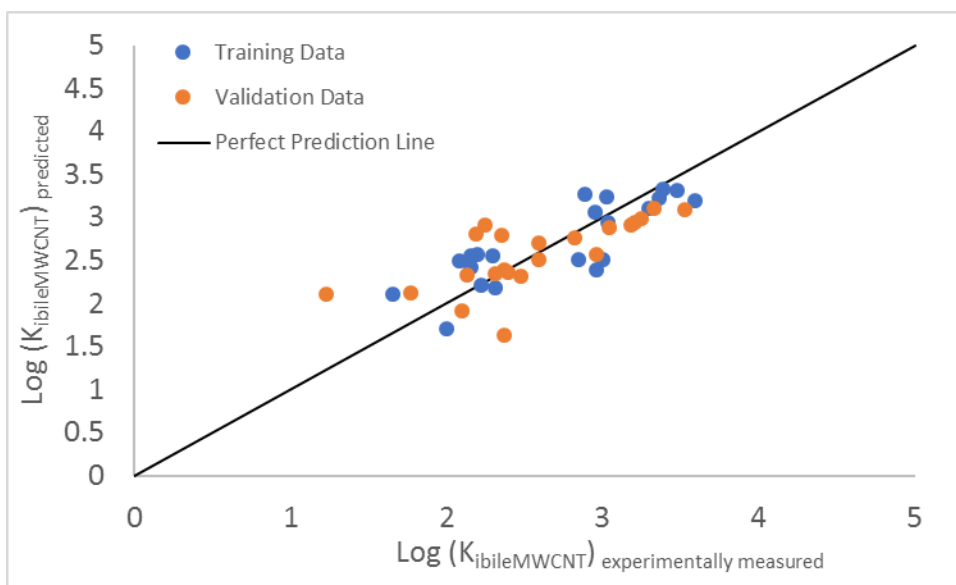


Figure 3.13. Plot of predicted distribution coefficient of PAH between bile and MWCNT ($K_{ibileMWCNT}$) against experimentally obtained values for the training and validation data set.

3.4 Conclusions

Overall, the results of this work support previous findings that the adsorption of PAHs by MWCNT is largely driven by the compound's chemical characteristics that contribute to hydrophobic forces and π - π interactions. However, the adsorption of small PAHs is particularly sensitive to the compound's morphology, where structure and aromatic character greatly influence the PAH's π electron system. Further, adsorption interactions observed were concentration sensitive, where the adsorption process switched from linear to nonlinear as the %

surface area coverage of MWCNT by PAH increased beyond 50%. Likewise, the contribution of PAH physicochemical properties to the adsorption process decreased with increasing surface area coverage, indicating that as available adsorption sites began to fill up the interactions driving the adsorption switched from specific to nonspecific. Similarly, the relationship between adsorption and resulting bioavailability of MWCNT-adsorbed PAH was concentration dependent. At low PAH concentrations when the adsorption process was still linear and the measured adsorption affinity (i.e. $\text{Log } K_d$) was ≥ 2.5 , only the aqueous fraction of PAH was bioavailable. However, bioavailability could not be estimated accurately when adsorption affinity was low. Incorporating both MWCNT adsorption affinity influences and the bioconcentration potential of PAHs by *P. promelas*, allowed bioavailability of MWCNT-adsorbed PAHs to be predictable. These findings indicate that bioavailability of CNT adsorbed contaminants is related to both adsorption and the bioaccumulative potential of the contaminant by the organism in question. Given the results, it is not likely that MWCNTs will enhance the bioavailability of PAHs to fish, although there is an adsorption affinity threshold at which MWCNTs can significantly reduce bioavailability of the adsorbed PAHs.

3.5 References

Aas, E.; Beyer, J.; Goksoyr, A. Fixed wavelength fluorescence (FF) of bile as a monitoring tool for polyaromatic hydrocarbon exposure in fish: an evaluation of compound specificity, inner filter effect and signal interpretation. *Biomarkers*. **2000**, 5 (1), 9-23.

Aihara, J. Reduced HOMO-LUMO gap as an index of kinetic stability for polycyclic aromatic hydrocarbons. *J. Phys. Chem. A*. **1999**, 103, 7487-7495.

Anderson-Sprecher, R. Model comparison and R^2 . *Am. Stat.* **1994**, 48 (2), 113-117.

Apul, O.; Karanfil, T. Adsorption of synthetic organic contaminants by carbon nanotubes: A critical review. *Water Res.* **2015**, 68, 34-55.

Apul, O.G.; Wang, O.; Zhou, Y.; Karanfil, T. Adsorption of aromatic organic contaminants by graphene nanosheets: Comparison with carbon nanotubes and activated carbon. *Water. Res.* **2013**, 47, 1648-1654.

Apul, O.G.; Wang, Q.; Shao, T.; Rieck, J.R.; Karanfil, T. Predictive model development for adsorption of aromatic contaminants by multi-walled carbon nanotubes. *Environ. Sci. Technol.* **2012a**, 47, 2295-2303.

Arnot, J.A.; Gobas, F.A.P.C. A review of bioconcentration factor (BCF) and bioaccumulation factor (BAF) assessments for organic chemical in aquatic organisms. *Environ. Rev.* **2006**, 14, 257-297.

Baun, A.; Sorensen, S.N.; Rasmussen, R.F.; Hartmann, N.B.; Koch, C.B. Toxicity and bioaccumulation of xenobiotic organic compounds in the presence of aqueous suspensions of aggregates of nano-C60. *Aquat. Toxicol.* **2008**, 86, 379-387.

Beckles, D.M.; Chen, W.; Hughes, J.B. Bioavailability of polycyclic aromatic hydrocarbons sequestered in sediment: microbial study and model prediction. *Environ. Tox. Chem.* **2007**, 26(5), 878-883.

Belsley, D.A.; Kuh, E.; Welsch, R.E. *Regression diagnostic: identifying influential data and sources of collinearity*; Wiley-Interscience: New York, **1980**.

Beyer, J.; Jonsson, G.; Krahn, M.M.; Arese, F. Analytical methods for determining metabolites of polycyclic aromatic hydrocarbon (PAH) pollutants in fish bile: A review. *Environ. Tox. Pharm.* **2010**, 30, 224-244.

Bjork, J.; Hanke, F.; Palma, C.; Samori, P.; Cecchini, M.; Persson, M. Adsorption of aromatic and anti-aromatic systems on graphene through π - π stacking. *J. Phys. Chem. Lett.* **2010**, 1, 3407-3412.

Bleeker, E.A.J.; Verbuggen, E.M.J. Bioaccumulation of polycyclic aromatic hydrocarbons in aquatic organisms. *RIVM report 601779002*; National Institute for Public Health and the Environment: Netherlands, **2009**.

Brooks, A.J.; Lim, H-N.; Kilduff, J.E. Adsorption uptake of synthetic organic chemicals by carbon nanotubes and activated carbons. *Nanotechnology*, **2012**, 23, 294008; doi:10.1088/0957-4484/23/29/294008.

Crittenden, J. C.; Sanongraj, S.; Bulloch, J. L.; Hand, D. W.; Rogers, T. N.; Speth, T. F.; Ulmer, M. Correlation of aqueous-phase adsorption isotherms. *Environ. Sci. Technol.* **1999**, 33, 2926-2933.

Debnath, S.; Cheng, Q.; Hedderman, T.; Byrne, H. A comparative study of the interaction of different polycyclic aromatic hydrocarbons on different types of single walled carbon nanotubes. 2010. *J. Phys. Chem. C*, 114 (18), 8167-8175.

Ferguson, P.L.; Chandler, G.T.; Templeton, R.C.; Demarco, A.; Scrivens, W.A.; Englehart, B.A. Influence of sediment-amendment with single-walled carbon nanotubes and diesel soot on bioaccumulation of hydrophobic organic contaminants by benthic invertebrates. **2008**. *Environ. Sci. Technol.* 42: 3879-3885.

German, D.P.; Nagle, B.C.; Villeda, J.M.; Ruiz, A.M.; Thomson, A.W.; Balderas, S.C.; Evans, D.H. Evolution of herbivory in a carnivorous clade of minnows (Teleostei: Cyprinidae): Effects on gut size and digestive physiology. *Physiol. Biochem. Zool.* **2009**, 83 (1), 000-000.

Gutman, I.; Durdević, J.; Balaban, A.T. A regularity for cyclic conjugation in acenaphthylene, fluoranthene and their congeners. *Polycyclic Aromatic Compounds*. **2009**, 29, 3-11.

Hofmann, T.; von der Kammer, F. Estimating the relevance of engineered carbonaceous nanoparticle facilitated transport of hydrophobic organic contaminants in porous media. *Environ. Pollut.* **2009**, 157, 1117-1126.

Hyung, H.; Kim, J.H. Natural organic matter (NOM) adsorption to multi-walled carbon nanotubes: effect of NOM characteristics and water quality parameters. *Environ. Sci. Technol.* **2008**, 42, 4416-4421.

Kah, M.; Zhang, X.; Jonker, M.T.O.; Hofmann, T. Measuring and modeling adsorption of PAHs to carbon nanotubes over a six order of magnitude wide concentration range. *Environ. Sci. Technol.* **2011**, 45 (14), 6011-6017.

Keiluweit, M.; Kleber, M. Molecular-level interactions in soils and sediments: the role of aromatic π -systems. *Environ. Sci. Technol.* **2009**, 43, 3421-3429.

Krygowski, T.M.; Ciesielski, A. Aromatic character of the benzene ring present in various topological environments in benzenoid hydrocarbons; nonequivalence of indices of aromaticity. *J. Chem. Inf. Comput. Sci.*, **1995**, 35, 203-210.

Kukkonen, J.; Pellinen, J. Binding of organic xenobiotics to dissolved organic macromolecules: comparison of analytical methods. **1994**. *Sci. Total Environ.* 152, 19-29.

Lawrence, M.A.M.; Davies, N.A.; Edwards, P.A.; Taylor, M.G.; Simkiss, K. Can adsorption isotherms predict sediment bioavailability? *Chemosphere*. **2000**, 41, 1091-1100.

Linard, E., Apul, O.G., Karanfil, T., van den Hurk, P.; Klaine S.J. Bioavailability of carbon nanomaterial-adsorbed polycyclic aromatic hydrocarbons to Pimphales promelas: influence of adsorbate molecular size and configuration. **2017**. *Environ. Sci. Technol.* DOI: 10.1021/acs.est.7b02164.

Linard, E.N.; van den Hurk, P.; Karanfil, T.; Apul, O.G.; Klaine, S.J. Influence of carbon nanotubes on the bioavailability of fluoranthene. *Environ. Tox. Chem.* **2015**, 34(3), 658-666.

Lotya, M.; Hernandez, Y.; King, P.J.; Smith, R.J.; Nicolosi, V.; Karlsson, L.S.; Blighe, F.M.; De, S.; Wang, Z.; McGovern, I.T.; Duesberg, G.S.; Coleman, J.N. Liquid phase production of graphene by exfoliation of graphite in surfactant/water solutions. *J. Am. Chem. Soc.* **2008**, 131, 3611-3620..

Mackay, D. Correlation of bioconcentration factors. *Environ. Sci. Technol.* **1982**, 16, 274-278.

Maldonado-Valderrama, J.; Wilde, P.; Macierzanka, A.; Mackie, A. The role of bile salts in digestion. *Adv. Colloid Interface Sci.* **2011**, 165, 36-46.

Manes, M. Activated carbon adsorption fundamentals. *Encyclopedia of Environmental Analysis and Remediation*; Meyers, R. A., Ed.; John Wiley & Sons: New York, **1998**.

Ormsby, J.L.; King, B.T. Clar valence bond representation of π -bonding in carbon nanotubes. *J. Org. Chem.* **2004**, 69, 4287-4291.

Pacák, P. Molar refractivity and interactions in solutions I. Molar refractivity of some monovalent ions in aqueous and dimethyl sulfoxide solutions. *Chem. Papers.* **1989**, 43(4), 489-500.

Pan, B.; Xing, B. Critical review: Adsorption of organic chemicals on carbon nanotubes. *Environ. Sci. Technol.* **2008**, 42(24), 9005-9013.

Peterson, E.J.; Pinto, R.A.; Landrum, P.F.; Weber, W.J. 2009. Influence of carbon nanotubes on pyrene bioaccumulation from contaminated soils by earthworms. *Environ. Sci. Technol.* **2009**, 43, 4181-4187.

Ruiz-Morales, Y. HOMO-LUMO gap as an index of molecular size and structure for polycyclic aromatic hydrocarbons (PAHs) and asphaltenes: A theoretical study I. *J. Phys. Chem. A.* **2002**, 106, 11283-11308.

Schwarzenbach, R.P.; Gschwend, P.M.; Imboden, D.M. *Environmental Organic Chemistry*; A John Wiley & Sons, Inc. publication: Hoboken, New Jersey, **2003**.

Singh, D.K.; Giri, P.K.; Iyer, P.K. Evidence for defect-enhanced photoluminescence quenching of fluorescein by carbon nanotubes. **2011**. *J. Phys. Chem. C*, 115, 24067-24072.

Su, Y.; Yan, X.; Pu, Y.; Xiao, F.; Wang, D.; Yang, M. Risks of single-walled carbon nanotubes acting as contaminants-carriers: potential release of phenanthrene in Japanese Medaka (*Oryzias latipes*). *Environ. Sci. Technol.* **2013**, 47, 4704-4710.

Sun, Y.; Yang, S.; Zhao, G.; Wang, Q.; Wang, X. Adsorption of polycyclic aromatic hydrocarbons on graphene oxides and reduced graphene oxides. *Chem. Asian. J.* **2013a**, 8, 2755-2761.

Suresh, C.H.; Gadre, S.R. Clar's aromatic sextet theory revisited via molecular electrostatic potential topography. *J. Org. Chem.*, **1999**, 64, 2505-2512.

Tarpey, T. A note on the Prediction Sum of Squares Statistic for Restricted Least Squares. *Am. Stat.* **2000**, 54 (2), 116-118.

Torreiro-Melo, A.G.; Silva, J.S.; Bianchini, A.; Zanardi-Lamardo, E.; de Carvalho, P.S.M. Bioconcentration of phenanthrene and metabolites in bile and behavioral alterations in the tropical estuarine guppy *Poecilia vivipara*. *Chemosphere*. **2014**, 132, 17-23.

Voutsas, E.; Magoulas, K.; Tassios, D. Prediction of the bioaccumulation of persistent organic pollutants in aquatic food webs. *Chemosphere*. **2002**, 48, 645-651.

Vuorinen, P.J.; Keinänen, M.; Vuontisjärvi, H.; Baršiene, J.; Broeg, K.; Förlin, L.; Gercken, J.; Kopecka, J.; Köhler, A.; Parkkonen, J.; Pempkowiak, J.; Schiedek, D. Use of biliary PAH metabolites as a biomarker of pollution in fish from the Baltic Sea. *Mar. Pollut. Bull.* **2006**, 53, 479-487.

Wang, J.; Chen, Z.; Chen, B. Adsorption of polycyclic aromatic hydrocarbons by graphene and graphene oxide nanosheets. *Environ. Sci. Technol.* **2014**, 48, 4817-4825.

Wang, L.; Forner, J.D.; Hou, L.; Zhang, C.; Kan, A.T.; Tomson, M.B.; Chen, W. Contaminant-mobilizing capability of fullerene nanoparticle (nC60): Effect of solvent-exchange process in nC60 formation. *Environ. Tox. Chem.* **2012**, 32(2), 329-336.

Wang, Z.; Zhao, J.; Song, L.; Mashayekhi, H.; Chefetz, B.; Xing, B. Adsorption and desorption of phenanthrene on carbon nanotubes in simulated gastrointestinal fluids. *Environ. Sci. Technol.* **2011**, 45, 6018-6024.

Xia, X.; Chen, X.; Zhao, X.; Chen, H.; Shen, M. Effects of carbon nanotubes, chars, and ash on bioaccumulation of perfluorochemicals by Chironomus plumosus Larvae in Sediment. *Environ. Sci. Technol.* **2012**, 46, 12467-12475.

Xia, X-R.; Monteiro-Riviere, N.A.; Riviere, J.E. An index for characterization of nanomaterials in biological systems. *Nat. Nano.* **2010**, 5, 671-675.

Yang, K.; Xing, B. Adsorption of organic compounds by carbon nanomaterials in aqueous phase: Polyani Theory and its application. *Chem. Rev.* **2010**, 110, 5989-6008.

Yang, K.; Xing, B. Desorption of polycyclic aromatic hydrocarbons from carbon nanomaterials in water. *Environ. Polln.* **2007**, 145, 529-537.

Yang, K.; Xing, B. Desorption of polycyclic aromatic hydrocarbons from carbon nanomaterials in water. *Environ. Poll.* **2007**, 145, 529-537.

Yang, K.; Zhu, L.; Xing, B. Adsorption of polycyclic aromatic hydrocarbons by carbon nanomaterials. *Environ. Sci. Technol.* **2006**, 40, 1855-1861.

Zhang, L.; Wang, L.; Zhang, P.; Kan, A.T.; Chen, W.; Tomson, M.B. Facilitated transport of 2,2',5,5'-Polychlorinated Biphenyl and phenanthrene by fullerene nanoparticles through sandy soil columns. *Environ. Sci. Technol.* **2011**, 45, 1341-1348.

Zhang, S.; Shao, T.; Bekargolu, S.S.K.; Karanfil, T. The impacts of aggregation and surface chemistry on carbon nanotubes on the adsorption of synthetic organic contaminants. *Environ. Sci. Technol.* **2009**, 43, 5719-5725.

Zhao, Q.; Yang, K.; Li, W.; Xing, B. Concentration-dependent polyparameter linear free energy relationships to predict organic compound sorption on carbon nanotubes. *Sci. Rep.* **2014**, 4:3888, 1-7.

Zhu, D.; Pignatello, J.J. Characterization of aromatic compound sorptive interactions with black carbon (charcoal) assisted by graphite as a model. *Environ. Sci. Technol.* **2005**, 39, 2033-2041.

Zou., H. The adaptive lasso and its oracle properties. *J. Am. Stat. Assoc.* **2006**, 101(476), 1418-1429.

CHAPTER FOUR

INVESTIGATING THE INFLUENCE OF COMPETITIVE ADSORPTION BY MWCNTS AND THE IMPACT ON ADSORBED-PAH BIOAVAILABILITY TO P. PROMELAS

4.1 Introduction

Carbon nanotubes (CNTs) released into the environment or processed in water treatment facilities will interact with a multitude of other components including natural organic matter and mixtures of contaminants. It has been widely observed that natural organic matter can outcompete other molecules for the available adsorption sites on CNT's surface due to both pore blockage and direct competition (Wang et al. 2009; Wang et al., 2008; Zhang et al., 2011; Sun et al., 2013). Such competition has been shown to increase the bioavailability of adsorbed contaminants, where increased competition for adsorption sites by NOM can lead to higher water concentrations of contaminant, likewise resulting in greater contaminant bioaccumulation (Shen et al., 2013). The degree to which the competitive interactions alter the adsorption affinity of other compounds depends on a wide array of factors including the size of NOM, the surface area and porosity of the adsorbent, and the adsorption affinity of the compound in question. The structure of the compound has been found to be of particular importance in competitive adsorption such that NOM competition was found to be more severe for non-planar organic contaminants compared with planar, hydrophobic contaminants (Zhang et al., 2011). Competition between polycyclic aromatic hydrocarbons (PAHs) on the surface of CNTs is largely driven by adsorption affinity and hydrophobic interactions, where the less hydrophobic PAHs with lower adsorption affinity are more easily outcompeted by those with higher adsorption affinity (Yang et al., 2006a). Though adsorption is similar for PAHs of similar physicochemical properties in single-solute systems (Ersan et al., 2016), in bi-solute systems the compound's structure is also a contributing factor to the competitive interaction (Yang et al.,

2006a). Further, competition between solutes in multi-solute mixtures were not always found to reduce adsorption capacity; there is evidence that in some cases compounds will interact with the sorbates that have already adsorbed to the CNT surface, thus creating a multilayer (Yang et al., 2010). In general, adsorption of compounds in bi-solute mixtures has been described as a more linear process where competition at the surface of the adsorbent and filling of adsorption sites leads to a more homogenous surface (Xi and Ball, 2000). Typically linear adsorption is considered weaker than nonlinear adsorption to heterogenous surfaces (Apul and Karanfil, 2015; Yang and Xing, 2010) and suggests greater potential for the adsorbent to act as a contaminant carrier (Haws et al., 2006). While these types of interactions in bi- and multi-solute mixtures have the potential to significantly alter the bioavailability of CNT-adsorbed contaminants, little to no work exists on this subject.

The primary aim of this study was to assess the role of competition on bioavailability of PAHs when adsorbed to multi-walled carbon nanotubes (MWCNTs) in a bi-solute mixture. Adsorption competition and the resulting bioavailability was investigated for two pairs of PAHs, that were chemically similar yet structurally different. The main objectives of this study were to (i) characterize the competitive interaction between (a) phenanthrene and anthracene, and (b) fluoranthene and pyrene, via bi-solute batch adsorption experiments and (ii) compare bioavailability of the PAHs to *Pimephales promelas* in single and bi-solute mixtures, using bile fluorescence analysis and HPLC peak comparison.

4.2 Materials and Methods

4.2.1 Materials

The four polycyclic aromatic hydrocarbons used for this study are phenanthrene (PHEN), 97% purity, and anthracene (ANT), 99% purity from ACROS Organics; fluoranthene (FLU), 98% purity, from ULTRA Scientific; and pyrene (PYR), 98% purity, from Sigma-Aldrich. Stock solutions were prepared in HPLC grade methanol and the PAH characteristics are presented in

Appendix A (Table A1). All solvents, including methanol and acetonitrile, used for solid-phase extraction (SPE) and high-performance liquid chromatography (HPLC), were HPLC grade. C18 SPE columns (200 mg/ 3 mL) were purchased from Thermo Scientific.

The multi-walled carbon nanotubes (MWCNT) were from the same batch as used in previous studies (Linard et al., 2017). As purchased from the manufacturer, Nanostructured & Amorphous Materials (Houston, TX), MWCNTs had a purity of +95%, length of 10-30 μm , outer diameter of 20-30 nm, and inner diameter 5-10 nm. MWCNTs were suspended via microtip sonication (Branson 450 digital sonifier at 60 watts) in moderately hard water with 2 mg C/L Suwannee River natural organic matter (NOM) collected from near the Suwannee River Visitor's Center (Fargo, GA). After sonication and suspension, MWCNTs length was 0.1-0.8 μm . The surface area and pore volumes of the MWCNTs before and after adsorption of dissolved organic carbon were determined via nitrogen adsorption with a physisorption analyzer (Micromeritics) and application of the Brunaur-Emmett-Teller (BET) equation, the Barrett-Joyner-Halendea (BJH) equation, and the density functional theory model (DFT) (Zhang et al. 2009). Surface area, micropore, mesopore and macropore volumes of MWCNTs with NOM adsorbed were approximately 98 m^2/g , $2.2 \times 10^{-4} \text{ cm}^3/\text{g}$, $5.1 \times 10^{-1} \text{ cm}^3/\text{g}$, and $4.2 \times 10^{-2} \text{ cm}^3/\text{g}$, respectively (Table B1).

4.2.2 Adsorption Isotherms

Single- and bi-solute adsorption isotherms were determined from duplicate tests using the batch equilibrium approach in a background solution of moderately hard water containing 2 mg C/L NOM. All experiments were conducted in 10 mL screw cap glass centrifuge tubes at $25^\circ\text{C} \pm 1^\circ\text{C}$ and allowed to come to equilibrium on a bench top shaker table for 96 hours. PAH stock solution was added to 1.5 mg/L MWCNT suspension, keeping the addition of methanol below 0.1% total solution to avoid any co-solvent effects. In single solute isotherms, the initial PAH concentration of PHEN, ANT, FLU and PYR ranged from 2.5-125, 0.5-25, 1.25-75, and 1.25-75

$\mu\text{g/L}$, respectively. Competitive sorption experiments were conducted in two discreet pairs, 1) PHEN and ANT; 2) FLU and PYR where bi-solute isotherm experiments were prepared identically as the single-solute isotherms except a fixed dose of the competing solute was added. Bi-solute experiments were conducted at two different fixed doses of the competing solute, 2.5 and 7.5 $\mu\text{g/L}$. Vials without MWCNTs were identically prepared to serve as positive controls; controls for the entire system were spiked with methanol only. After equilibrium was reached, the vials with and without MWCNTs were centrifuged (Eppendorf 5804 R) at $\sim 1500g$ for 1 hour and the remaining aqueous supernatant was then concentrated using solid phase extraction (protocol described in a following section). The concentration of the PAHs in the eluent was analyzed via normal-phase HPLC at a flow rate of 1 mL/min equipped with a fluorescence detector at the fluorescence excitation/emission wavelengths 252/366 nm for PHEN and ANT, and 275/420 nm for FLU and PYR. For samples containing PHEN and/or ANT, the mobile phase of the HPLC was at a gradient methanol and water mixture increasing from 75:25 to 90:10 where the retention times were 11.1 and 11.9 mins for PHEN and ANT, respectively. For samples containing FLU and/or PYR, the mobile phase of the HPLC was at an isocratic acetonitrile and water mixture of 80% and 20% where retention times were 9.2 and 10.2 for FLU and PYR, respectively. Analysis of PAH concentration in vials without MWCNT showed negligible change from the initial concentration; therefore, the sorption of PAHs by MWCNTs was calculated as the difference in concentration between positive controls and MWCNT vials.

4.2.3 Adsorption Models

Work in previous studies showed the Freundlich model and Polyani theory to be the most accurate in describing the adsorption of PAHs by MWCNTs; therefore, both were employed in this study (Yang et al., 2006a). The model equations and definition of the parameters are listed in Table 4.1, where q_e (mg/g) and C_e (mg/L) represent the adsorbed concentration and aqueous

concentration, respectively, of PAH at equilibrium. The goodness of model fit was assessed by residual root mean square error (RMSE) and the correlation coefficients (R^2).

Table 4.1. Nonlinear sorption models used to fit adsorption isotherms of PAHs to MWCNTs.

Model	Equation	Parameters
Freundlich (FM)	$q_e = K_F \cdot C_e^{1/n}$	K_F [(mg/g)/(mg/L) ^{1/n}], Freundlich affinity coefficient; $1/n$, Freundlich exponential coefficient
Polyani-Manes (PMM)	$\log q_e = \log q_{\max} + a \cdot (C_{sw}/V_s)^b$ $C_{sw} = RT \cdot \ln(C_s/C_e)$	q_{\max} (mg/g), maximum adsorbed capacity; C_{sw} (J/mol), effective adsorption potential; C_s (mg/L), adsorbate water solubility V_s (cm ³ /mol), molar volume of solute; a [(cm ³) ^{b+1} / (mol J ^b)] and b , fitting parameters; R [8.314 J/(K mol)], universal gas constant; T (K), absolute temperature

4.2.4 Solid-phase extraction

Reverse-phase solid-phase extraction (SPE) of PAHs from aqueous solutions, including the adsorption isotherm experiments and water samples from the bioavailability assays, was done using HYPERSEP C18 cartridges (200 mg/ 3mL). Before loading the samples, the cartridges were conditioned with 3 mL of acetonitrile, followed by 3 mL of methanol, and then 2 mL of nanopure water amended with 10% or 15% methanol to match the aqueous samples that would be processed. Samples containing PHEN and ANT were modified with 10% methanol, while samples containing FLU and PYR were modified with 15% methanol. Amending water samples with an organic solvent helps to keep the octadecyl chains of the solid phase activated and can help increase the solubility of PAHs (Marcé and Borrull, 2000). After conditioning, 13 mL of sample were loaded on the cartridges at a flow rate of ~2.5 mL/min. The cartridges were then rinsed with 2mL of nanopure water and dried using a vacuum filter for 10 mins. Due to the lower hydrophobicity of PHEN and ANT vs FLU and PYR (i.e. Log Kow = 4.6 vs 5.2, respectively), two different eluents were used to improve the recovery. PHEN and ANT were eluted by 1.5 mL methanol, while FLU and PYR were eluted by 1.5 mL acetonitrile via gravity. Preliminary tests showed improved recovery of FLU and PYR with acetonitrile as the eluent over methanol. The

eluent was then transferred to 1 mL amber septa-capped vials for later HPLC analysis. Preliminary tests showed that using the above mentioned methanol amendments to water samples and organic solvent eluents gave the highest recoveries (>80% for all PAHs) and negligible breakthrough.

4.2.5 Bioavailability Assays

Bioavailability assays were conducted using adult *Pimephales promelas* (fathead minnows) weighing greater than or equal to 1 g wet in the same exposure conditions as in previously published work (Linard et al., 2017). Exposures were conducted in replicates with 4 fish per treatment in 16 hour static conditions, full water changes every 4 hours. Average response of fish, represented by bile fluorescence, from a single aquarium was considered a single measurement unit during statistical analysis. Water samples were collected at the beginning and end of each water change to verify PAH concentrations via SPE and HPLC analysis. For a single replicate, 6 treatments in addition to a control existed, where the response of fish was measured when exposed to single solute solutions of each PAH and bi-solute solutions of the PAHs, both with and without the addition of 1.5 mg/L of suspended MWCNT. A schematic of the treatments and exposure set up is depicted in Figure 4.1 where PAH A and PAH B denote the two different PAHs used in the assay. Solutions for each treatment were tumbled in 4L amber glass containers on a rotary tumbler to reach equilibrium prior to fish exposure. The two pairs of PAHs were used in bi-solute exposures where 1) PHEN and ANT, and 2) FLU and PYR. The pairs were selected based on having similar physiochemical properties (Table A1), but differing in either structure (i.e. linear vs angular) for pair 1 or aromatic character (i.e. alternate vs non-alternate) in pair 2. The spiked concentrations of each PAH were determined from the developed adsorption isotherms where competition between the two PAHs was apparent. The same concentration was used in single-solute and bi-solute solution where all PAHs were each

spiked at 5 µg/L. No mortality or abnormal behavior was observed throughout the duration of the assays.

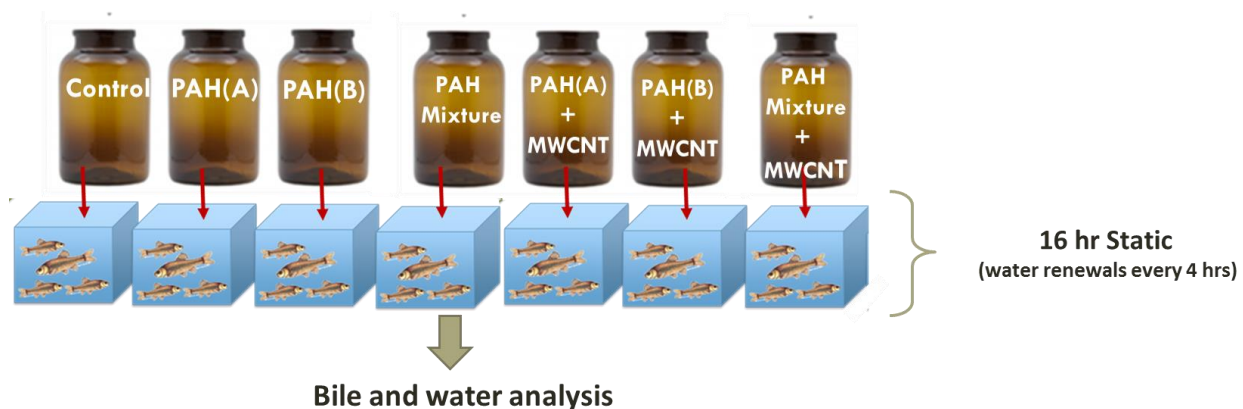


Figure 4.1. Schematic of experimental set up of bioavailability assays. PAH A and PAH B denote the two different PAHs used in the assay.

4.2.6 Bile Analysis

Fish were euthanized at the end of each exposure and the bile was collected for analysis of PAH metabolites. Collected bile was initially diluted to 1:5 with the addition of 50 µL of nanopure water, vortexed and centrifuged at 14000 rpms (Eppendorf 5804 R) to sediment the gallbladder skin. The supernatant was diluted to 1:30 with 200 µL of methanol for samples containing PHEN and/or ANT or with acetonitrile for samples containing FLU and/or PYR. Acetonitrile was used over methanol for FLU and PYR bile samples to remain consistent with the mobile phase used; acetonitrile in the mobile phase over methanol was used to reduce the retention time of FLU and PYR on the HPLC column. The diluted bile samples were then analyzed using a Waters-HPLC affixed with a UV-fluorescence detector at the fluorescence excitation/emission wavelengths 252/366 nm for PHEN and ANT, and 275/420 nm for FLU and PYR. The mobile phase and flow were identical to those previously described for the water samples. The retention times only slightly deviated from the water sample analysis and were 11.3 mins for PHEN, 11.8 mins for ANT, 9.5 mins for FLU and 10.7 mins for PYR.

Following methods and definitions put forth by Torreiro-Melo et al. (2015), the relative concentration of PAH in bile was calculated as PAH equivalents using calibration curves of PAHs prepared in the same background solution used to analyze the bile fluorescence via HPLC (i.e. 100% methanol for PHEN and ANT; 100% acetonitrile for FLU and PYR). The observed area under the fluorescent peaks of individual PAHs was directly correlated of the concentration of PAH in solution; the linear equations for each PAH are as follows:

$$Peak Area_{PHEN} = 1243 * C \quad (4.1)$$

$$Peak Area_{ANT} = 4166 * C \quad (4.2)$$

$$Peak Area_{FLU} = 567 * C \quad (4.3)$$

$$Peak Area_{PYR} = 350 * C \quad (4.4)$$

Previous work also showed a linear relationship between PAH exposure and bile fluorescence intensity (Table C1). As such, the PAH equivalent concentration calculated in bile samples allowed for a bile bioconcentration factor (BCF_{bile}) to be established. BCF_{bile} was calculated as the ratio between the concentration of PAH in the bile (PAH_{bile}) compared to the concentration of the PAH water concentration (PAH_{water}) as represented by the following equation (Torreiro-Melo et al., 2015):

$$BCF_{bile} = \frac{PAH_{bile}}{PAH_{water}} \quad (4.5)$$

This allowed for changes in BCF_{bile} to be assessed for each PAH due to the presence of another PAH and the presence of MWCNT.

4.2.7 Statistical Analysis

JMP Pro 12 software from SAS Institute Inc was used to perform all statistical tests. Analysis of covariance (ANCOVA), where the covariant was the concentration of the “competitor PAH”, was used to compare adsorption isotherms in log-log form for each PAH. Student’s T test was used to compare the concentration of each PAH in bile (PAH_{bile}) within the PAH pairs, between single solute and bi-solute exposures and treatments with and without

MWCNT. Least squared mean contrast was used to compare the difference in bioavailability of the MWCNT-adsorbed PAH between single-solute and bi-solute treatments. Shapiro-Wilk's test was used to test normality of bile fluorescence residuals; Brown and Forsythe test was used to test homogeneity of variance within treatments. Unless otherwise denoted, the significance level of all tests was set at 0.05.

4.3 Results and Discussion

4.3.1 Single-Point Competitive Adsorption

Competition was specifically investigated within two discrete pairs of PAHs, (1) PHEN and ANT and (2) FLU and PYR. PAHs within these pairs had similar chemical characteristics, but differed structurally (Table A1). Figure 4.2 shows the competition between the PAHs of each pair at the initial concentration of the primary adsorbate when the concentration of the competitor PAH ranged from 0-7.5 $\mu\text{g/L}$. Single-point adsorption descriptors ($K_d = q_e/C_e$) of both PHEN and ANT at 2.5 $\mu\text{g/L}$ drastically decreased with the presence of the competitor PAH (p-value <.0001 for both) (Figure 4.2. [A] & [B]). For PHEN, K_d values decreased with increasing competitor concentration (i.e. ANT) even as PHEN concentration also increased (Figure 4.2. [A]). In contrast, when ANT was the primary adsorbate, K_d values were not influenced by increasing competitor concentration (i.e. PHEN) at higher equilibrium concentrations of ANT (Figure 4.2. [B]). This indicates that ANT has greater potential to outcompete PHEN for adsorption sites and is attributed to the difference in PAH structure. Though the two compounds are nearly identical in physiochemical properties, the linear structure of ANT likely allows it to better align with the curved surface of the MWCNT than angular PHEN (Apul et al., 2012). The increased contact between the MWCNT surface and the compound likewise increases the π - π interactions and strength of adsorption (Gotovac et al., 2007).

The change in K_d values for FLU and PYR had distinctly different trends than that observed for the PHEN and ANT pair. When both compounds were the primary adsorbate, the addition of 2.5 $\mu\text{g/L}$ of the competitor PAH caused an initial increase in K_d values (Figure 4.2. [C] & [D]). This was most pronounced at the low equilibrium concentration (i.e. 2.5 $\mu\text{g/L}$) of the primary adsorbate, while the trend was suppressed at higher primary adsorbate concentrations (i.e. 45 $\mu\text{g/L}$). Wang et al. (2014), suggested that such a “turning point” in K_d values indicate high energy adsorption up to that point, after which the adsorption of molecules has a greater distribution of lower energy adsorption sites resulting in the characteristic decrease of K_d values with continual increase of equilibrium concentration (Wang et al., 2014). It may be that the adsorption of a small amount of the competitor PAH altered the surface morphology of the MWCNT in a way that enhanced adsorption; when either the competitor or primary solute increased in concentration beyond some threshold the compounds then became competitive. Interactions between PAHs have been likened to the π - π interactions that PAHs undergo with the surface of carbon nanomaterials (Podeszwa, 2010; Feng et al., 2009) and may allow for PAH binding and stacking on one another on the surface of MWCNT (Yang et al., 2010; Yang et al., 2006a). Wang et al. (2012) has likewise observed a synergistic effect in bi-solute systems where the adsorption of planar compound enhanced the adsorption of another. For FLU, even at the highest concentration of the competitor PYR, K_d values were similar to those observed in adsorption experiment without the competitor present (Figure 4.2 [C]). In contrast, K_d values of PYR at the highest competitor concentration were found to be lower than if the competitor were not present (Figure 4.2 [D]). This suggests that PYR adsorption is altered by simultaneous low FLU adsorption, and is more susceptible to competition when FLU is present at a higher concentration. Overall, the interactions between the two PAHs were distinctly different for each pair (i.e. (1) PHEN and ANT, (2) FLU and PYR) There were significant interactions between the

primary solute and competitor PAH at low concentrations, but similarly to Yang et al. (2006a), the interactions became insignificant at high concentrations.

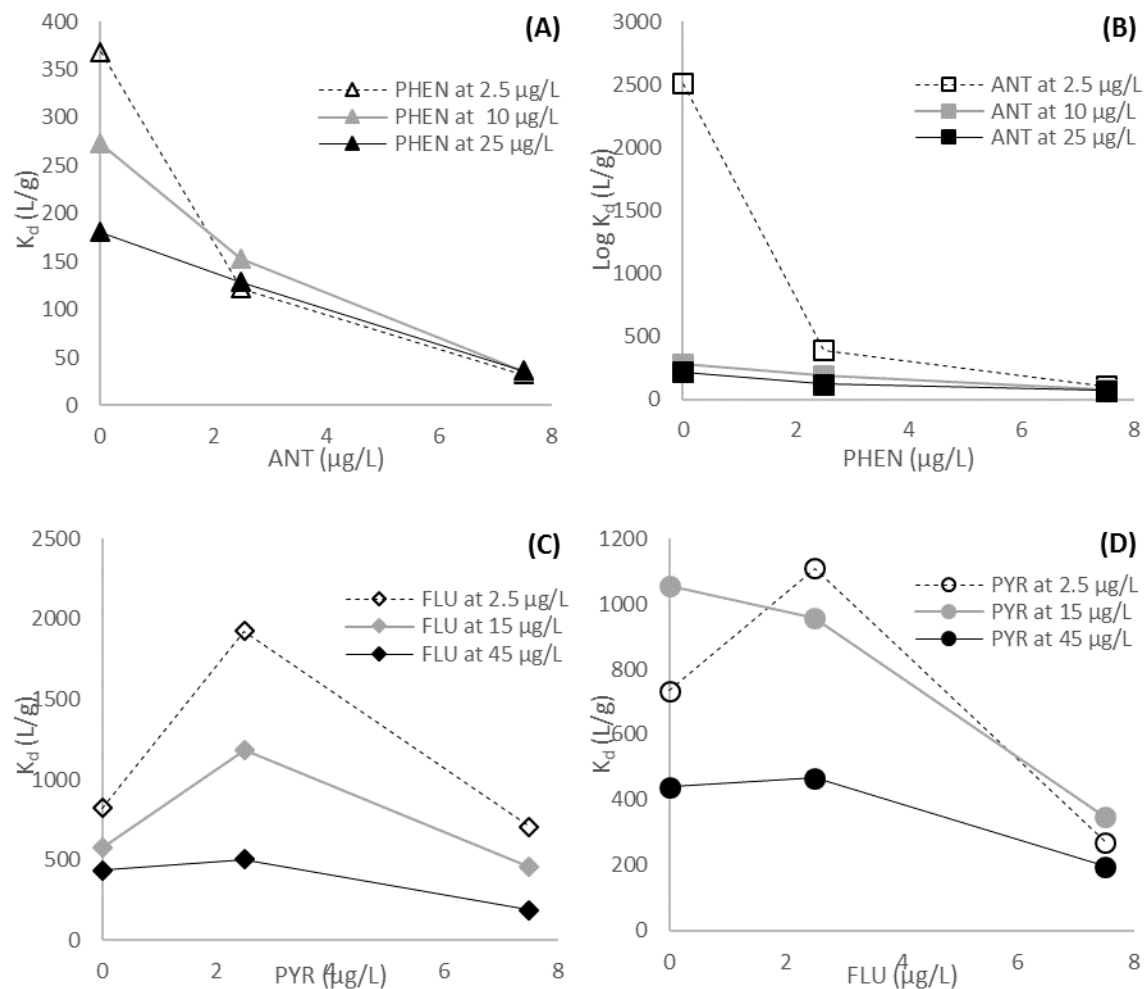


Figure 4.2. Single point adsorption descriptors (K_d) of the primary adsorbate. (A) PHEN, (B) ANT, (C) FLU and (D) PYR, at different concentrations plotted against the competitor adsorbate. $K_d = q_e/C_e$

4.3.2 Adsorption in Bi-solute Systems

Adsorption isotherms of PHEN, ANT, FLU and PYR by MWCNTs without and with the competitor PAH are shown in Figure 4.3. The corresponding fitting parameters of the Freundlich (FM) and Polyani-Manes (PMM) models are given in Table 4.2. As previously observed, PAHs

of similar physicochemical characteristics were similarly adsorbed by MWCNT when in single solute solutions (Yang et al., 2006a). As such, MWCNT has a similar adsorption capacity for PHEN and ANT represented by the Freundlich K_F value without the competitor present (Table 4.2). Although it appeared that MWCNTs had a greater adsorption capacity for FLU over PYR (i.e. K_F values 118 vs 77.6, respectively), ANCOVA of the linearized single-solute isotherms showed that there was not a significant difference in adsorption of the two compounds. In general, adsorption capacity of MWCNT for the primary adsorbate decreased with the increasing concentration of the competitor PAH (Table 4.2 and Figure 4.3). However, the mechanism of adsorption and interaction between the primary and competitor PAHs differed for the two PAH pairs, i.e. (1) PHEN and ANT and (2) FLU and PYR.

Both FM and PMM fit the data well as seen with high correlation coefficients, although the PMM fit generally had lower RMSE values (Table 4.2). There were a few exceptions in which the models did not fit the data accurately, suggesting another type of model may better explain the adsorption process. The FM was not able to adequately fit the PHEN + 7.5 $\mu\text{g/L}$ ANT isotherm ($R^2 = 0.80$), which was attributed to the nonlinearity of the isotherm at higher equilibrium concentrations (Figure 4.3. [A]). This is supported by the high value of the PMM fitting parameter b (i.e. 7.75), where increases in b above one are indicative of increasing nonlinearity (Yang and Xing, 2010). Fitting of the isotherm with the Langmuir model improved the fit ($R^2 = 0.90$), suggesting that the competition by ANT changed the heterogeneity of the adsorption sites available to PHEN, thus leading to an adsorption process that more closely resembled monolayer formation (Kah et al., 2011; Yang et al., 2006b). In contrast, the adsorption of ANT in the presence of PHEN became an increasingly more linear process as the concentration of the competitor increased from 2.5 to 7.5 $\mu\text{g/L}$, though the adsorption capacity (i.e. K_F values) was still lower compared to adsorption of ANT alone (Figure 4.2. [B]; Table 4.2). ANCOVA of the linearized ANT adsorption isotherms showed that this trend was

dependent on the competitor concentration. The isotherm slope (i.e. FM $1/n$ value) of ANT with 2.5 $\mu\text{g/L}$ PHEN was significantly greater than ANT alone ($p\text{-value} = 0.023$) and further increased with the addition of 7.5 $\mu\text{g/L}$ PHEN ($p\text{-value} = 0.002$). A number of studies have similarly observed the suppression of isotherm nonlinearity in bi-solute systems, and have attributed it to the limit of competition (Xi and Ball, 2000; Yang et al., 2006a). A linear isotherm is reached when the adsorbed molecules could no longer be outcompeted by other molecules present (Yang et al., 2006a). This is also in line with the previously discussed findings of competition effects between PHEN and ANT on the single-point adsorption descriptors; ANT significantly reduces the adsorption of PHEN in bi-solute systems while PHEN has limited impact on ANT adsorption.

For FLU and PYR, competitive interactions were not observed until a higher ratio of primary solute to competitor PAH concentration was reached. The decrease in adsorption capacity from the single-solute solutions to the bi-solute solutions with 2.5 $\mu\text{g/L}$ was not significant for either FLU or PYR. Only with the addition of 7.5 $\mu\text{g/L}$ of the competitor PAH did the adsorption capacity of the MWCNT for FLU and PYR significantly decrease ($p\text{-value} = .0271$ and 0.0003 , respectively). Further, for FLU isotherms, the addition of 7.5 $\mu\text{g/L}$ of PYR led to a significant change in isotherm slope ($p\text{-value} 0.0085$), corresponding with a decrease in both the FM exponent, $1/n$, and PMM exponent, b . This indicated an increase in surface heterogeneity and adsorption energy potential, possibly suggesting improved adsorption of FLU due to the presence of PYR (Yang et al., 2010). This was similar to the observed increase in single-point adsorption descriptor with the addition of 2.5 $\mu\text{g/L}$ of PYR, as previously discussed. ANCOVA was used to compare the adsorption isotherms of FLU and PYR, each in the presence of 2.5 and 7.5 $\mu\text{g/L}$ of the competitor. Similar to comparison of the isotherms when no competitor was present, there was no significant difference in adsorption of FLU and PYR when in the presence of 2.5 $\mu\text{g/L}$ competitor PAH. However, with 7.5 $\mu\text{g/L}$ of the competitor present, the adsorption

isotherms of FLU and PYR were significantly different (p -value = 0.0023). Adsorption of FLU was significantly higher than that of PYR at the low equilibrium concentration, but at higher equilibrium concentrations there was no difference in adsorption of the two compounds. This is attributed to the similar molecular structure and physicochemical properties of the two compounds, thus leading to substantial and comparative competition when each is present at high concentrations in a bi-solute system (Yang et al., 2006a). The results indicate a preference of MWCNT to adsorb FLU over PYR, but only at higher concentrations of PYR, are PYR molecules able to overcome the competition and dominate adsorption. Although the four fused benzene rings in PYR allow for an extremely stable π - electron delocalization cloud that can contribute greatly to the π - π interactions with the surface of MWCNT, this structure also causes PYR to be quite rigid (Apul and Karanfil, 2015; Schwarzenbach et al., 2003). Though FLU has a lower π -bonding potential, the non-aromatic ring that lacks double carbon bonds in its structure allows FLU molecules to flex more than PYR (Zhu and Pignatello, 2005; Martinex and Iverson, 2012; Schwarzenbach et al. 2003). This may allow FLU to more easily curve with the surface of MWCNT, thus creating more contact between FLU and the nanomaterial surface than PYR (Zhang et al., 2009) and likely leading to the greater competition potential of FLU over PYR.

Table 4.2. Fitting parameters of Freundlich and Polyani-Manes nonlinear models to adsorption isotherms of PAHs on MWCNT

Freundlich Model (FM)						
Primary adsorbate	Competitor (conc. in $\mu\text{g/L}$)	$K_F (\text{mg/g})/(\text{mg/L})^{1/n}$	1/n	RMSE	R^2	
phenanthrene	None	42.58±5.00	0.63±0.04	0.34	0.99	
	ANT (2.5)	24.53±5.22	0.60±0.07	0.41	0.96	
	ANT (7.5)	5.19±1.97	0.49±0.13	0.23	0.80	
anthracene	None	34.45±12.43	0.51±0.08	0.45	0.95	
	PHEN (2.5)	31.23±7.23	0.62±0.06	0.18	0.98	
	PHEN (7.5)	26.20±5.94	0.74±0.06	0.09	0.98	
fluoranthene	None	118.78±31.76	0.67±0.07	0.64	0.99	
	PYR (2.5)	76.80±12.73	0.54±0.04	0.45	0.99	
	PYR (7.5)	22.04±4.74	0.40±0.06	0.48	0.97	
pyrene	None	77.64±18.40	0.56±0.06	0.79	0.98	
	FLU (2.5)	96.18±10.01	0.54±0.03	0.48	0.99	
	FLU (7.5)	42.10±5.68	0.56±0.04	0.28	0.99	
Polyani-Manes Model (PMM)						
Primary adsorbate	Competitor (conc. in $\mu\text{g/L}$)	$\text{Log } q_{\text{max}}$	a	b	RMSE	R^2
phenanthrene	None	1.83±0.46	-0.04±0.06	0.89±0.31	0.04	0.99
	ANT (2.5)	0.84±0.11	-8.4e6±1.85e-5	2.69±0.48	0.07	0.98
	ANT (7.5)	0.21±0.02	-1.4e-14±4.24e-14	7.75±0.77	0.02	0.99
anthracene	None	0.77±0.29	-5.72e-3±0.02	1.16±0.77	0.16	0.91
	PHEN(2.5)	0.55±0.15	-1.15e-3±2.3e-3	1.63±0.45	0.13	0.97
	PHEN (7.5)	8.89±113	-8.09±112.6	0.035±0.45	0.04	0.97
fluoranthene	None	1.14±0.28	-5.6e-5±2.7e-4	2.22±1.04	0.18	0.96
	PYR (2.5)	1.43±0.62	-2.6e-3±0.02	1.25±0.94	0.14	0.95
	PYR (7.5)	1.32±0.57	-0.04±0.11	0.76±0.47	0.08	0.97
pyrene	None	1.04±0.07	-2.8e-7±8.5e-7	3.48±0.67	0.09	0.99
	FLU (2.5)	1.26±0.10	-2.6e-4±4.2e-4	1.88±0.34	0.10	0.98
	FLU (7.5)	0.94±0.09	-6.7e-4±1.04e-3	1.71±0.34	0.06	0.99

*All estimated parameter values and their standard errors were determined by JMP Pro 12 software (SAS Institute Inc.); Mean ± Standard Error

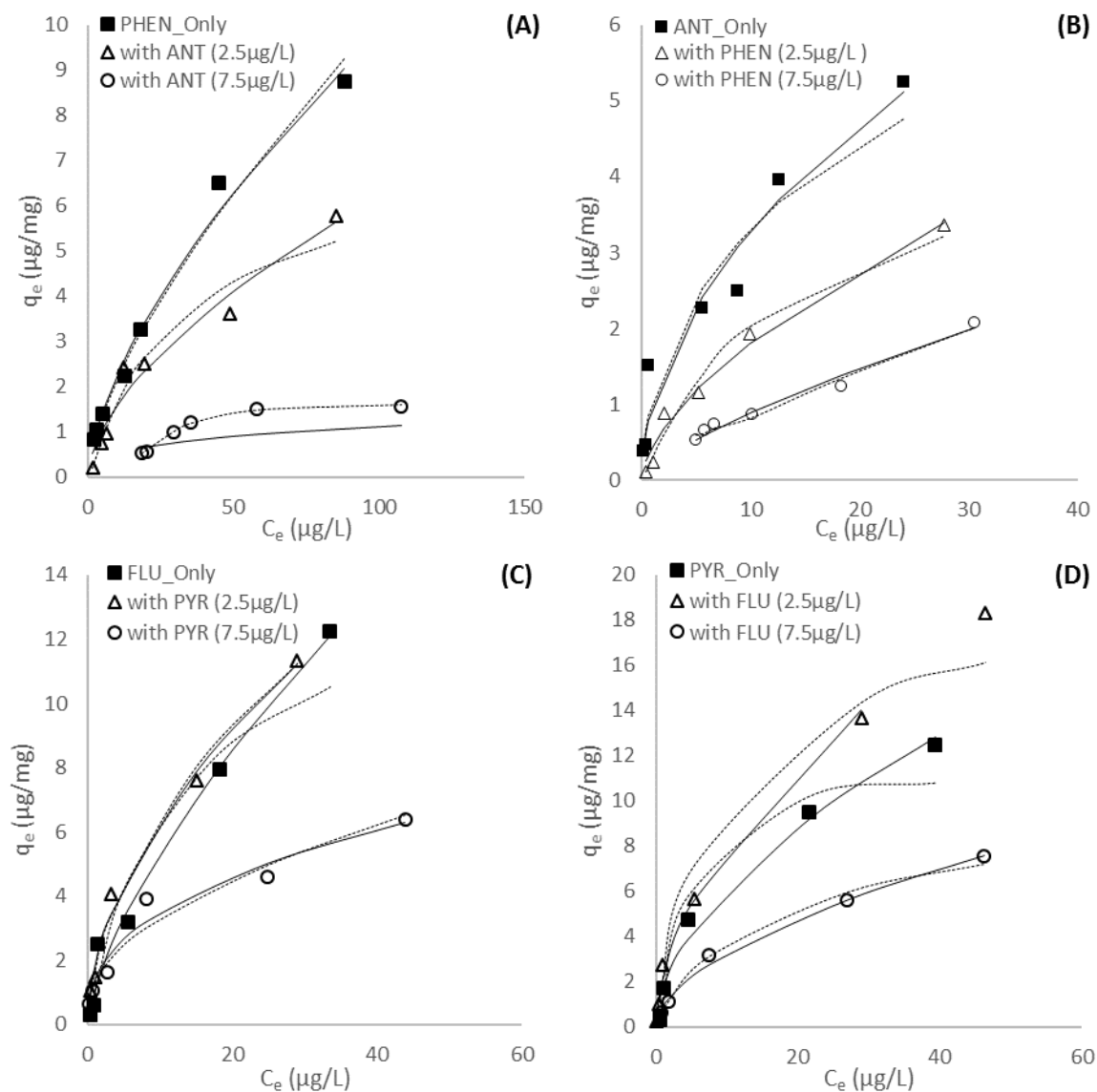


Figure 4.3. Adsorption isotherms of PAHs by MWCNTs without and with competitor at two concentrations (i.e. 2.5 and 7.5 µg/L). (A) phenanthrene (PHEN) alone and with anthracene (ANT) as competitor; (B) ANT alone and with PHEN as competitor; (C) fluoroanthene (FLU) alone and with pyrene (PYR) as competitor; and (D) PYR alone and with FLU as competitor. Solid lines are the Freundlich model fit and dashed lines are the Polanyi-Manes model fit.

PMM correlation curves of each PAH alone and in the presence of the competitor were plotted in Figure 4.4 and used to further assess competition between chemically similar PAHs in

a bi-solute system. The underlying assumptions of the Polyani theory are that adsorption (1) depends on the distance of the molecule from the surface of the adsorbate, (2) the process is independent of temperature and (3) adsorption is independent of the state of aggregation (Yang and Xing, 2010; Yang et al., 2010). Additionally, given that all adsorption space is accessible, correlation curves of different adsorbates for a single adsorbent should collapse onto a single line when adsorption potential is normalized to the molecule's molar volume (Wang et al., 2008; Xia and Ball et al., 2000; Yang and Xing, 2010). However, the correlation curves of PHEN and ANT, without a competitor present were significantly different, indicating that different adsorption sites were accessible for the two molecules (Figure 4.4. [A]). Wang et al. (2008) suggested that differences in correlation curves are indicative of different specific interactions happening between the compound and the adsorbent surface. Interestingly, the correlation curve of PHEN with 7.5 $\mu\text{g/L}$ of ANT as a competitor was more similar to the correlation curves of all the ANT adsorption isotherms. This is attributed to the increased competition of ANT on PHEN adsorption, possibly inhibiting the ability of PHEN to access the adsorption sites it would normally access in the absence of a competitor (Yang et al., 2006a). The correlation curves of FLU and PYR largely fell on a single line. However, the correlation curve for both FLU and PYR as the primary PAH deviated from a single line at high equilibrium concentrations when the competitor was present at 7.5 $\mu\text{g/L}$ (Figure 4.4. [B]). This suggests that FLU and PYR were accessing the same adsorption sites on MWCNT, but when the competitor was at a higher concentration than the primary solute, access to adsorption sites for the primary solute were blocked (Yang et al., 2006a).

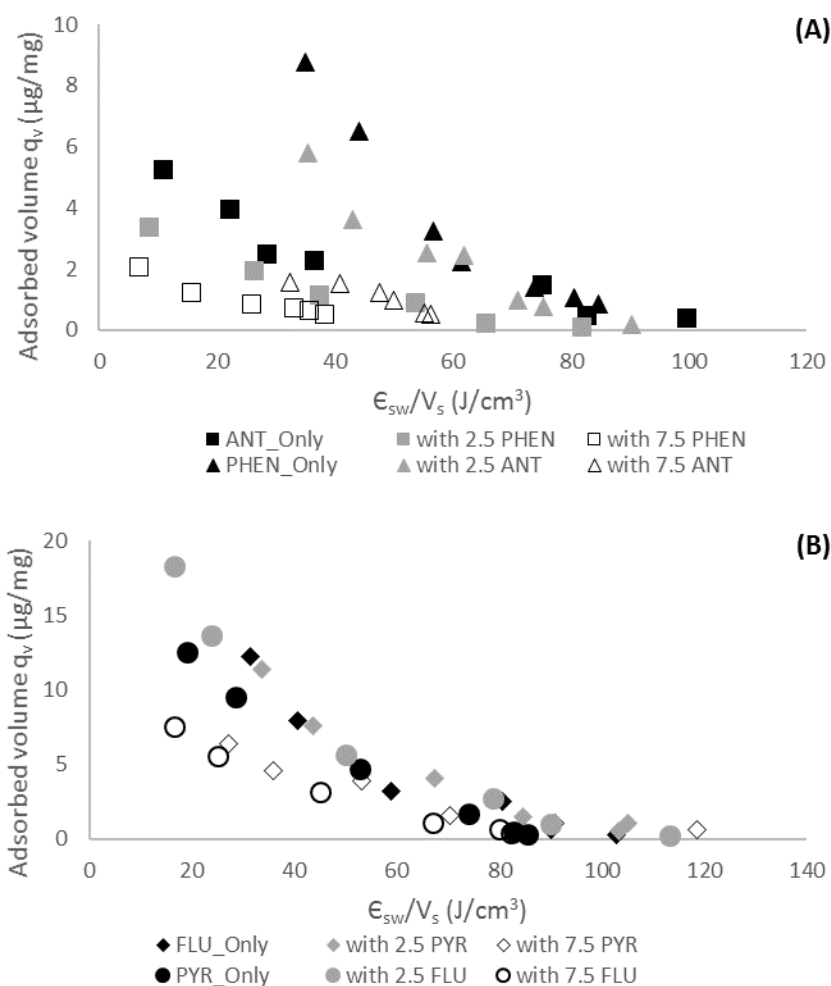


Figure 4.4. Polyani-model based correlation curves of PAHs adsorbed by MWCNT alone and in the presence of the competitor PAH at two concentrations (i.e. 2.5 and 5 µg/L). (A) PHEN and ANT and (B) FLU and PYR.

4.3.3 Bioavailability of MWCNT Adsorbed PAHs in Single and Bi-solute Systems

From the single and bi-solute adsorption experiments, it was determined that at 5 µg/L of the primary and competitor PAH, the single point adsorption descriptors (Log K_d) were similar for pairs (1) PHEN and ANT and (2) FLU and PYR. Log K_d values for PHEN and ANT in single solute solutions were 2.52 and 2.61, respectively; in the bi-solute solutions Log K_d values were 1.45 and 1.9, respectively. For FLU and PYR, Log K_d values in single solute solutions were 3.3 and 3.2, respectively and was 2.79 for both PAHs in bi-solute solutions. The concentration of

PAH in the bile (i.e. PAH_{bile}) of *P. promelas* exposed to single and bi-solute treatments of each PAH, with and without MWCNT was compared and is shown in Figure 4.5. In single solute treatments, MWCNTs decreased the concentration of PHEN and ANT measured in the bile by ~50%, and decreased the concentration of FLU and PYR by ~85%. However, due to the higher variation in response of fish to PHEN adsorbed to MWCNTs, the difference was not significant at the 95% confidence level. This is similar to previously reported results and is attributed to the greater adsorption affinity of MWCNT for FLU and PYR than PHEN and ANT, and the lower bioconcentration factor (BCF_{bile}) of PHEN than the other PAHs.

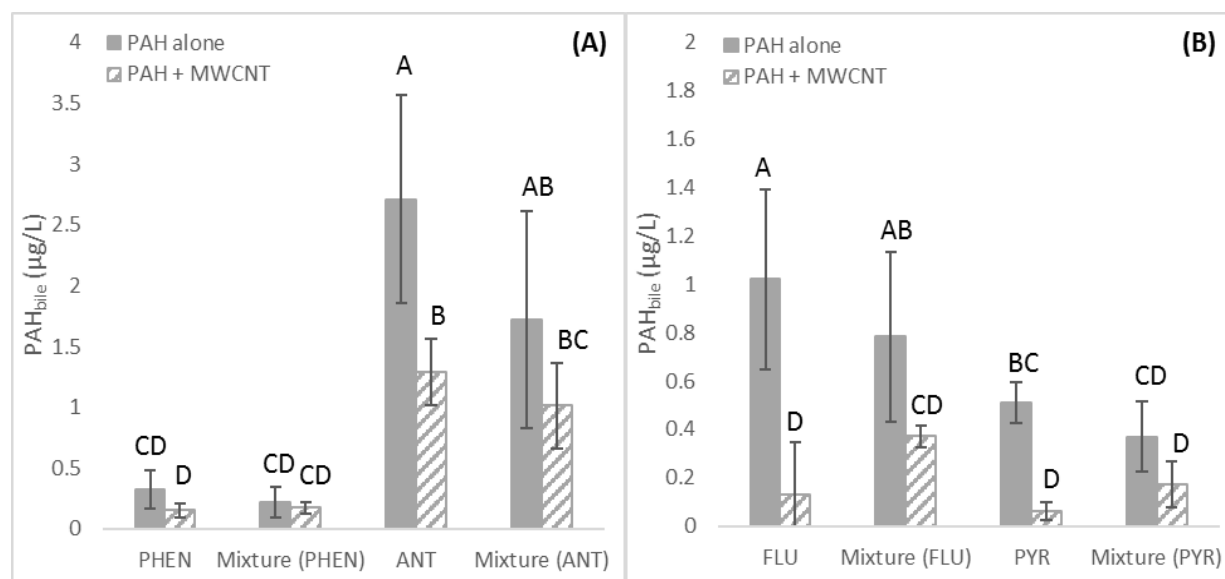


Figure 4.5. Comparison of the concentration of PAH measured in bile of fish exposed to treatments with and without MWCNT in single and bi-solute exposures. The initial concentration was 5 $\mu\text{g/L}$ of either (A) PHEN and ANT or (B) FLU and PYR. Error bars represent the 95% confidence level of the mean and levels not connected by the same letter are statistically different based on Student's T test and least squared means (p-value < 0.05).

In bi-solute solutions, the PHEN concentration in the bile of MWCNT exposed fish was not significantly different to that of fish exposed to the bi-solute solution without MWCNT.

There was a 40% reduction in the concentration of ANT in bile due to adsorption by MWCNTs, though due to variation in response, the reduction was not considered significant at a 95% confidence level. This indicates that due to competitive interactions between PHEN and ANT, there was a lack of significant effect of MWCNT on the bioavailable fraction of either PAH. This is attributed to decreased adsorption affinity of both PAHs when present in mixtures. Within the FLU_PYR bi-solute mixture, the reduction of FLU in the bile due to the presence of MWCNTs was significantly lower than without MWCNTs (p-value = 0.0275). However, the reduction in PYR bile concentration was not significant at the 95% confidence level. Least squared means analysis was used to compare PAH_{bile} values in single solute and bi-solute exposures, as it related to the difference in treatments with and without MWCNTs. The observed change in PHEN and ANT treatments due to the presence of MWCNTs in single solute treatments was not significantly different from the change observed in bi-solute treatments. In contrast, the change observed in bile concentration of FLU and PYR due to the presence of MWCNT was significantly greater in the single solute treatments than the bi-solute treatments (p-value = 0.0001 and 0.0365 for FLU and PYR respectively). This was attributed to greater competition between FLU and PYR, than PHEN and ANT. Due to weaker adsorption of PHEN and ANT compared with FLU and PYR, PHEN and ANT were more vulnerable to competitive interactions leading to a more drastic decrease in adsorption capacity by MWCNT; thus MWCNT appeared to have a limited influence on bioavailability of PHEN and ANT in bi-solute systems. In contrast, the difference in FLU bile concentration in bi-solute exposures with and without MWCNT was significantly greater than the difference observed for PYR (p-value 0.048), suggesting that the bioavailability of PYR is more susceptible to competition by FLU as similarly observed in the bi-solute adsorption experiments.

Plotting of the % reduction in PAH_{bile} as a function of adsorption by MWCNT showed a strong linear correlation ($R^2 = 0.86$) (Figure 4.6). Regardless of whether the exposure solutions

were single- or bi-solute, the concentration of PAH in the bile appeared to be directly related to adsorption where the concentration of PAH was estimated to be nearly zero with Log K_d values surpassing 3.5. This would seem to imply that interactions between multiple solutes at the surface of MWCNT has little effect on bioavailability of the adsorbed molecules beyond the influence of altered adsorption affinity.

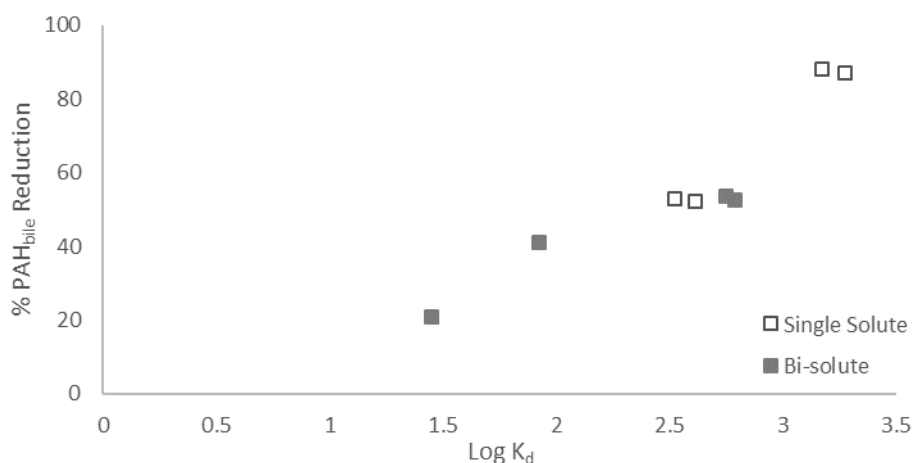


Figure 4.6. The reduction in bile concentration (%) of PAHs as a function of adsorption. Adsorption is represented by the single point adsorption descriptor (Log K_d) at the exposure concentrations.

The partition coefficient of PAH from MWCNT into the bile ($K_{\text{ibileMWCNT}}$) was calculated to further assess any changes in bioavailability of adsorbed PAHs due to competition and bi-solute interaction. Assuming that steady state had been reached in the system, $K_{\text{ibileMWCNT}}$ was calculated for each MWCNT exposure as follows.

$$K_{\text{ibileMWCNT}} = \frac{C_e * K_{\text{ibile}}}{C_s * K_{\text{iMWCNT}}} = \frac{BCF_{\text{bile}}}{K_d} \quad (4.6)$$

Where C_e is the equilibrium concentration measured in the system, BCF_{bile} is the ratio of PAH measured in the bile compared with the water concentration, and K_d is the single point adsorption descriptor of the system. $K_{\text{ibileMWCNT}}$ essentially normalizes the concentration of PAH observed

in the bile by the concentration that is adsorbed to ingested MWCNTs. This type of parameter can provide additional information on the bioavailability of MWCNT adsorbed PAHs, beyond just the change in concentration of the PAH in the bile (Haw et al., 2006). Least squared means was used to compare $K_{\text{ibileMWCNT}}$ of each PAH in single-solute and bi-solute exposures. Only for FLU was a significant increase of $K_{\text{ibileMWCNT}}$ observed in bi-solute exposures compared with the single solute exposure (p-value = 0.0068), indicating that a greater amount of FLU is absorbed into the organism when bi-solute adsorption is occurring. This is attributed to the interactions between PYR and FLU at the MWCNT surface. Although the adsorption work showed PYR to be more sensitive to FLU competition, molecules of similar structure and physicochemical characteristics have the greatest competition (Yang et al., 2006a) (Figure 4.2). It may be that though FLU outcompetes PYR in an aqueous system, the lowered adsorption affinity allows it to more easily desorb once ingested by an organism. Additionally, during the adsorption experiments there was a distinct trend in which the adsorption of FLU appeared to increase at low levels of PYR adsorption (Figure 4.2). If multilayer adsorption is the mechanism occurring in bi-solute FLU and PYR solutions, then it may be that the outer layers of adsorbed FLU more readily desorb when ingested by an organism (Yang et al. 2006a; Yang et al., 2010; Wang et al., 2011).

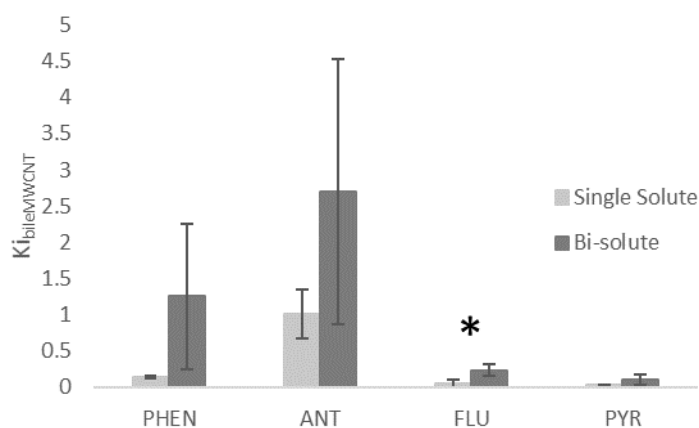


Figure 4.7. Comparison of the uptake of each PAH from MWCNT into bile, represented by $K_{\text{bileMWCNT}}$, in single solute and bi-solute exposures. Error bars represent the standard deviation about the mean. Asterisks indicate a significant difference, as determined by least squared means, in $K_{\text{bileMWCNT}}$ between the single solute and bi-solute exposure (p-value < 0.05).

4.4 Conclusions

The results of this work indicate that while molecules of similar physicochemical characteristics may adsorb similarly to a given adsorbent in single-solute solutions, differences in structure are a major driving force in the competitive interactions that occur in bi-solute systems. In cases where structure allowed for the PAH molecules to have greater contact with the MWCNT surface, the PAH was shown to outcompete its isoform. In this study the linear structure of ANT and the more flexible structure of FLU, were shown to improve their contact with the surface of MWCNT and were likely the reason they were able to outcompete angular PHEN and rigid PYR, respectively. Similar to previous reports, competitive interactions were more significant at lower concentrations of the two solutes and largely became insignificant at higher concentrations (Yang et al., 2006a). The bioavailability of the adsorbed PAHs in bi-solute systems closely followed the observed adsorption trends and was largely attributed to changes in adsorption affinity due to competition at the MWCNT surface. However, the results indicated

that the uptake of FLU into the exposed organism from ingested MWCNTs ($K_{ibileMWCNT}$) was greater in a bi-solute system compared with the bioavailability of the single solute system.

Although the overall concentration of FLU in the bile was still lower than in treatments without MWCNT, this may indicate that in multi-solute systems, as expected in the natural environment, MWCNTs have a greater potential to act as a “contaminant transporter”. Further, the potential of competitor adsorption to enhance the adsorption of another solute should be further studied as this may significantly impact the bioavailability of adsorbed molecules in an unpredictable way.

4.5 References

- Apul, O.; Karanfil, T. Adsorption of synthetic organic contaminants by carbon nanotubes: A critical review. *Water Res.* **2015**, 68, 34-55.
- Apul, O.G.; Shao, T.; Zhang, S.; Karanfil, T. Impact of carbon nanotube morphology on phenanthrene adsorption. *Environ. Tox. Chem.* **2012**, 31(1), 783-788.
- Ersan, G.; Apul, O.G.; Karanfil, T. Linear solvation energy relationships (LSER) for adsorption of organic compounds by carbon nanotubes. *Water Res.* **2016**, 98, 28-38.
- Feng, C.; Lin, C.S.; Fan, W.; Zhang, R.Q.; Van Hove, M.A. Stacking of polycyclic aromatic hydrocarbons as prototype for graphene multilayers, studied using density functional theory augmented with a dispersion term. *J. Chem. Phys.* **2009**, 131, 194702-1-8.
- Gotovac, S.; Honda, H.; Hattori, Y.; Takahashi, K.; Kanoh, H.; Kaneko, K. Effect of nanoscale curvature of single-walled carbon nanotubes on adsorption of polycyclic aromatic hydrocarbons. *Nano Letters.* **2007**, 7(3), 583-587.
- Haws, N.W.; Ball, W.P.; Bouwer, E.J. Modeling and interpreting bioavailability of organic contaminant mixtures in subsurface environments. *J. Contam. Hydro.* **2006**, 82, 255-292.
- Kah, M.; Zhang, X.; Jonker, M.T.O.; Hofmann, T. Measuring and modeling adsorption of PAHs to carbon nanotubes over a six order of magnitude wide concentration range. *Environ. Sci. Technol.* **2011**, 45 (14), 6011-6017.
- Linard, E., Apul, O.G., Karanfil, T., van den Hurk, P.; Klaine S.J. Bioavailability of carbon nanomaterial-adsorbed polycyclic aromatic hydrocarbons to *Pimphales promelas*: influence of adsorbate molecular size and configuration. **2017**. *Environ. Sci. Techn.* DOI: 10.1021/acs.est.7b02164.
- Marcé, R.M.; Borrull, F. Review: Solid-phase extraction of polycyclic aromatic compounds. *J. Chromatogr. A.* **2000**, 885, 273-290.
- Martinez, C. R.; Iverson, B.I. Rethinking the term “pi-stacking”. *Chem. Sci.* **2012**, 3, 2191-2201.
- Podeszwa, R. Interactions of graphene sheets deduced from properties of polycyclic aromatic hydrocarbons. *J. Chem. Phys.* **2010**, 132, 44704-1-8.
- Schwarzenbach, R.P.; Gschwend, P.M.; Imboden, D.M. *Environmental Organic Chemistry*; A John Wiley & Sons, Inc. publication: Hoboken, New Jersey, **2003**.
- Shen, M.; Xia, X.; Zhai, Y.; Zhang, X.; Zhao, X.; Zhang, P. Influence of carbon nanotubes with preloaded and coexisting dissolved organic matter on the bioaccumulation of polycyclic aromatic hydrocarbons to *Chironomus plumosus* larvae in sediment. *Environ. Tox. Chem.* **2013**, 33(1), 1-8.
- Sun, H.; Song, Q.; Luo, Q.; Wu, W.; Wu, J. Sorption of phenanthrene on single-walled carbon nanotubes modified by DOM: effects of DO molecular weight and contact time. *Environ. Sci. Process. Impact.* **2013**, 15, 307-314.

Torreiro-Melo, A.G.; Silva, J.S.; Bianchini, A.; Zanardi-Lamardo, E.; de Carvalho, P.S.M. Bioconcentration of phenanthrene and metabolites in bile and behavioral alterations in the tropical estuarine guppy *Poecilia vivipara*. *Chemosphere*. **2014**, 132, 17-23.

Wang, J.; Chen, Z.; Chen, B. Adsorption of polycyclic aromatic hydrocarbons by graphene and graphene oxide nanosheets. *Environ. Sci. Technol.* **2014**, 48, 4817-4825.

Wang, S.; Ng, C.W.; Wang, W.; Li, Q.; Hao, Z. Synergistic and competitive adsorption of organic dyes on multiwalled carbon nanotubes. *Chem. Eng. J.* **2012**, 197, 34-40.

Wang, X.; Lu, J.; Xing, B. Sorption of organic contaminants by carbon nanotubes: influence of adsorbed organic matter. *Environ. Sci. Technol.* **2008**, 42, 3207-3212.

Wang, X.; Tao, S.; Xing, B. Sorption and competition of aromatic compounds and humic acid on multiwalled carbon nanotubes. *Environ. Sci. Technol.* **2009**, 43, 6214-6219.

Wang, Z.; Zhao, J.; Song, L.; Mashayekhi, H.; Chefetz, B.; Xing, B. Adsorption and desorption of phenanthrene on carbon nanotubes in simulated gastrointestinal fluids. *Environ. Sci. Technol.* **2011**, 45, 6018-6024.

Xia, G.; Ball, W.P. Polyani-based models for the competitive sorption of low-polarity organic contaminants on a natural sorbent. *Environ. Sci. Technol.* **2010**, 34, 1246-1253.

Yang, K.; Wang, X.; Zhu, L.; Xing, B. Competitive sorption of pyrene, phenanthrene, and naphthalene on multiwalled carbon nanotubes. *Environ. Sci. Technol.* **2006a**, 40, 5804-5810 .

Yang, K.; Wu, W.; Jing, Q.; Jiang, W.; Xing, B. Competitive adsorption of naphthalene with 2,4-dichlorophenol and 4-chloroaniline on multiwalled carbon nanotubes. *Environ. Sci. Technol.* **2010**, 44, 3021-3027.

Yang, K.; Xing, B. Adsorption of organic compounds by carbon nanomaterials in aqueous phase: Polyani Theory and its application. *Chem. Rev.* **2010**, 110, 5989-6008.

Yang, K.; Zhu, L.; Xing, B. Adsorption of polycyclic aromatic hydrocarbons by carbon nanomaterials. *Environ. Sci. Technol.* **2006**, 40, 1855-1861.

Zhang S, Shao T, and Karanfil T. The effects of dissolved natural organic matter on the adsorption of synthetic organic chemicals by activated carbons and carbon nanotubes. *Water Res.* **2011**, 45, 1378-1386.

Zhang, S.; Shao, T.; Bekargolu, S.S.K.; Karanfil, T. The impacts of aggregation and surface chemistry on carbon nanotubes on the adsorption of synthetic organic contaminants. *Environ. Sci. Technol.* **2009**, 43, 5719-5725.

Zhang, S.; Shao, T.; Bekargolu, S.S.K.; Karanfil, T. The impacts of aggregation and surface chemistry on carbon nanotubes on the adsorption of synthetic organic contaminants. *Environ. Sci. Technol.* **2009**, 43, 5719-5725.

Zhu, D.; Pignatello, J.J. Characterization of aromatic compound sorptive interactions with black carbon (charcoal) assisted by graphite as a model. *Environ. Sci. Technol.* **2005**, 39, 2033-2041.

CHAPTER FIVE

CONCLUSIONS

The potential risk of carbon nanomaterials (CNMs) to act as contaminant transporters or the potential use of such materials for pollution remediation of organic contaminants is strongly linked to the material's adsorptive capabilities. While current literature has laid a good base of how CNMs can influence the bioavailability or toxicity of some compounds in specific scenarios, there is still a gap in our understanding of the mechanisms driving bioavailability of CNM-adsorbed contaminants. The aim of this work was to establish a more holistic understanding of the correlation between adsorption behavior and the resulting bioavailability of the adsorbed compounds. By working with a single class of contaminants, polycyclic aromatic hydrocarbons (PAHs), I could systematically assess and characterize how the physicochemical properties of the adsorbent and adsorbate may be predominant modifiers of bioavailability.

As carbon nanotubes and graphene are both made up of sp^2 hybridized carbon atoms in a hexagonal honeycomb arrangement, it was not surprising that the mechanisms of adsorption of PAHs in this study were found to be largely similar in objective one. Although the results suggested that the dominant adsorbate-adsorbent interaction differed for multi-walled carbon nanotubes (MWCNTs) and exfoliated graphene (GN), the bioavailability of each of the PAHs when adsorbed to MWCNT or GN was found to be similar. However, bioavailability of PAHs adsorbed to MWCNTs appeared to be influenced by adsorbate size while bioavailability of PAHs adsorbed to GN were influenced by adsorbate morphology. This indicated that bioavailability of CNM-adsorbed PAHs was driven by the ability of the PAH molecules to access the available adsorption sites rather than the specific interactions occurring between the PAH and the CNM surface. Given these findings, it is likely that CNMs with similar carbon bond hybridization will impact the bioavailability of adsorbed compounds by a similar mechanism regardless of the materials physical structure. Extrinsic properties of the materials

such as surface area, degree of functionalization and edge length are expected to also influence adsorption capacity and subsequent bioavailability of adsorbed compounds, though again these effects are expected to be consistent within sub-classes of CNMs (i.e. sp , sp^2 , sp^3 hybridized carbons).

From the second objective, the adsorption studies were in agreement with previously published findings where compound properties contributing to hydrophobic interactions and π - π bonding (e.g. size, polarizability, and aromaticity) largely drove the strength and capacity of adsorption. However, similar to objective one the results of this study again suggested that the compound's physical characteristics significantly influenced the adsorption interactions occurring. For small PAHs that were limited in their inherent aromatic and hydrophobic character, this was found to be especially important; molecular morphology that decreased or inhibited π electron cycling within the adsorbate molecule significantly decreased the compound's adsorption affinity by MWCNT. Additionally, increasing concentrations of the adsorbate resulted in a change of adsorption interactions from specific to non-specific interactions which was associated with weaker adsorption affinities. Small, less hydrophobic PAHs were particularly sensitive to this change in adsorption interactions, suggesting that in highly concentrated scenarios CNMs would only be effective at removing compounds with higher hydrophobic character from the water column.

While bioavailability of MWCNT-adsorbed PAHs was inversely related to adsorption affinity determined in the aqueous system, it was not a direct correlation. The bioavailability of the adsorbed PAH was driven by the opposing forces of the strength of adsorption between the PAH and MWCNT vs. the absorption potential of the PAH across the organism's cell membranes. Both of these interactions can be influenced by PAH physicochemical characteristics, though not necessarily in parallel trends. For example, though small, less hydrophobic PAHs, like naphthalene and fluorene, both have a low adsorption affinity for

MWCNT, the uptake potential of fluorene is significantly higher than that of naphthalene. This demonstrates that while compound physicochemical characteristics may drive adsorption in aqueous systems in a predictable manner, the bioaccumulative potential of that compound needs to also be taken into consideration when describing the adsorption-bioavailability relationship between different classes of compounds and CNMs.

The final objective of this work was to assess how the adsorption-bioavailability relationship may change when PAHs are present in a mixture rather than a single solute system. Though PAH isoforms adsorbed similarly in single-solute solutions to MWCNTs, competitive interactions occurred in bi-solute solutions thus altering adsorption of one or both of the PAHs present. Co-solute adsorption led to a decrease in adsorption affinity of both PAHs and consequently increased bioavailability of the adsorbed PAH in a similar manner. This indicates that in the natural environment with many different compounds present, bioavailability of CNM-adsorbed contaminants may be greater than anticipated given single-solute adsorption studies.

In support of findings from the previous two objectives, it was also observed that PAHs that outcompeted their chemically similar isoform had a molecular structure or morphology that allowed greater contact with the MWCNT surface. Interestingly, findings from the bi-solute adsorption and bioavailability study of the high hydrophobic PAH pair (e.g. fluoranthene and pyrene), suggested that at low concentrations there appeared to be a synergistic adsorption interaction rather than a competitive interaction. An enhanced uptake of fluoranthene in *P. promelas* was then observed raising concerns about enhanced bioavailability of contaminants from multi-solute systems due to the presence of CNMs.

Overall, the results of this work indicate that it is not likely that MWCNT, GN or other similarly structured CNMs will enhance the bioavailability of PAHs to fish in a natural system at current estimated CNM concentrations. However, CNMs with a different carbon hybridization or crystalline structure, such as fullerenes, may alter bioavailability in a different manner than

observed in this study. Additionally, this work showed that beyond the influence of the adsorbate's chemical properties the adsorbate's physical and morphological traits significantly impact both adsorption and bioavailability of CNM-adsorbed compounds. This provides additional insight into adsorbate and CNM interactions pertaining to adsorbate structure where current literature has previously lacked assessment. By systematically assessing bioavailability of several PAHs adsorbed to MWCNTs in single and bi-solute systems at different concentrations in the presence of natural organic matter, I was able to provide the most holistic and environmentally relevant understanding of the adsorption-bioavailability relationship. The results showed that factors influencing CNM adsorption affinity of compounds prior to organismal ingestion, such as concentration and competition, also influence bioavailability of the CNM-adsorbed PAHs in a similar manner. Once ingested, bioaccumulative potential of the adsorbed compound is a near equal and opposing force to adsorption affinity, the combined interactions controls the adsorption-bioavailability relationship. While this work indicated adsorption behavior of PAHs by CNMs is not a perfect prediction of the resulting uptake of PAH into *P. promelas* bile, inclusion of additional biotic processes will likely improve the ability to predict the bioavailability of other CNM-adsorbed compounds. Understanding and modeling the adsorption-bioavailability relationship of CNM-adsorbed PAHs is the first step to assessing the potential use of CNMs for pollution remediation and/or their indirect risk when released into the environment.

Future studies should focus on assessing whether other types of contaminants, beyond planar aromatics, show a similar relationship between adsorption affinity and resulting bioavailability when adsorbed to CNMs. This may provide clarity in the variable results that have been observed in the literature in terms of whether or not a CNM-adsorbed contaminant is bioavailable and to what degree bioavailability was affected. Also, attention should be given to understanding the influence of solution chemistry on the relationship between adsorption affinity


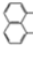





and bioavailability of CNM-adsorbed contaminants. Solution chemistry, while not as influential on neutral aromatic compounds, such as PAHs, can be highly influential on the adsorption behavior of ionizable compounds or those with functional groups. Further by investigating the mechanism by which desorption occurs in the digestive solution of organisms and the relationship with absorption of the CNM-adsorbed contaminants into the organism, we can better understand what alters bioavailability beyond adsorption interactions that occurred prior to organismal uptake. Although this work is based on a single contaminant class, the results show that the structural makeup of contaminants is particularly important in driving competitive interactions and influencing the bioavailability of the CNM-adsorbed solutes. Mixtures between different types of contaminants and with environmental components needs to be assessed to more accurately understand the biologically implications of CNMs entering the environment.

APPENDICES

Appendix A

Chemical Characteristics

Table A1 Adsorbate physico-chemical properties

Compound	Structure	MW ^a (g/mol)	Density ^a (g/cm ³)	Log K _{ow} ^a	C _{sw} ^a (mg/L)	Molecular Size ^c (Å x Å x Å)	Surface Area ^b (Å ²)	Volume ^d (cm ³ /mol)	Polarizability ^e (Å ³)	p ^a	Ionization Potential ^b (eV)	Resonance energy (eV)	HOMO-LUMO gap ^e (eV)	Dipole Moment ⁱ (D)	Refractive Index ³	Molar refractivity ^m (cm ³ /mol)
Naphthalene (NAP)		128.2	0.9	3.33	31	9.2 x 7.4 x 3.9	155.8	142.44	17.5 [14.6-17.5] ^{4e}	0.2	8.1 ± 0.02	1.35 ^g [0.39-3.2] ^{hi}	4.3 [0.18-8.4] ^{hi}	0.0	1.58	37.23
Acenaphthene (ACE)		154.2	1.2	4.20	3.9	9.2 x 8.6 x 3.9	180.8	146.86	16.8 [17.8-20.5] ^{4e}	0.2	7.7 ± 0.05	3.1 ⁱ	4.2 [0.17-8.3] ^{hi}	0.82	1.61	47.69
Fluorene (FLO)		166.2	1.05	4.32	1.69	11.4 x 7.5 x 4.2	194	138.5	19.1 [19.4-21.3] ^{4e}	0.2	7.9 ± 0.05	4.1 ⁱ	4.5 [0.19-7.3] ^{hi}	0.48	1.65	54.80
Phenanthrene (PHEN)		178.2	0.98	4.57	1.15	11.6 x 8.0 x 3.9	198	181.84	24.6 [20.4-25.0] ^{4e}	0.26	7.903	1.95 ^g [0.55-4.8] ^{hi}	4.2 [0.17-8.2] ^{hi}	0.042	1.59	51.27
Anthracene (ANT)		178.2	1.25	4.68	0.045	11.6 x 7.4 x 3.9	202.2	142.56	24.6 [20.6-25.0] ^{4e}	0.26	7.4 ± 0.06	1.6 ^g [0.48-4.6] ^{hi}	3.2 [0.13-7.3] ^{hi}	0.0	1.60	48.43
Fluoranthene (FLU)		202.3	1.25	5.23	0.260	11.1 x 9.2 x 3.9	218	161.84	28.8 [23.2-28.8] ^{4e}	0.2	7.9 ± 0.1	2.19 ^g [0.58] ^{hi}	3.6 [0.15-7.7] ^{hi}	0.33	1.10	10.55
Pyrene (PYR)		202.3	1.27	5.13	0.135	11.6 x 9.2 x x3.9	213	159.29	23.0 [22.9-28.7] ^{4e}	0.29	7.4 ± 0.1	2.13 ^g [0.60] ^{hi}	3.4 [0.14-7.2] ^{hi}	0.0	1.85	71.22

MW = molecular weight, K_{ow} = octanol-water partitioning coefficient, C_{sw}, water solubility limit, β = H-acceptor, HOMO-LUMO gap = energy difference between highest occupied molecular orbital and lowest unoccupied molecular orbital, molar refractivity was calculated using Lorenz-Lorentz expression $[R = \frac{n^2 - 1}{n^2 + 2} \frac{M}{\rho}]$, where n = refractive index, M = molar mass, ρ = density

^aSchwarzenbach et al. 2003, ^bDabestani & Ivanov, 1999, ^cde Lima Ribeiro & Ferreira, 2003, ^dDatabase T3BD, ^eDatabase ChemSpider, ^fMatscheko et al. 2002, ^gHendon and Ellzey, 1974, ^hAlhara, 1996, ⁱPauling and Sherman, 1933, Wang et al., 2007, ^jDatabase NIST, ^kLu et al. 2007, ^mPacik, 1988

REFERENCES

- Aihara, J. Bond resonance energies of polycyclic benzenoid and non-benzenoid hydrocarbons. *J. Chem. Soc. Perkin Trans.* **1996**, 2, 2185-2195.
- ChemSpider: Search and share chemistry. <http://www.chemspider.com/> (accessed Aug 25, 2015)
- Dabestani, R.; Ivanov, I.N. Invited review: A compilation of physical, spectroscopic and photophysical properties of polycyclic aromatic hydrocarbons. *J. Photochem. Photobiol.*, **1999**, 70(1), 10-34.
- de Lima Ribeiro, F.A.; Ferreira, M.M.C. QSPR models of boiling point, octanol-water partition coefficient and retention time index of polycyclic aromatic hydrocarbons. *J. Mol. Struct.* **2003**, 663, 109-126.
- Herndon, W.C.; Ellzey, M.L. Jr. Resonance theory. V. Resonance Energies of benzenoid and nonbenzenoid π systems. *J. Am. Chem. Soc.* **1974**, 96 (21), 6631-6642.
- Lu, G-N.; Dang, Z.; Tao, X-Q.; Yang, C.; Yi, X-Y. Estimation of water solubility of polycyclic aromatic hydrocarbons using quantum chemical descriptors and partial least squares. *QSAR Comb. Sci.* **2007**, 27 (5), 618-626.
- Matscheko, N.; Lundstedt, S.; Svensson, L.; Harju, M.; Tysklind, M. Accumulation and elimination of 16 polycyclic aromatic compounds in the earthworm (*Eisenia fetida*). *Environ. Tox. Chem.* **2002**, 21(8), 1724-1729.
- NIST PAH Database. <http://pah.nist.gov/beta/index.html> (accessed Sept 15, 2016)
- Pacák, P. Molar refractivity and interactions in solutions I. Molar refractivity of some monovalent ions in aqueous and dimethyl sulfoxide solutions. *Chem. Papers.* **1989**, 43(4), 489-500
- Pauling, L.; Sherman, J. The nature of chemical bond. VI. The calculation from thermochemical data of the energy of resonance of molecules among several electronic structures. *J. Chem. Phys.*, **1933**, 1, 606-617.
- Schwarzenbach, R.P.; Gschwend, P.M.; Imboden, D.M. *Environmental Organic Chemistry*; A John Wiley & Sons, Inc. publication: Hoboken, New Jersey, 2003.
- Toxin and Toxin Target Database (T3DB). <http://www.t3db.ca/toxins/> (accessed Sept 15, 2016)
- Wang, S.; Sheng, Y.; Feng, M.; Leszczynski, J.; Wang, L.; Tachikawa, H.; Yu, H. Light-induced cytotoxicity of 16 polycyclic aromatic hydrocarbons on the US EPA priority pollutant list in human skin HaCaT keratinocytes: relationship between phototoxicity and excited state properties. *Environ. Toxicol.* **2007**, 22(3), 318-327.

CNM Characterization

Table B1. Morphological characteristics of adsorbents measured before and after adsorption of 2 mg C/L NOM

Adsorbent	Length ^a (μm)	OD ^a (mm)	Thickness ^a (mm)	SSA _{BET} ^b (m^2/g)	V _{TOTAL} ^b (cm^3/g)	V _{micro} ^b (<2 nm) (cm^3/g)	V _{meso} ^b (2-50 nm) (cm^3/g)	V _{micro} ^b (>50 nm) (cm^3/g)
Pristine_GN	2.5	N/A	6.8	32	0.12	4.4×10^{-4}	4.7×10^{-2}	6.6×10^{-2}
Pristine_MWCNT	0.5-5	20-30	NR	132	0.80	1.3×10^{-2}	6.0×10^{-1}	1.8×10^{-1}
NOM_GN	2.5	N/A	6.8	17	0.10	3.0×10^{-5}	6.1×10^{-2}	2.0×10^{-1}
NOM_MWCNT	0.5-5	20-30	NR	98	0.71	2.2×10^{-4}	5.1×10^{-1}	4.2×10^{-2}

NOM = natural organic matter; GN = exfoliated graphene; MWCNT = multiwalled carbon-nanotube; OD = outer diameter; SSA = specific surface area; V_{TOTAL} = total pore volume; V_{micro} = micro pore volume; V_{meso} = meso pore volume; V_{macro} = macro pore volume

^a Provided by manufacturer.

^b Data represents average of triplicate measurements

Table B2. Micro Raman of exfoliated graphene (GN) and multi-walled nanotubes (MWCNT) with PAHs adsorbed

	Pristine		NAP		PHEN		ANT		FLU	
	Position ^a (cm ⁻¹)	FWHM ^b (cm ⁻¹)	Position (cm ⁻¹)	FWHM (cm ⁻¹)	Position (cm ⁻¹)	FWHM (cm ⁻¹)	Position (cm ⁻¹)	FWHM (cm ⁻¹)	Position (cm ⁻¹)	FWHM (cm ⁻¹)
GN	1581.6	15.1	1590.7	18.3	1590.1	36.2	1591.9	24.0	1591.5	28.5
MWCNT	1586.5	40.3	1609.5	34.9	1595.1	42.3	1593.3	37.4	1593.2	46.2

GN = exfoliated graphene; MWCNT = multiwalled carbon-nanotube; FWHM = Full Width at Half Maximum; NAP =

naphthalene; PHEN = phenanthrene; ANT = anthracene; FLU = fluoranthene

^a Position of G-band.^b Measure of Raman peak that reflects structural distribution.

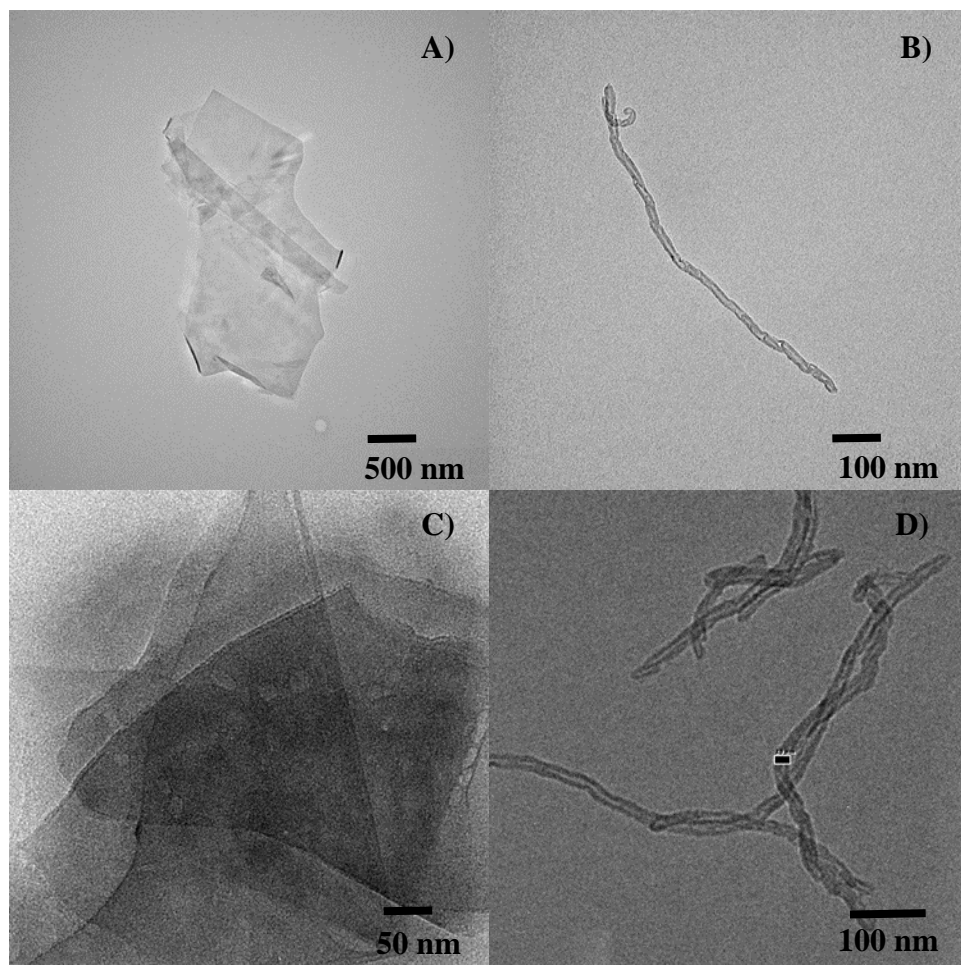


Figure B1. TEM images of (A, C) exfoliated graphene and (B,D) MWCNT in moderately hard water and in the presence of 2 mg C/L NOM respectively.

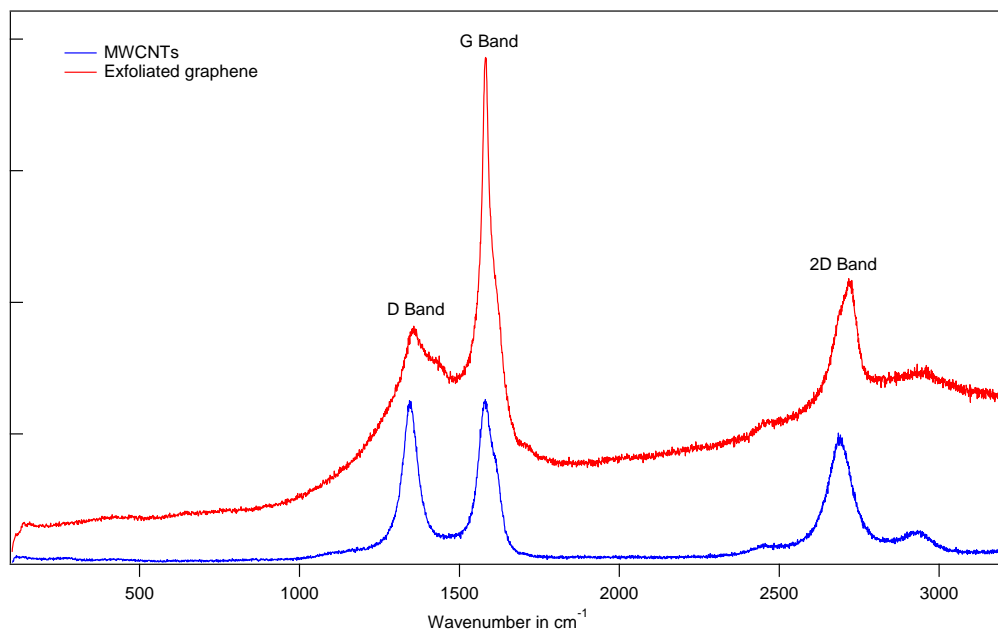


Figure B2. Raman spectra for MWCNTs and exfoliated graphene.

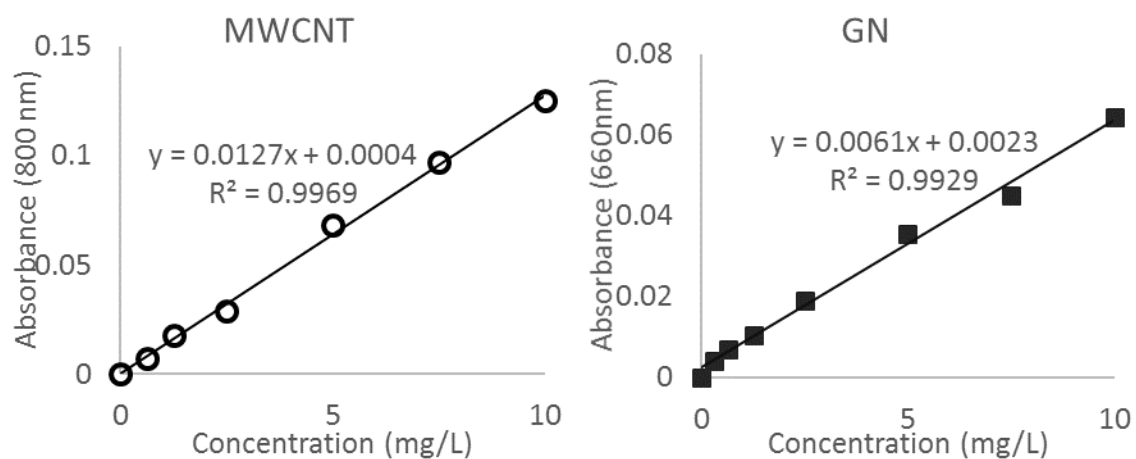


Figure B3. Concentration of MWCNTs and GN suspended in 2 mg C/L NOM measured via UV-vis absorbance at 800 nm and 660 nm, respectively.

Appendix C

Supporting Information for Organismal PAH and CNM Exposure

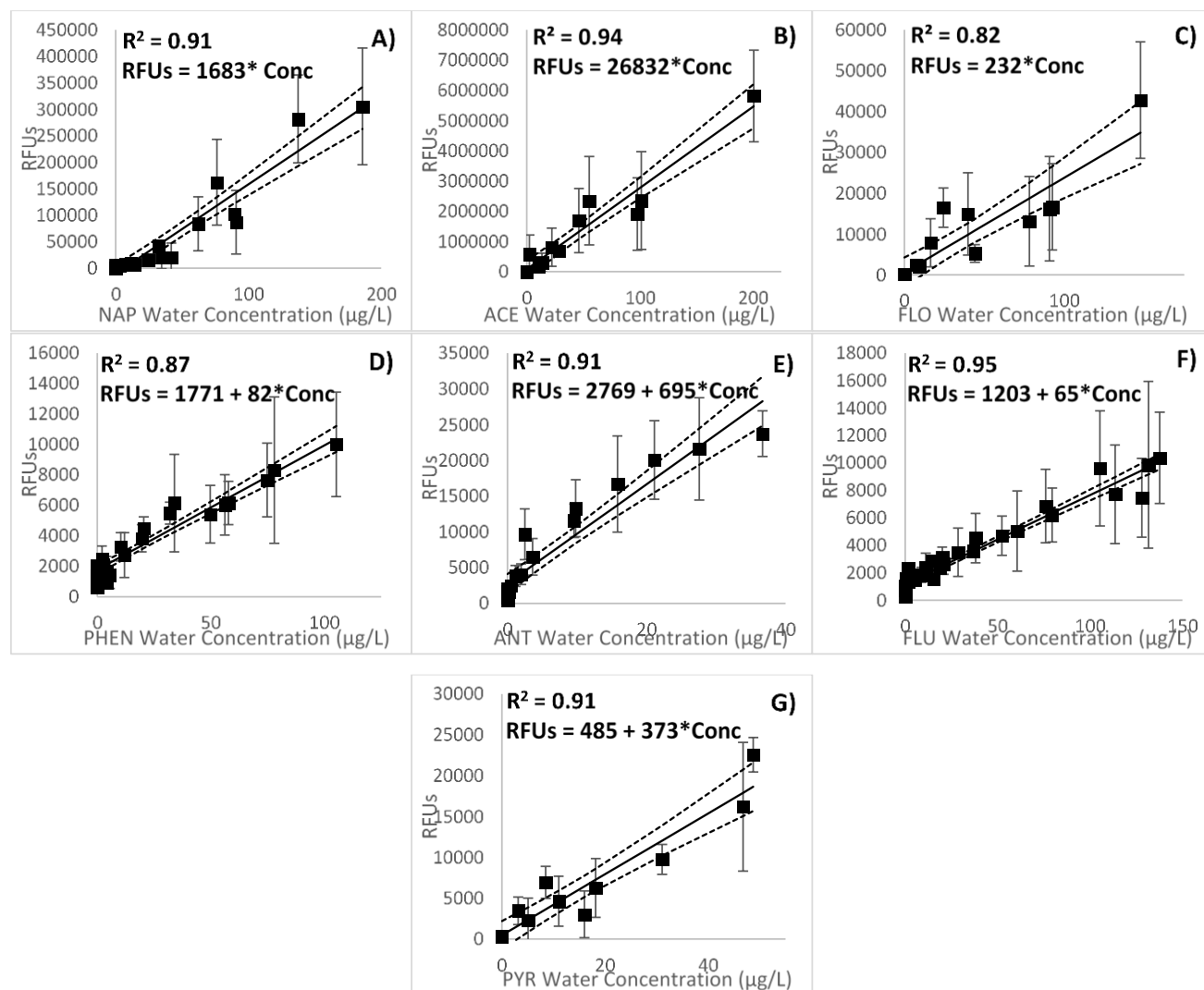


Figure C1. Dose response of *P. promelas* exposed to aqueous PAH. Bile fluorescence, as relative fluorescent units (RFUs), is plotted as a function of A) NAP, B) ACE, C) FLO, D) PHEN, E) ANT, F) FLU and G) PYR measured aqueous concentration. Individual data points represent the average bile fluorescence expressed by fish from the same aquarium, where the error bars represent the standard deviation of response from individuals within that aquaria. The correlation coefficients (R^2) and prediction lines of the dose-response curve were calculated using linear regression where response and concentration per aquaria represent the measurement units. The solid line represents the prediction line developed from the experimental data points, while the dashed lines give the 95% confidence interval around the prediction line.

Table C1. Standard curves of PAHs used to calculate PAH equivalent concentration in bile samples and the calculated bile bioconcentration factor (BCF_{bile}).

PAH	Excitation/Emission λ	Calibration Equation	Background Solution ^a	Log BCF_{bile}
NAP	276/330	$RFU_{NAP} = 1018.4 * C$	100% Methanol	1.56
ACE	285/330	$RFU_{ACE} = 2656 * C$	100% Methanol	2.80
FLO	260/310	$RFU_{FLO} = 248.1 * C$	50:50 Methanol/nano-pure water	2.62
PHEN	250/363	$RFU_{PHEN} = 51.1 * C$	50:50 Methanol/nano-pure water	2.82
ANT	252/399	$RFU_{ANT} = 205.5 * C$	50:50 Methanol/nano-pure water	3.25
FLU	280/440	$RFU_{FLU} = 97.1 * C$	50:50 Methanol/nano-pure water	2.27
PYR	270/390	$RFU_{PYR} = 284.1 * C$	50:50 Methanol/nano-pure water	3.08

C = concentration ($\mu\text{g/L}$)

^aSolution is the exact same as used to dilute and analyze the bile samples for each PAH.

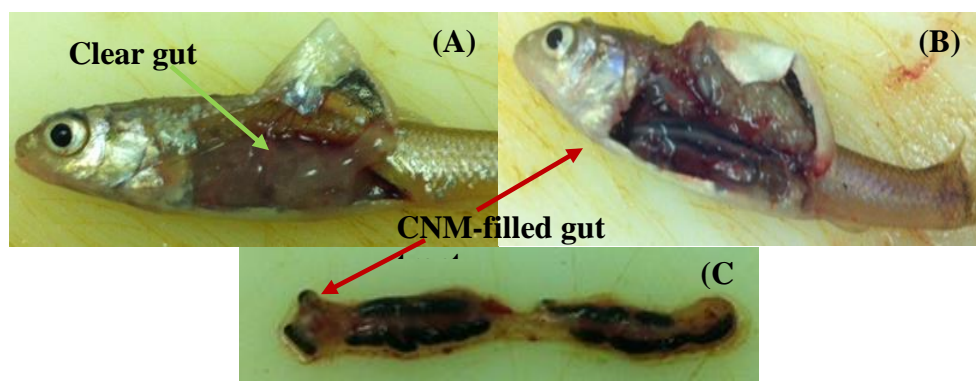


Figure C2. Images of *P. promelas* intestinal tract from the (A) PAH only treatments containing no PAH, (B) CNM treatments with PAH and CNM present, and (C) an enlargement of the CNM filled intestinal tract.

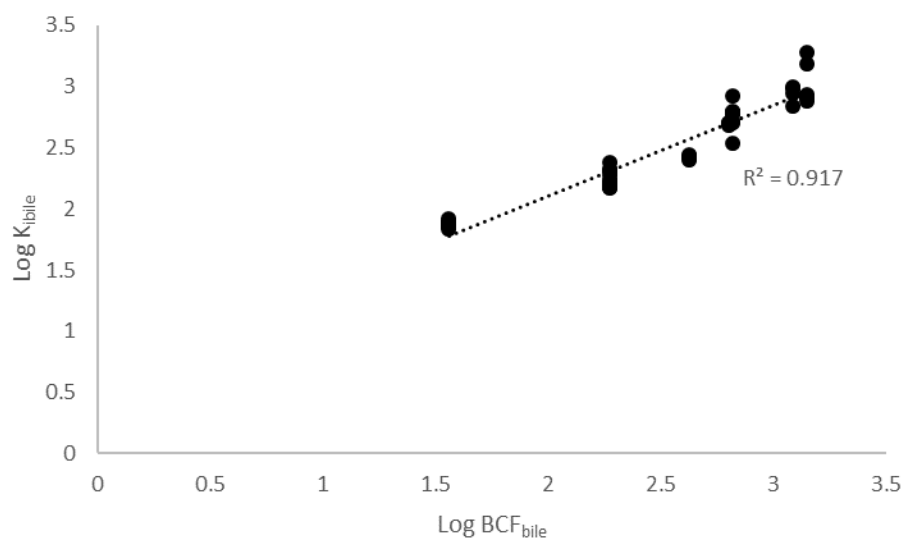


Figure C3. Relationship between single $\text{Log BCF}_{\text{bile}}$ values for each PAH and the measured partitioning of PAHs into bile from the bioavailability assays ($\text{Log K}_{\text{bile}} = \text{Log} \left(\frac{\text{PAH}_{\text{bile}}}{C_n} \right)$).

Appendix D

Adsorption Model Fitting

Table D1. Freundlich model fitting parameters of adsorption isotherms above and below the “isotherm transition point”

<i>Freundlich Model (FM) Below</i>				
	$K_F \text{ (mg/g)/(mg/L)}^{1/n}$	$1/n$	RMSE	R^2
<i>naphthalene</i>	30.32±10.65	0.56±0.086	0.212	0.981
<i>acenaphthene</i>	17.45±11.82	0.47±0.15	0.397	0.943
<i>fluorene</i>	11.27±16.58	0.46±0.30	0.425	0.767
<i>phenanthrene</i>	71.91±35.77	0.61±0.10	0.266	0.987
<i>anthracene</i>	379.68±102.32	0.88±0.046	0.056	0.999
<i>fluoranthene</i>	99.50±8.50	0.53±0.023	0.163	0.997
<i>pyrene</i>	203.2±156.1	0.60±0.12	0.454	0.982
	2			
<i>Freundlich Model (FM) Above</i>				
	$K_F \text{ (mg/g)/(mg/L)}^{1/n}$	$1/n$	RMSE	R^2
<i>naphthalene</i>	52.88±13.73	0.73±0.154	1.93	0.942
<i>acenaphthene</i>	20.88±0.86	0.51±0.019	0.124	0.999
<i>fluorene</i>	15.96±5.44	0.46±0.156	0.751	0.911
<i>phenanthrene</i>	44.32±4.16	0.59±0.036	0.455	0.987
<i>anthracene</i>	29.88±13.81	0.45±0.113	0.494	0.89
<i>fluoranthene</i>	76.02±19.56	0.49±0.095	2.65	0.90
<i>pyrene</i>	74.27±66.03	0.48±0.265	3.75	0.81

Appendix E

JMP Outputs for LFER Models

JMP Outputs for LFER Model (eq. 3.3)

Independent Variable	Log $K_{0.01}$
Dependent Variables	π , β , V
RSquare (R^2)	0.86
RSquare Adj	0.81
Root Mean Square Error	0.29
Mean of Response	2.57
Observations (or Sum Wgts)	14

ANOVA table for LFER Model (eq.3.3)

Source	DF	Sum of Squares	Mean Square	F Ratio	p-value
Model	3	4.92	1.64	19.99	0.0002
Error	10	0.82	0.08		
C. Total	13	5.74			

Parameter Estimated for LFER Model (eq.3.3)

Term	Estimated Coefficient	Std Error	t Ratio	p-value	VIF
Intercept	0.20	0.84	0.24	0.81	.
V	-0.02	0.01	-2.06	0.07	2.15
π	0.13	0.03	4.56	0.001	2.06
β	9.16	2.84	3.23	0.01	1.74

JMP Outputs for LFER Model (eq.3.4)

Independent Variable	Log $K_{0.1}$
Dependent Variables	π , β , V
RSquare (R^2)	0.81
RSquare Adj	0.77
Root Mean Square Error	0.26
Mean of Response	2.44
Observations (or Sum Wgts)	17

ANOVA table for LFER Model (eq.3.4)

Source	DF	Sum of Squares	Mean Square	F Ratio	p-value
Model	3	3.94	1.31	18.77	<.0001
Error	13	0.91	0.07		
C. Total	16	4.85			

Parameter Estimated for LFER Model (eq.3.4)

Term	Estimated Coefficient	Std Error	t Ratio	p-value	VIF
Intercept	0.93	0.65	1.43	0.18	.
V	-0.02	0.01	-3.99	0.00	1.71
π	0.13	0.02	6.56	<.0001	1.40
β	7.64	2.12	3.60	0.00	1.30

JMP Outputs for LFER Model (eq.3.5)

Independent Variable	Log $K_{0.01}$
Dependent Variables	π , β , V, Structure
RSquare (R^2)	0.97
RSquare Adj	0.95
Root Mean Square Error	0.15
Mean of Response	2.57
Observations (or Sum Wgts)	14

ANOVA table for LFER Model (eq.3.5)

Source	DF	Sum of Squares	Mean Square	F Ratio	p-value
Model	5	5.55	1.11	47.53	<.0001
Error	8	0.19	0.02		
C. Total	13	5.74			

Parameter Estimated for LFER Model (eq.3.5)

Term	Estimated Coefficient	Std Error	t Ratio	p-value	VIF
Intercept	1.81	0.72	2.50	0.04	.
V	-0.02	0.01	-2.87	0.02	5.55
π	0.11	0.02	5.39	0.00	3.31
β	7.03	1.63	4.32	0.00	2.01
Structure[Clustered]	0.40	0.09	4.47	0.00	2.36
Structure[Linear]	-0.34	0.08	-4.11	0.00	3.00

JMP Outputs for LFER Model (eq.3.6)

Independent Variable	Log $K_{0.1}$
Dependent Variables	π , β , V, Structure
RSquare (R^2)	0.95
RSquare Adj	0.93
Root Mean Square Error	0.14
Mean of Response	2.44
Observations (or Sum Wgts)	17

ANOVA table for LFER Model (eq.3.6)

Source	DF	Sum of Squares	Mean Square	F Ratio	p-value
Model	5	4.62	0.92	44.82	<.0001
Error	11	0.23	0.02		
C. Total	16	4.85			

Parameter Estimated for LFER Model (eq.3.6)

Term	Estimated Coefficient	Std Error	t Ratio	p-value	VIF
Intercept	1.76	0.60	2.95	0.01	.
V	-0.02	0.01	-3.53	0.00	8.09
π	0.09	0.02	5.38	0.00	3.74
β	8.18	1.23	6.67	<.0001	1.48
Structure[Clustered]	0.35	0.07	5.14	0.00	2.59
Structure[Linear]	-0.28	0.09	-3.16	0.01	4.35

Appendix F

JMP Outputs for Bioavailability Model

JMP Outputs for Bioavailability Model

Independent Variable	Log (C_{ibile}^{ex}/C_{MWCNT})
Dependent Variables	Log BCF, Log K_d
RSquare (R^2)	0.68
RSquare Adj	0.65
Root Mean Square Error	0.34
Mean of Response	2.71
Observations (or Sum Wgts)	21

ANOVA table for Bioavailability Model

Source	DF	Sum of Squares	Mean Square	F Ratio	p-value
Model	2	4.45	2.22	19.47	<.0001
Error	18	2.06	0.11		
C. Total	20	6.50			

Parameter Estimated for Bioavailability Model

Term	Estimated Coefficient	Std Error	t Ratio	p-value	VIF
Intercept	2.55	0.45	5.63	<.0001	.
Log BCF	0.63	0.15	4.12	0.0006	1.00
Log K_d	-0.52	0.11	-4.96	0.0001	1.00